

2010

Miocene - Quaternary tectonic evolution of the northern eastern California shear zone

Kurt L. Frankel

Georgia Institute of Technology - Main Campus

Jeffrey Lee

Central Washington University, jeff@geology.cwu.edu

Kim Bishop

California State University - Los Angeles

Nancye Dawers

Tulane University

Plamen Ganey

University of Southern California

See next page for additional authors

Follow this and additional works at: <http://digitalcommons.cwu.edu/cotsfac>



Part of the [Geology Commons](#), and the [Tectonics and Structure Commons](#)

Recommended Citation

Frankel, K.L., Lee, J., et al. (2010). Miocene-Quaternary tectonic evolution of the northern eastern California shear zone. In H.E. Clifton & R. Ingersol (Eds.), *Geologic excursions in California and Nevada: Tectonics, stratigraphy, and hydrogeology* (Book 108, 173-231). Upland, CA: Pacific Section, SEPM (Society for Sedimentary Geology).

Authors

Kurt L. Frankel, Jeffrey Lee, Kim Bishop, Nancye Dawers, Plamen Ganev, Jeff Unruh, and Lewis A. Owen

Miocene - Quaternary tectonic evolution of the northern eastern California shear zone

Kurt L. Frankel¹, Jeff Lee², Kim Bishop³, Nancye Dawers⁴, Plamen Ganey⁴, Jeff Unruh⁵, and Lewis A. Owen⁶

¹*School of Earth and Atmospheric Sciences, Georgia Institute of Technology, Atlanta, GA 30332, USA, kfrankel@gatech.edu*

²*Department of Geological Sciences, Central Washington University, Ellensburg, WA 98926, USA*

³*Department of Geological Sciences, California State University, Los Angeles, CA 90032, USA*

⁴*Department of Earth and Environmental Sciences, Tulane University, New Orleans, LA 70118, USA*

⁴*Department of Earth Sciences, University of Southern California, Los Angeles, CA 90089, USA*

⁵*Fugro William Lettis & Associates, Inc., Walnut Creek, CA 94596, USA*

⁶*Department of Geology, University of Cincinnati, Cincinnati, OH 45221, USA*

ABSTRACT

The northern eastern California shear zone is an important component of the Pacific–North America plate boundary. This region of active transtensional deformation east of the San Andreas fault extends from the Garlock fault northward along the east side of the Sierra Nevada and into western Nevada. The eastern California shear zone is thought to accommodate nearly a quarter of relative plate motion between the Pacific and North America plates. Recent studies in the region, utilizing innovative methods such as cosmogenic nuclide geochronology, airborne lidar, structural mapping, and (U-Th)/He geochronology, are helping elucidate deformation histories for many of the major structures that comprise the eastern California shear zone. This field trip includes 12 stops focused on the active tectonics of the Sierra Nevada, Inyo Mountains, Coso Range, Poverty Hills, Volcanic Tableland, Fish Lake Valley, and Queen Valley. Trip participants will explore a rich record of the spatial and temporal tectonic evolution of the northern eastern California shear zone from the Miocene through the Holocene. Discussion will focus on the constancy of strain accumulation and release, timing of offset on faults, the origin and evolution of structures, distribution of strain, the various techniques used to determine fault displacements and slip rates, and the role and evolution of the eastern California shear zone as an increasingly important component of the Pacific–North America plate boundary.

Keywords: faults, neotectonics, earthquakes, strain distribution, eastern California.

In Clifton, H.E., and Ingersoll, R.V., eds., 2010, Geologic excursions in California and Nevada: tectonics, stratigraphy and hydrogeology: Pacific Section, SEPM (Society for Sedimentary Geology) Book 108, p. 173-231.

INTRODUCTION

The eastern California shear zone is an ideal natural laboratory to study the spatial and temporal evolution of active plate boundary fault systems. As such, the region has been the focus of a number of field-based studies in recent years, each with the goal of unraveling the spatial and temporal histories of fault displacements and slip rates. Results of this research highlight the importance of the eastern California shear zone in understanding the evolution of the Pacific–North America plate boundary.

The eastern California shear zone is an evolving component of the Pacific–North America plate boundary system (e.g., Faulds et al., 2005; Wesnousky, 2005). This region of predominantly right-lateral strike-slip faults is thought to accommodate ~20%–25% of total relative motion between the Pacific and North American plates (Bennett et al., 2003; Dixon et al., 2000, 2003; Dokka and Travis, 1990; Hearn and Humphreys, 1998; Humphreys and Weldon, 1994; McClusky et al., 2001; Thatcher et al., 1999). The area of active deformation extends northward from the eastern end of the Big Bend of the San Andreas fault near Palm Springs for ~500 km through the Mojave Desert and along the western edge of the Basin and Range east of the Sierra Nevada (Fig. 1).

In the Mojave Desert, south of the left-lateral Garlock fault, the eastern California shear zone comprises a 100-km-wide network of NNW–trending right-lateral faults. Geodetic data indicate that elastic strain is accumulating across this zone at a rate of 12 ± 2 mm/yr (Savage et al., 1990; Gan et al., 2000; McClusky et al., 2001; Miller et al., 2001; Peltzer et al., 2001). Seismological and paleoseismological data also indicate that this part of the eastern California shear zone releases strain at a relatively rapid rate; portions of several of these faults ruptured during the 1992 moment magnitude (M_w) 7.3 Landers and 1999 M_w 7.1 Hector Mine earthquakes. Moreover, paleoseismologic data indicate that these two earthquakes are part of an ongoing, ~1000-yr-long seismic cluster (Rockwell et al., 2000). However, such evidence for data, which suggest that the long-term, cumulative slip rate across the Mojave part of the eastern California shear zone is much slower. Recent work in the Mojave section of the eastern California shear zone indicates the total long-term slip rate across this fault system is on the order of 5–7 mm/yr, or about half of the current rate of strain accumulation determined from space-based geodesy (Oskin and Iriondo, 2004; Oskin et al., 2007, 2008). These observations suggest a pronounced strain rate transient across the Mojave section of the eastern California shear zone.

The Garlock fault bisects the eastern California shear zone, forming a major geologic and physiographic boundary between the Mojave Desert and western Basin and Range (Fig. 1; Davis and Burchfiel, 1973). Since the late Pleistocene, there has been at least 18 km of offset along the fault, yet little to no significant earthquake activity has occurred over at least the past ~300 yr (Carter, 1980; Dawson et al., 2003; McGill and Sieh, 1991). The Garlock fault is somewhat enigmatic in that nowhere does it appear to offset, or be offset by, NW-trending eastern California shear zone faults. A large remaining question in eastern California shear zone tectonics is how Pacific–North America plate boundary strain is transferred through, or around, the Garlock fault.

Nevertheless, displacement from the southern part of the eastern California shear zone in the Mojave Desert is funneled northward across the Garlock fault onto four main fault systems; the Owens Valley, Panamint Valley–Hunter Mountain–Saline Valley, Death Valley–Fish Lake Valley, and Stateline fault zones (Fig. 1). The only fault in the northern eastern California shear zone to experience significant seismic activity is the Owens Valley fault, which last ruptured in a M_w 7.6(?) earthquake near the town of Lone Pine in 1872 (Beanland and Clark, 1994; Hough and Hutton, 2008). A series of down-to-the-NW normal faults transfer slip between the Owens Valley, Panamint Valley–Hunter Mountain–Saline Valley, and Death Valley–Fish Lake Valley

faults (Fig. 1; Dixon et al., 1995; Lee et al., 2001a; Reheis and Dixon, 1996). In contrast to the strain transient south of the Garlock, the region-wide rate of dextral shear across these four faults appears to have remained constant at 9–10 mm/yr over late Pleistocene to recent time scales (Bacon and Pezzopane, 2007; Bennett et al., 2003; Frankel et al., 2007a; Guest et al., 2007; Lee et al., 2001a, 2009; Oswald and Wesnousky, 2002).

Farther north, dextral motion between the Sierra Nevada block and North America is focused on two faults bounding the east and west sides of the White Mountains: the White Mountains fault zone to the west and the Fish Lake Valley fault zone to the east. Of these two, global positioning system (GPS) data suggest that the Fish Lake Valley fault system is storing at least 75% of the elastic strain accumulating in this region (Dixon et al., 2000). However, recent late Pleistocene slip rate studies on these two faults reveal a geologic versus geodetic rate discrepancy similar to that in the Mojave, whereby the White Mountains and Fish Lake Valley faults account for less than half of the region-wide rate of shear determined from GPS data (Bennett et al., 2003; Frankel et al., 2007b; Kirby et al., 2006).

Across this same region, extension is accommodated on the Round Valley fault in the west, across the Volcanic Tableland, White Mountains fault, and Fish Lake Valley fault to the east (Berry, 1997; Ganev et al., 2010; Kirby et al., 2006; Sheehan, 2007). Unlike the dextral component of shear in this region, when compared with short-term rates of extension, late-Pleistocene extension rates appear to agree well with geodetic data (e.g., Bennett et al., 2003; Ganev et al., 2010; Wesnousky, 2005). The mismatch between short- and long-term rates of right-lateral deformation and the good temporal correlation among rates of extension have important implications for lithospheric dynamics, the distribution of deformation, and strain transfer along this important component of the Pacific-North America plate boundary. Although most of the structures in the northern eastern California shear zone are relatively well characterized, there are some regions where debate still exists as to the exact origin and significance of landforms. For example, the Poverty Hills, which are located along the dominantly right-lateral Owens Valley fault, have been explained as both a thrust-bound pop-up structure (e.g., Taylor and Dilek, 2001; Taylor, 2002) and as a large landslide (e.g., Bishop and Clements, 2006). Critical to understanding the role of the eastern California shear zone in plate boundary deformation is unraveling the origin and importance of enigmatic features such as the Poverty Hills.

This field guide reviews some of the newest results bearing on the formation, displacement, exhumation, and slip rate histories for many of the faults and landforms in the northern eastern California shear zone. We begin with a discussion of deformation across the Coso Range and southern-most Owens Valley fault, Miocene to recent exhumation of the Inyo Mountains, and the origin and significance of the Poverty Hills. We then move on to spatial and temporal variations in strain accumulation and release along the Fish Lake Valley and Queen Valley fault systems and the implications of these deformation rates for the strain transfer from the northern eastern California shear zone to the Walker Lane belt of western and central Nevada. We finish with a discussion of the role of the Volcanic Tableland and Sierra Nevada frontal fault system in accommodating extension across the northern ECSZ. The second part of the guidebook serves as a road log to 12 field sites that we feel provide an excellent representation of the late Miocene to Holocene deformational history of the northern eastern California shear zone.

QUATERNARY TECTONISM OF THE NORTHWESTERN COSO RANGE

The Coso Range is a tectonically and volcanically active region along the southeastern margin of the Sierra Nevada (“Sierran”) microplate, which moves about 13 mm/yr northwest with respect

to stable North America (Argus and Gordon, 1991; 2001; Dixon et al., 1995; 2000). Northwest motion of the Sierran microplate is accommodated by distributed strike-slip and normal faulting in a 100-km-wide zone of active deformation bordering the eastern Sierra Nevada that is variously referred to as the eastern California shear zone and Walker Lane belt (Dokka and Travis, 1990; Unruh et al, 2003).

Active crustal extension in the Coso Range primarily is driven by a releasing transfer of dextral motion from the Airport Lake fault to the Owens Valley fault, two major right-lateral strike-slip faults that form the eastern tectonic boundaries of the Sierran microplate southeast and northwest, respectively, of the Coso Range (stop 1 in Fig. 1; Unruh et al., 2002; Monastero et al., 2005). In detail, the Airport Lake fault zone splits into several branches at the southern end of the step-over region (Fig. 2). An eastern branch, consisting of north- to NNE-striking normal faults in northeastern Indian Wells Valley, extends northward across eastern Coso Basin and into the southern end of Wild Horse Mesa, where it continues northward and forms a dramatic series of scarps in Pliocene volcanic flows. The faults with the largest scarps in Wild Horse Mesa exhibit a left-stepping pattern (Fig. 2). A central branch, consisting of a zone of short NNE-striking, left-stepping surface traces, crosses the White Hills anticline south of Airport Lake playa and becomes the Coso Wash fault, which is characterized by a single trace along the southeastern flank of the Coso Range. A western branch of the Airport Lake fault zone, consisting of a series of short, discontinuous scarps, extends NNW across the basin south of the southern Coso Range and joins the Little Lake fault zone in southern Rose Valley (Fig. 2). Transfer of motion from all of these structures to the Owens Valley fault is described in greater detail below.

Oblique extension in the step-over region across the Coso Range has been accompanied by late Quaternary rhyolitic volcanism and hydrothermal activity (Duffield and Bacon, 1981). The Coso geothermal field, located in the central Coso Range (GF; Fig. 2), is a world class electrical-grade geothermal resource. As discussed below, Monastero et al. (2005) proposed that the Coso geothermal field and associated normal faults may be the surface manifestations of an actively developing metamorphic core complex. If this hypothesis is correct, then the modern Coso Range may be an analogue for other well-exposed core complexes, such as the Neogene Black Mountains core complex in Death Valley, in the early stages of their development (Unruh et al., 2008).

Slip Transfer and Oblique Extension Across the Central Coso Range

Based on the geomorphic expression of faults in late Quaternary deposits, the bulk of Holocene deformation in the Coso Range appears to be associated with the central branch of the Airport Lake fault zone (Fig. 2). The most significant structure in this branch is the Coso Wash fault, which consists of a series of NNE-striking normal faults that dip both to the south-southeast and the west-northwest. This fault zone extends from the White Hills anticline northward to Haiwee Spring in northern Coso Wash (Fig. 2), and is interpreted to be the principal locus for transferring active dextral shear through the Coso Range (Unruh et al., 2008). The Coso Wash fault zone can be traced about 9 km north of Airport Lake playa as a single southeast-dipping trace that has excellent geomorphic expression as scarps in Holocene alluvial fan deposits. The fault along this reach consists of a series of alternating short NNE- and NW-striking reaches. At the southern margin of the Coso geothermal field (Fig. 2), the fault splays out into a series of west-northwest-dipping traces that step northwest (left) into the bedrock of the Coso Range, and dip toward the main geothermal production zones. The west- northwest-dipping fault segments are geomorphically well expressed by northwest-facing scarps in bedrock and alluvium, and the

faults locally pond alluvium in their down-dropped hanging wall blocks upstream of the scarps.

At the latitude of the geothermal field, the east-dipping Coso Wash fault and the WNW-dipping normal faults collectively bound a prominent north-northeast-trending basement ridge that separates Coso Wash from the main production area of the Coso geothermal field (Walker and Whitmarsh, 1998). The basement ridge is at least 10 km long (Fig. 2), locally exhibits up to 550 meters of relief, and is best expressed between the geothermal field and Haiwee Spring. The basement ridge is essentially a horst block and may be analogous to the “central ridge” that Dooley et al. (2004) observed in scaled analog models of transtensional releasing stepovers that include a ductile substratum beneath a simulated brittle upper crust (quartz sand). North of the geothermal field, the Coso Wash fault dips consistently east-southeast and can be traced as a series of east-facing scarps in Holocene alluvium northward to the area around Haiwee Springs, where it loses its surface expression (Fig. 2). North of Haiwee Springs, Coso Wash terminates as a Quaternary basin and narrows to a steep canyon cut in Cretaceous bedrock and Pliocene basalts of Wild House Mesa. Analysis of stereo aerial photography of this segment of the fault indicates east-facing bedrock scarps, and possibly fault-related east-facing bedrock slopes. These features probably represent Quaternary faulting, as recognized earlier by Walker and Whitmarsh (1998). The step-faulted terrain associated with the eastern branch of the Airport lake fault and the Coso Wash fault appear to merge at this location to form a rhombic array of faults at the southern end of Upper Centennial Flat (Fig. 2), north of the termination of the basement ridge.

At the latitude of Haiwee Spring, the locus of active deformation steps west from Coso Wash to a series of NNE-striking, left-stepping normal faults that bound the western margins of Quaternary basins in the northwestern Coso Range such as McCloud Flat and Lower Cactus Flat (Fig. 2). The geomorphic expression and relative activity of these structures appear to increase northward as slip dies out on the Coso Wash fault and basement ridge to the east. The left step in the locus of deformation across the Coso Range is associated with a elongated, NW-trending zone of low P-wave and S-wave velocities in the depth range of about 5 to 12 km (Reasenberget al., 1980; Wilson et al., 2003; Hauksson and Unruh, 2007). The base of seismicity is distinctly elevated above the low velocity zone (Monastero and Unruh, 2002), suggesting that hot fluids (brines and/or magma) are present below about 5 km (Wilson et al., 2003; Hauksson and Unruh, 2007).

At least two faults that display evidence for late Quaternary dextral offset can be traced north from Lower Cactus Flat into the northwestern Coso Range piedmont (Faults A and B; Figs. 2 and 3). The easternmost of the two faults (A) transfers slip in a restraining stepover across NW-plunging, basement-involved anticlines to the Red Ridge fault zone, a zone of short NNE striking, en echelon normal faults that extends from Red Ridge northward to the margin of Owens Lake basin (Fig. 3). The westernmost of the two faults (B) is part of a zone of short, discontinuous NW-striking fault segments that trend toward the southern end of the Owens Valley fault (Fig. 3). Slemmons et al. (2008) have documented dextral offset of Holocene beach ridges of Owens Lake along this fault trend, which they attribute to surface rupture during the 1872 Owens Valley earthquake. A Pleistocene pediment that fringes the northern Coso Range is deformed by WNW-trending folds in the triangular region between faults A and B (Fig. 3). The coeval NNE-SSW shortening and WNW-ESE extension of the pediment surface in the triangular region between fault trends A and B is consistent with northwest dextral shear passing through the northwestern Coso Range.

The Red Ridge fault zone, which is mapped in detail by Slemmons et al. (2008), may transfer slip to the Central Valley fault zone, a NW-striking fault in Owens Lake basin interpreted

by Neponset and Aquila (1997) from analysis of seismic reflection data (Fig. 3). The “Central block” bounded by this structure and the Owens Valley fault to the west has subsided episodically during the Quaternary (Neponset and Aquila, 1997), possibly during large earthquakes. The NW-trending folds in the pediment surface may be the surface expression of reverse slip on blind, WNW-striking splays of the southern Owens Valley fault, also mapped by Neponset and Aquila (1997) from interpretation of reflection data (Fig. 3).

The Central Coso Range as a “Nascent” Metamorphic Core Complex

Monastero et al. (2005) proposed that the central Coso Range is a “nascent” metamorphic core complex; i.e., an extensional domain where active normal faults root into an elevated brittle ductile transition zone beneath the Coso geothermal field, but which has not undergone sufficiently large extensional strains to unroof and exhume the ductile rocks beneath the brittle upper crustal carapace. Workers have inferred the structure of core complexes early in their deformation history at low cumulative strains from palinspastic reconstruction of exhumed examples (e.g., Serpa and Pavlis, 1996), but natural examples of nascent, actively developing core complexes are sparsely documented. As discussed by Unruh et al. (2008), the upper crustal structure of the central Coso Range has many similarities to exhumed core complexes, and may be an example of a core complex forming as a consequence of oblique extension in a transtensional tectonic regime.

A basic structural model for an exhumed metamorphic core complex is shown in Figure 4A. Brittle deformation occurs above a breakaway fault at the locus of maximum extension, with numerous high-angle normal faults that accommodate that extension (Fig. 4A). These faults become listric with depth and/or are rotated into a near horizontal orientation above the footwall (Spencer, 1984; Buck, 1988). The boundary that separates brittle behavior in the upper plate from ductile flow in the lower plate, referred to as the main detachment zone, commonly is bowed upward into an antiformal structure directly adjacent to the breakaway fault zone. This zone is at its shallowest near the breakaway fault, deepens with increasing distance from the breakaway, and presumably becomes more brittle (Gans et al., 1985) because it is farther from the locus of uplift of the lower plate which is advecting heat to the near-surface. The distal termination of this detachment zone is characterized by one or more fault-bounded sedimentary basins that commonly have associated antithetic faults (Fillmore et al., 1994; Ingersoll et al., 1996; Fillmore and Walker, 1996; Gans et al., 1985). These supra-detachment basins principally receive sediments from the center of the uplifting core complex and commonly have admixed tuffs and lava flows from contemporaneous volcanism. Although the specific structural elements of any given core complex may differ from this basic model, all core complexes show a majority of these features.

A comparison of the structure of the central Coso Range (Fig. 4B) with the general model for a metamorphic core complex in Figure 4A reveals several key similarities, the most important of which is a series of normal faults that accommodate brittle extension above a shallow brittle-ductile transition zone (BDT). The BDT locally is elevated above magma or lithostatically pressured brines that occur in the 6 to 12 km depth range beneath the Coso Range (Hauksson and Unruh, 2007). Active normal faults mapped in the central Coso Range and locally by seismic reflection methods root into the elevated BDT and form localized zones of fracture permeability that facilitate hydrothermal convection in the Coso geothermal reservoir (Unruh et al., 2008; Fig. 4B). Coso Wash is interpreted to be analogous to the primary “breakaway basin” in the classic exhumed core complex model, and the basin-bounding Coso Wash fault is interpreted to sole into

the BDT as it dips eastward away from the zone of elevated heat flow beneath the central Coso Range.

The key difference between Coso and the general core complex model is in the geometry of the upper plate. In many exhumed core complexes, the upper plate has been arched into an antiform (Fig. 4A), presumably a consequence of localized unroofing of the lower plate in the center of the structure with progressive extension. With sufficient cumulative deformation and exhumation, the end result of this process is surface exposure of the brittle-ductile transition zone and underlying crust that has been deformed by ductile flow. Because the Coso structure has experienced only a few kilometers or less of horizontal extension (Monastero et al., 2005), the unroofing process is in an early stage and has not yet produced significant antiformal relief on the upper plate. Well-developed “supra-detachment basins”, presumably resulting from significant extension of the upper plate, also are not present in the central Coso Range.

Southern Owens Valley fault, Northwest Coso Range

The field trip stop along state highway 190 affords an excellent opportunity to look at, stand on and walk around evidence for surface rupture during the 1872 Owens Valley earthquake. Figure 5 is a slightly oblique aerial view of the field trip stop, looking toward the southeast. The highway parallels an abandoned shoreline of Owens Lake, and a series of gravelly late Holocene beach ridges are present on the north side of the highway. The photo shows a series of northwest-trending lineaments south of the highway that project to the broad bend in the road. These features are the surface expression of the zone of discontinuous fault segments that can be traced northwest of Fault A in Figure 3, and they trend toward the southern end of the Owens Valley fault zone mapped by Neponset and Aquila (1997) in southeastern Owens Lake basin (Fig. 3). D.B. Slemmons and his colleagues discovered that the Holocene beach ridges north of the highway are offset about 1.5 m in a right lateral sense along the trend of the lineaments. Slemmons et al. (2008) argue that the offset beach ridges represent surface rupture during the 1872 earthquake on the Owens Valley fault zone. If this is correct, then the 1872 rupture extended at least to the southern end of Owens Lake basin, and probably south into the Coso Range piedmont (Slemmons et al., 2008).

This stop is a good location to observe other tectonic-geomorphic evidence that northwest dextral shear extends from the southern end of the Owens Valley fault into the northwest Coso Range, thus establishing kinematic linkage with the northern extent of the Airport Lake fault. There is a large hill about 3 km south of the road, on trend with the lineaments in Figure 5, where the associated fault segment terminates or makes a poorly expressed left step (Fig. 3). The hill is cut by a series of left-stepping, west-facing scarps (Fig. 6). About 3-4 km south of highway 190 there is a prominent north-facing wave-cut scarp at about 1160 m (3800 ft) elevation bordering the northern Coso Range piedmont. The shoreline of Owens Lake last reached the elevation of this escarpment about 24 ka during a Tioga-age pluvial highstand (Bacon et al., 2006). The shoreline scarp is visibly warped by a series of low-amplitude folds west of the Red Ridge fault zone (Fig. 3); the fold deformation is best observed from highway 190 in low-angle, early morning light when the escarpment is shadowed (Fig. 7). Although not readily visible from the field trip stop, the Red Ridge fault zone is expressed as a series of horst and graben in a middle(?) to late Pleistocene pediment surface south of the 1160 m shoreline escarpment (Figs. 7 and 8).

EXHUMATION OF THE INYO MOUNTAINS

One of the most prominent geomorphic features in the northern ECSZ, the Inyo Mountains range is ~95 km long and 20-25 km wide with a maximum relief of ~3000 m, rising to its highest point at 3390 m above sea level (east of stop 2 in Fig. 1). The Inyo Mountains are located within a unique kinematic configuration in this part of the Basin and Range Province and ECSZ. These mountains are the southern continuation of the White Mountains, an east-tilted normal fault block, and are parallel to and lie east of the Sierra Nevada, a west-tilted normal fault block. The Inyo Mountains form the northern termination of the Hunter Mountain fault, a NW-striking dextral fault that connects the relatively shallow Panamint Valley (<1 km to basement at the northern end; Blakely and Ponce, 2001) and much deeper Saline Valley (4.0-4.5 km; Blakely and Ponce, 2001) pull apart basins (Fig. 1). The Inyo Mountains are bounded along its east flank by an active, east-dipping normal fault system, the Eastern Inyo fault zone (EIFZ) which can be traced for ~40 km from Daisy Canyon in the south to Waucoba Wash to the north (Fig. 9).

The Inyo Mountains expose several Mesozoic granitic plutons that intrude into sedimentary rocks including Precambrian through Paleozoic miogeocline strata and Mesozoic marine and nonmarine volcanic and epiclastic strata. In the southwestern Inyo Mountains, Paleozoic and Mesozoic metasedimentary rocks were complexly folded and faulted during the Permian, Jurassic, and Cretaceous. In the southeastern Inyo Mountains, a middle to late Miocene sedimentary basin was deposited over, but not cut by, the southern extension of the EIFZ (Conrad, 1993). Late Cenozoic faults, including the EIFZ, a dominantly normal-slip fault, and the Hunter Mountain fault zone, a dominantly dextral fault, bound the east flank of the Inyo Mountains (Fig. 1).

Faulting Along the Eastern Inyo Fault Zone

The following summary on faulting is based on the work of Lee et al. (2009a). The EIFZ consists of two major geometric segments that connect the northern termination of the Hunter Mountain fault with NE-striking normal faults that cut the Saline Range, thereby defining a right-step within a dextral fault system (Figs. 1 and 9). Well-developed and fresh landforms, such as triangular facets, wineglass-shaped drainages, small alluvial fan size at the range front, fault scarps developed across late Pleistocene alluvial fans, vertically offset drainages, and a steep range-front escarpment, up to 39° just north of McElvoy Canyon indicates recent slip along the EIFZ.

The southern segment of the EIFZ bounds the steep eastern flank of the Inyo Mountains (Fig. 9). Here, the main trace of the EIFZ extends along strike for 24 km from Daisy Canyon to Willow Creek. This N26W striking, E-dipping, dominantly normal fault zone is composed of bedrock fault planes and fault scarps cutting alluvial fan deposits. The height of the footwall escarpment above the valley floor is impressive ranging from ~2.5 km at Willow Creek to ~3.0 km at McElvoy Canyon (Fig. 9). Gravity data indicate that maximum depth to basement in Saline Valley is 4.0-4.5 km and located approximately east of the mouth of McElvoy Canyon (Blakely and Ponce, 2001). These observations yield a minimum vertical offset of 7.0-7.5 km across this segment. Along the southern two-thirds of this segment, primarily west-facing, discontinuous fault scarps cut and offset latest Pleistocene alluvial fan surfaces. Where these scarps cut and offset debris flow levees, field observations indicate both a vertical and dextral component of slip. Differential GPS surveying of offset debris flow levee apices at McElvoy Canyon yields a weighted mean dextral offset of 3.1 ± 0.7 m and vertical offset of 2.4 ± 0.2 m, likely the result of

a single earthquake. Assuming a fault dip of 50-70° yields horizontal extension of 1.5 ± 0.7 m and an oblique slip offset of 3.4 ± 0.7 m at $353 \pm 12^\circ$ since the abandonment of this surface at 18.3 ± 4.4 ka (^{10}Be TCN model age).

The northern segment of the EIFZ extends from Willow Creek northeastward (Fig. 9) and is characterized by ~15 km-wide zone of ~N10-60E striking, dominantly SE-dipping, but also and between $4.9 +2.2/-1.8$ and $11.7 +5.7/-3.5$ km, respectively. Combining the dip-slip and horizontal extension measurements that accumulated since onset of extension at 15.6 ± 2.4 Ma yields a middle Miocene dip-slip rate of between 0.6 ± 0.1 and $0.9 +0.4/-0.2$ mm/yr and horizontal extension rate of between $0.3 +0.2/-0.1$ and $0.8 +0.4/-0.2$ mm/yr.

The second episode of normal slip at ~2.8 Ma also signaled the onset of dextral slip along the Hunter Mountain fault. This age of initiation for dextral slip along the Hunter Mountain fault is the same, within error, to that for the Owens Valley-White Mountains fault zone (Stockli et al., 2003), and consistent with Jones et al.'s (2004) hypothesis that dextral shear increased within the western part of the ECSZ during the Pliocene. The magnitude of dextral offset across the Hunter Mountain fault was measured at 9.3 ± 1.4 km (Burchfiel et al., 1987; Sternlof, 1988), which combined with age of onset of slip, yields a Pliocene dextral slip rate of 3.3 ± 1.0 mm/yr. This Pliocene slip rate is the same, within error, as Sternlof's (1988) calculated early Pleistocene dextral slip rate and Oswald and Wesnousky's (2002) estimated latest Pleistocene slip rate, suggesting that the dextral slip rate along the Hunter Mountain fault has remained constant through time. Summing dextral geologic slip rates, calculated parallel to the Pacific-North America plate motion (N47°W) (Dixon et al., 2000), along the Hunter Mountain fault, along the Owens Valley fault (Holocene rate of 1.0 ± 0.4 mm/yr; Bacon and Pezzopane, 2007), Death Valley fault (late Pleistocene rate of $4.2 +1.9/-1.1$ to $4.7 +0.9/-0.6$; Frankel et al., 2007), and Stateline fault (present day rate of ~1 mm/yr; Wernicke et al., 2004; Hill and Blewitt, 2006; Guest et al., 2007) yields a net geologic dextral slip rate across the ECSZ of $9.3 +2.2/-1.4$ to $9.8 +1.4/-1.0$ mm/yr at a latitude of ~36.5°, the same, within error, as calculated geodetic rates (Bennett et al., 2003).

THE POVERTY HILLS

The Poverty Hills (stop 3 in Fig. 1) are a mass of metamorphosed late Paleozoic sedimentary and Mesozoic granitic rock situated in the axial part of the alluviated Owens Valley (Fig. 1). Occupying 5 km², the hills stand as high as 300 m above the surrounding alluvial plain. The Paleozoic meta-sedimentary rocks comprising the western part of the hills consist mostly of Pennsylvania/Permian Keeler Canyon Formation and minor Permian Lone Pine Formation (Fig. 11). Granitic rocks occupying the eastern part are assigned to the Tinemaha Granodiorite (Fig. 11; Bateman, 1965), a rock unit also exposed to the west in the Sierra Nevada and to the southeast in the Inyo Mountains, where the unit forms the Santa Rita Flat pluton (Ross, 1962,1965, 1967,1969). The hills are adjacent to the active right-lateral Owens Valley fault that displays recent scarps both north and south of the hills (Fig. 11).

Origin of the Poverty Hills

Two models have been advocated for the origin of the Poverty Hills. One model proposes that the hills are a transpressional uplift at a left-step along the Owens Valley fault (Martel, 1984, 1989; Taylor and Dilek, 2001; Taylor, 2002). A second model proposes that the hills represent an ancient long-runout landslide mass derived from either the Sierra Nevada to the west (Pakisier et al., 1964) or the Inyo Mountains to the east (Bishop and Clements, 2006). The model advocated here is the landslide model.

A problem with the transpressional uplift model is that the Fish Springs fault at the north-west side of the Poverty Hills is a pure dip-slip fault. The fault cuts a Pleistocene tephracone (Fig. 11) and survey of the offset demonstrates no right-lateral displacement (Martel, 1989). Without right-lateral displacement on the Fish Springs fault, the transpressional model does not account for the presence of the western half of the Poverty Hills, where the highest elevations occur.

The main line of evidence for the landslide interpretation is the brecciated nature of the granitic and metasedimentary rock throughout much of the hills. Excellent exposures of the breccia are seen in roadcuts along Tinemaha Road, which will be visited during this field trip. Good breccias exposures are also present at the highest elevation of the hills on the west, in abandoned mine prospects scattered throughout the hills, and in outcrops at the southeast side of the hills. The brecciated zones, up to several tens of meters thick, display important characteristics of rock avalanche origin including preservation of stratigraphy and large clast-to-matrix ratio (Yarnold and Lombard, 1989). Along Tinemaha Road, an exposure of a brecciated stratigraphic layer in meta-sedimentary rock is contorted and distorted in a manner quite similar to that of a layer in the Blackhawk landslide, which is a classic Pleistocene rock avalanche deposit in the southern Mojave Desert (Fig. 12).

The most likely source area for the Poverty Hills landslide is the northern Santa Rita Flat pluton area southeast of the hills in the Inyo Mountains (Fig. 1). In this area, the granitic rocks of the pluton are in contact with Keeler Canyon Formation rocks, just as they are in the Poverty Hills. Assuming the northern end of the pluton is the source for the landslide, the Poverty Hills mass has likely been cut-off by the Owens Valley fault and displaced northward from an eastern part of the landslide. The eastern part is postulated to have been down-dropped by down-to-the-east displacement on the fault and consequently buried beneath recent alluvium. An important notion from this scenario is that the Owens Valley fault continues northward along the eastern side of the Poverty Hills and into the Owens River flood plain to the northeast, where it is buried under recent alluvium.

FISH LAKE VALLEY FAULT ZONE

The Death Valley-Fish Lake Valley fault (DV-FLVF) is a major fault system in the eastern California shear zone (ECSZ) which extends for ~300 km northward from its intersection with the Garlock fault (stops 3, 4, and 6 in Fig. 1). Along the northern part of the DV-FLVF prominent dextral offsets, steep normal faults scarps, ponded drainages, and shutter ridges developed in late Pleistocene and Holocene alluvium along the eastern White Mountains piedmont and are indicative of recent fault activity (Sawyer, 1990; Brogan et al., 1991; Reheis, 1992; Reheis et al., 1993; Reheis et al., 1995; Frankel et al., 2007a; 2007b; Ganey et al., 2010). Right-lateral motion on the DV-FLVF is thought to have begun ~10 Ma (Reheis and Sawyer, 1997), while the extensional component, responsible for the opening of Fish Lake Valley, most likely began ~5 Ma (Reheis and Sawyer, 1997; Petronis et al., 2002; 2009; Petronis, 2005). Changes in strike as well as strain transfer to the north along the fault system affect the components of strike-slip vs. normal displacement. For example, the northern part of Death Valley fault and the southern and central sections of the FLVF strike predominantly north-northwest, whereas the northern part of the fault is characterized by numerous north- and northeast-striking strands that splay out into Fish Lake Valley from the main, range-bounding fault (Fig. 1; Sawyer, 1990; Reheis and Sawyer, 1997; Frankel et al., 2007a; b).

Late Pleistocene to Holocene Displacements, Ages, and Slip Rates

Recently, an airborne lidar survey was conducted along the DV-FLVF zone which is allowing displacement of late Pleistocene and Holocene fault-related landforms to be precisely mapped (Figs. 13 to 18). This survey resulted in several studies that quantified the amount of right-lateral and extensional slip along the northern DV-FLV fault system (Frankel et al., 2007a, 2007b; Ganev et al., 2010). Offset alluvial fan deposits have been dated using ^{10}Be and ^{36}Cl cosmogenic nuclide geochronology at six sites covering the northern ~140 km of the fault system; this makes for one of the most extensive quantitative slip rate compilations on an ECSZ fault. From south to north, the following type of slip rates were obtained: 1) dextral slip rate at the Red Wall Canyon alluvial fan in northern Death Valley (Frankel et al., 2007a); 2) dextral slip rate at Cucomongo Canyon in Fish Lake Valley (Frankel et al., 2008a, in review); 3) dextral and extensional slip rates at Furnace Creek in Fish Lake Valley (stop 4 in Fig. 1; Figs. 13 and 14; Frankel et al., 2007b; Ganev et al., 2010); 4) extensional slip rate at Wildhorse Creek in Fish Lake Valley (Ganev et al., 2010); 5) extensional slip rate at Perry Aiken in Fish Lake Valley (stop 5 in Fig. 1; Fig. 15; Ganev et al. 2010); and 6) dextral and extensional slip rates at Indian Creek in Fish Lake Valley (stop 6 in Fig. 1; Figs. 16, 17, and 18; Frankel et al., 2007b, 2008a; Ganev et al., 2010).

Cosmogenic surface exposure ages of the offset landforms vary from mid-Holocene (7 ± 1.8 ka) at Indian Creek (Frankel et al., 2008, in review) to late Pleistocene (121 ± 14 ka) at Wildhorse Creek (Ganev et al., 2010), allowing geologic slip rates across different temporal and spatial scales to be determined. The combination of cosmogenic nuclide ages and measured right-lateral displacement or extensional offset at each of the sites mentioned above, provides slip rates that span the northern half of the DV-FLV fault zone. The right-lateral slip rates from south to north are as follows: Red Wall Canyon - $4.2 +1.9/-1.1$ mm/yr (~70 ka age); Cucomongo Canyon - ≤ 5 mm/yr (~40 ka age); Furnace Creek - $3.1 +0.4/-0.4$ mm/yr (~90 ka age; Fig. 14); and Indian Creek - $2.5 +0.4/-0.4$ and $2.1 +0.7/-0.6$ mm/yr (~70 ka and ~7 ka age, respectively; Figs. 17 and 18) (Frankel et al., 2007a, 2007b, 2008). In each case these rates should be considered minima because the channels used as piercing lines formed at some undetermined time following alluvial fan deposition.

Extension rates along the DV-FLV fault zone are calculated by combining vertical components of displacement, fan surface ages, and an assumed 60° fault dip. From south to north the extension rates are: Furnace Creek - $0.1 +0.1/-0.1$ (~90 ka age; Fig. 15); Wildhorse Creek - $0.3 +0.2/-0.2$ (~120 ka age); Perry Aiken Creek - $0.7 +0.3/-0.1$ (~70 ka age; Fig. 17); and Indian Creek - $0.5 +0.2/-0.1$ (~70 ka age; Fig. 18) (Ganev et al., 2010). Note that a steeper dip would result in slower rates of extension and shallower dip would produce faster rates.

Spatial Variations in Fault Slip Rates

As documented by Frankel et al. (2007b), the strike-slip rate decreases northward along the DV-FLVF, from ~4.2 mm/yr at Red Wall Canyon in northern Death Valley to ~2.5 mm/yr at Indian Creek in northern Fish Lake Valley. The decrease in right-lateral slip rate is simultaneously accompanied by an increase in the extension rates from ~0.1 mm/yr at Furnace Creek (Fig. 13) in south-central Fish Lake Valley to ~0.7 and ~0.5 mm/yr at Perry Aiken Creek (Fig. 15) and Indian Creek (Fig. 16) in northern Fish Lake Valley (Ganev et al., 2010). These rate data allow for a better understanding of the style and location of northward strain transfer from the northern ECSZ faults through the Silver Peak-Lone Mountain extensional complex and Mina

deflection into the Walker Lane belt.

The FLVF terminates just north of Indian Creek (Fig. 1), and slip from this fault, is transferred northeastward across the left-lateral Mina Deflection. onto oblique normal-right lateral faults of the Walker Lane belt. In general, both the northward increase in extension rates documented by Ganev et al. (2010) and the northward decrease in dextral slip rates illustrated by Frankel et al. (2007b) reflect transfer of slip off the FLVF and on to northeast-trending normal faults as part of a distributed zone of deformation transfer in the Silver Peak-Lone Mountain extensional complex (Fig. 1; e.g., Frankel et al., 2007b, 2008, in review; Ganev et al., 2010; Hoeft and Frankel, 2010, in review; Oldow et al., 1994; Petronis et al., 2002).

Temporal Variations in Strain Accumulation and Release

When combined with the geologic slip rates (right-lateral and extensional) on the ECSZ faults to the west of DV-FLVF system, the long-term deformation budget can be compared with the short-term geodetic rate of strain accumulation across the northern ECSZ. For example, summing the preferred right-lateral slip rates from the Owens Valley, Hunter Mountain, Stateline, and Death Valley-Fish Lake Valley fault zones yields a total long-term geologic slip rate of 8.5 to 10 mm/yr at the latitude of northern Death Valley, which is indistinguishable from geodetic measurements of $9.3 \pm 0.2/-0.2$ mm/yr (Fig. 1; Bennett et al., 2003; Frankel et al., 2007b; Lee et al., 2009a).

However, to the north, at the latitude of central Fish Lake Valley, summing the long term rates on the two major strike-slip structures at $\sim 37.5^\circ\text{N}$, the White Mountains and Fish Lake Valley faults, results in a long-term deformation budget that is only approximately one-third that of the short-term geodetic rate (Fig. 1; Bennett et al., 2003; Frankel et al., 2007b; Kirby et al., 2006). As such, this mismatch between the short-term and long-term rates of deformation at this latitude suggest a strain transient similar to that in the Mojave segment of the ECSZ (e.g., Oskin et al., 2008) or implies that strain is distributed across a broad region extending from the Sierra Nevada range-front faults and Long Valley caldera in the west to the Silver Peak-Lone Mountain extensional complex in the east (e.g., Frankel et al., 2007b). Note, however, that rates of right lateral shear have remained constant over late Pleistocene to Holocene timescales, at least along the northern part of the system at Indian Creek (Figs. 17 and 18).

In order to compare long-term rates of normal faulting from the FLVFZ with short-term geodetic rates of extension, Ganev et al. (2010) resolved the extension vectors to a direction of $\text{N}65^\circ\text{E}$ (perpendicular to the orientation of the Pacific-North America plate boundary; Bennett et al., 2003; Wesnousky, 2005). When combined with the extension rates reported for the other ECSZ faults to the west of the FLVF system (i.e., Round Valley fault, distributed faulting in the Volcanic Tableland, and White Mountains fault), the geologic extension rate sums to ~ 1.1 mm/yr (Fig.1; Berry, 1997; Sheehan, 2007; Kirby et al., 2006, Ganev et al., 2010). This long-term extension rate is not significantly different from the ~ 1 mm/yr determined by Wesnousky (2005) based on geodetic data from Bennett et al. (2003) for the northern ECSZ. Comparison of long term geologic extensional rate data with short-term geodetic data at $\sim 37.5^\circ\text{N}$ illustrates that the average rate of extensional strain storage and release over the late Pleistocene is, within error, the same as the short-term year rate of extension in the northern ECSZ.

Summary of Deformation on the Fish Lake Valley Fault Zone

The late Pleistocene dextral slip rate on the Death Valley–Fish Lake Valley fault zone

decreases from ~4.5 mm/yr in northern Death Valley to ~2.5 mm/yr at Indian Creek in northern Fish Lake Valley. Conversely, rates of extension increase from ~0.1 mm/yr at Furnace Creek in south-central Fish Lake Valley to ~0.7 mm/yr in northern Fish Lake Valley. Combining right lateral slip rates from the northern Death Valley–Fish Lake Valley and White Mountains fault zones, the two major faults at latitude ~37.5°N, indicates that the late Pleistocene rate of dextral shear is less than half that determined from geodetic data. This suggests either the existence of a strain transient in the northern eastern California shear zone or that deformation is distributed across other structures in the region; long-term and short-term rates of extension appear to coincide with each other. The spatial variation in right-lateral and extensional rates suggest that deformation is distributed through the Silver Peak-Lone Mountain extensional complex as strain is transferred northward across the Mina Deflection into the Walker Lane. The excellent agreement between the Holocene and late Pleistocene rates of strike-slip deformation at Indian Creek in northern Fish Lake Valley indicate that these rates have remained constant over the past ~70 ka.

QUEEN VALLEY: KINEMATICS OF FAULT SLIP TRANSFER

At the northern end of the White Mountains is Queen Valley, a ~16 km long, NE-trending basin (Fig. 19). Queen Valley (stops 7 and 8 in Fig. 1) is located in the southwestern part of the Mina deflection, which is a major right-step in the dextral shear dominated ECSZ-WLB. Geologic mapping, tectonic geomorphologic, and terrestrial cosmogenic nuclide (TCN) geochronologic data document the geometry, style, kinematics, and slip rates on late Quaternary faults within the Queen Valley, California-Nevada area (Lee et al., 2009b). These data provide important insight into the kinematics of fault slip transfer from the dextral White Mountains fault zone northward into the right-stepping Mina deflection.

Rock Units and Ages

The following summary on rock units and geochronology in Queen Valley are based on the work of Lee et al. (2009b). Mesozoic granitic and metasedimentary rocks, and Tertiary basalt lava and rhyolite tuff underlie the ranges surrounding Queen Valley, and alluvial fan deposits underlie the Queen Valley basin. Exposed at the western end of Queen Valley is unit Tb, a Pliocene(?) plagioclase ± olivine ± pyroxene phryic basalt lavas (Fig. 19). Locally overlying unit Tb is unit Trt, a quartz + feldspar, lithic-bearing rhyolite tuff. In turn, this unit is overlain by unit Tts, a tan weathering, weakly bedded, lithic-bearing quartz + feldspar tuffaceous sandstone. The Queen Valley basin proper is underlain by four major late Pleistocene to Holocene alluvial fan surfaces. These surfaces have been subdivided into two groups, Qf surfaces which cover the southwestern two-thirds of the valley and Qqf surfaces that cover the northeastern third of the valley (Figs. 19 and 20). Alluvial fan surfaces in each group are further subdivided (from oldest, Qf1 or Qqf1, to youngest, Qf4 or Qqf4) based on tone and fan surface morphology, including terrace height, presence or absence of bar and swale morphology, degree of fan dissection, and inset geometry (Figs. 19 and 20). Poorly exposed playa deposits, Qp, are exposed at the western end of Queen Valley (Figs. 19 and 20b).

Quartz-rich granite samples were collected from the top of in situ boulders for ¹⁰Be terrestrial cosmogenic nuclide (TCN) surface exposure age determination of four of the alluvial fan surfaces. Boulder samples collected from the Morris Creek Qf2 surface yielded a mean age of 77.1 ± 0.8 ka (±standard error, se) (Fig. 19). Boulder samples collected from a Qf3c surface in the

hanging wall of the Orchard Spring normal fault scarp yielded a mean age of 16.9 ± 0.2 ka (\pm se) (Fig. 19). At the mouth of Queen Canyon, a single boulder on Qqf1, the oldest surface in the field area, yielded an exposure age of 98 ± 6 ka (\pm 2s). Boulder samples from the next youngest alluvial fan surface, Qqf2, from the Queen Canyon catchment yielded a mean age of 53.6 ± 1.2 ka (\pm se) (Fig. 19).

Apatite samples from the footwall of the QVF yield (U-Th)/He ages that decrease with decreasing elevation and exhibit an inflection point at ~ 2200 m (Stockli et al., 2000). Below the inflection point samples yield an elevation invariant mean age of 3.0 ± 0.5 Ma which dates the onset of exhumation and formation of the Queen Valley pull-apart structure (Stockli et al., 2000). Because the Queen Valley pull-apart structure forms the northern termination of the dextral White Mountains-Owens Valley fault system, the opening of the basin at ~ 3 Ma reflects the onset of right-lateral strike-slip faulting.

Faults, Magnitude of Offset, Slip Rates, and Kinematics of Fault Slip Transfer

The following summary on faulting and fault kinematics is based on the work of Lee et al. (2009b). Four active fault types and fault orientations cut undifferentiated pre-Tertiary bedrock, Tertiary basalt lava, rhyolite tuff, and tuffaceous sandstone, and the late Pleistocene alluvial fan surfaces across Queen Valley: (1) A series of NE-striking, NW- and SE-dipping normal faults and fault scarps, the Queen Valley fault, cut and offset bedrock and Qf1, Qf2, Qf3, Qqf1, Qqf2, and Qqf3 surfaces along the SE-side of the valley (Figs. 19 and 20); (2) A set of discontinuous NE-striking, sinistral faults cut Qf2 surfaces on the N-side of the valley (Fig. 19); (3) A NW-striking dextral fault, the Coyote Springs fault, cuts and offsets Tertiary basalt lava, and Qf1, Qf2, and Qf3 surfaces, along the SW-side of the valley (Figs. 19 and 20b); and this fault merges with (4) en echelon WNW- to EW-striking N-dipping and south(?) -dipping thrust faults which cut Tertiary basalt lava and Qf1 and Qf2 surfaces (Figs. 19 and 20b).

A transect, perpendicular to the strike of fault scarps cutting Qqf2 surfaces at the mouth of Queen Canyon, yields a minimum 9.4 ± 4.4 m of horizontal extension (assuming a fault dip of $60 \pm 10^\circ$) towards 282° (Fig. 19). Combining this calculated horizontal extension measurement with the ^{10}Be model Qqf2 surface age of 53.6 ± 10.7 ka yields a minimum horizontal extension rate of 0.2 ± 0.1 mm/yr. At Orchard Spring, Qf3c has been deposited across the Queen Valley fault, which offsets a Qf2 surface a minimum of 6.1 ± 0.3 m (Fig. 19). Combining this offset measurement with ^{10}Be model surface ages of 77.1 ± 15.4 ka for Qf2 in the footwall and 16.9 ± 3.4 ka for Qf3c in the hanging wall yields an estimated vertical slip rate bracketed between ~ 0.1 - 0.4 mm/yr and horizontal extension rate bracketed between ~ 0.1 - 0.3 mm/yr (assuming a fault dip of $60 \pm 10^\circ$) towards 300° . These late Pleistocene horizontal extension rates are the same, within error, to somewhat slower than the minimum 0.3 ± 0.1 mm/yr Pliocene horizontal extension rate across the Queen Valley fault based on apatite (U-Th)/He age of 3.0 ± 0.5 Ma for onset of normal slip (Stockli et al., 2003) and minimum vertical offset of 1370 m across the fault. Measurable offset markers are not present across the NW-striking dextral and EW-striking thrust faults.

Documented fault geometries and slip orientations across Queen Valley suggest that fault slip transfer models, the extensional displacement transfer (Oldow et al., 1994), block rotation (McKenzie and Jackson, 1983, 1986), and simple shear couple models (Wilcox et al., 1973), within a dextral fault system are not applicable to this part of the Mina deflection. Rather, dextral fault slip is transferred by both a restraining westward step into a flower structure and a releasing eastward step into a normal fault and hangingwall basin. Our results, combined with published slip rates for the dextral White Mountain fault zone (Kirby et al., 2006) and the eastern sinistral

Coaldale fault (Bradley, 2005), suggest that transfer of dextral slip into the Mina deflection is partitioned into three different components: horizontal extension along the Queen Valley fault, thrust faulting that merges into the dominantly dextral slip along the Coyote Springs fault, and dominantly sinistral slip along the Coaldale fault. A velocity vector diagram of fault slip partitioning across Queen Valley predicts a small component of Pliocene to present day contraction across the Coyote Springs and western Coaldale faults. Contraction across the Mina deflection is consistent with GPS data (Bennett et al., 1999).

VOLCANIC TABLELAND

The Volcanic Tableland (stops 9 and 10 in Fig. 1), located north of Bishop in northern Owens Valley, is a plateau formed from ash-flow deposits of the 758.9 ± 1.8 ka (Sarna-Wojcicki et al., 2000) Bishop eruption of what is now Long Valley caldera (Fig. 21) The overall form of the Tableland is that of a broad, southward-sloping, anticlinally warped sheet that extends southward from Long Valley caldera to the town of Bishop, where it becomes buried by younger sediment (Bateman, 1965). The brittle character of the Bishop Tuff, particularly its upper erosion-resistant capping unit, provides an ideal surface for preserving deformation, as it is inferred to have undergone little erosion since its emplacement (e.g., Bateman, 1965; Dawers et al., 1993). Cosmogenic nuclide data indicate that erosion over some of the Volcanic Tableland scarps amounts to only one to two meters (Goethals et al., 2009).

Tableland Normal Faults

Distributed across the Tableland are numerous, N-S striking normal fault scarps that collectively record ~1-2% E-W extensional strain that post-dates the Bishop eruption (Fig. 21; Pinter, 1995; Sheehan, 2007). Though some large en echelon arrays may kinematically accommodate a regional strike-slip component (Bateman, 1965), individual fault segments are clearly normal faults (Bateman, 1965; Dawers et al., 1993; Pinter, 1995; Ferrill et al., 1999; Ferrill and Morris, 2001). Hundreds of faults mapped here by Bateman (1965) and later by Pinter (1995) span a length range from decimeters up to the > 12 km long Fish Slough fault (Fig. 21). Because of this size range and preservation of along-strike displacement variations, the Volcanic Tableland has become a classic field area for studies of fault displacement-length scaling (Dawers et al., 1993), fault segment interaction (Willemse et al., 1996), fault linkage (Dawers and Anders, 1995; Ferrill et al., 1999), relay ramp geometry and kinematics (Ferrill and Morris, 2001), and distribution of strain on small faults (Sheehan, 2007). The Volcanic Tableland fieldtrip stops in this guidebook are sites that well illustrate these processes.

SIERRA NEVADA FRONTAL FAULT ZONE

The Sierra Nevada is one of the most prominent geomorphic features within this region with a mean elevation of 2800 m above sea level. It is bounded along its east flank by a normal fault system (stop 12 in Fig. 1), the Sierra Nevada frontal fault zone (SNFFZ), and a few kilometers farther east by a dextral fault zone, the Owens Valley fault. The SNFFZ and Owens Valley fault define the western boundary of both the ECSZ and Basin and Range Province, a region where NW dextral shear has been superimposed on E-W extension (Fig. 1).

The SNFFZ was long considered to have formed by regional Basin and Range extension (e.g. Bateman and Wahrhaftig, 1966). More recently, data from GPS, topographic, geoid, and

Quaternary fault slip studies were used to hypothesize that NW-dextral shear and EW-extension within the ECSZ resulted from translation of the Sierra Nevada both parallel and perpendicular to the Pacific-North American plate boundary in consequence of plate tractions and gravitational potential energy, respectively (e.g. Flesch et al., 2000; Bennett et al., 2003; Hammond and Thatcher, 2004). Data from petrological, geochemical, and geophysical studies investigating Sierra Nevada lithospheric structure and young deformation along the western boundary of the Basin and Range Province led Jones et al. (2004 and references therein) to suggest that removal of lithosphere beneath the Sierra Nevada at ~3.5 Ma initiated uplift and increased extensional strain rates. They also postulated that a combination of locally derived internal forces (gravitational potential energy) and plate boundary forces drive fault kinematics along the western boundary of the ECSZ and Basin and Range Province. In contrast to these hypotheses, the orientation of normal and strike-slip faults along the eastern margin of the Sierra Nevada relative to the small circles to the Sierra-Nevada-North America Euler pole, coupled with kinematic inversions of earthquake focal mechanisms, led Unruh et al. (2003) to hypothesize that most of the normal faulting along the eastern flank of the Sierra Nevada is related to plate boundary driven NW-translation of this rigid block rather than to Sierra Nevada uplift or Basin and Range extension.

For these hypotheses, motion of the Sierra Nevada block should be accommodated within the upper crust along its eastern flank by either oblique fault slip or spatially partitioned slip into normal and dextral components within a single stress regime, or by temporally partitioned slip into normal and dextral components within an alternating normal and strike-slip stress regimes. Detailed geologic mapping, tectonic geomorphologic and terrestrial cosmogenic radionuclide (TCN) geochronologic results along the southern part of the SNFFZ (stop 12 in Fig. 1; Fig. 22) bear on how Sierra Nevada motion is accommodated by fault slip (Le et al., 2007).

Rock Units and Ages

The following summary on rock units and ages is based on the work of Le et al. (2007). The southern escarpment of the SNFFZ, between Oak and Lubkin creeks, offsets granite- and metamorphic-derived Quaternary coarse- to fine-grain alluvial fan, glacial, and rockslide deposits (Figs. 22 and 23). Seven Quaternary alluvial fan surfaces of distinct ages were mapped on the basis of surface morphology, terrace height, and inset geometry. Quartz-rich granite boulder samples were collected for model TCN ^{10}Be exposure age dating of these surfaces; ^{10}Be model ages reported are recalculated assuming an erosion rate of 0.3 cm/k.y.

At the apex of drainage basins along the eastern range front of the Sierra Nevada remnants of the oldest alluvial surfaces, Qf1, typically appear as 30-100 m high mounds. Qf1 surfaces are partly varnished, highly dissected, and strongly weathered with scarce boulder deposits. Model ^{10}Be ages for boulder samples collected from an offset Qf1 surface located just south of Bairs Creek yielded a mean surface exposure age of 123.7 ± 16.6 ka (Fig. 22).

Based on the degree of surface dissection and inset geometry, Qf2 surfaces, comprising the next youngest surface, have been subdivided into two surfaces. The older Qf2a surfaces are characterized by a ridge and ravine topographic pattern and by their lack of boulders (Fig. 23). Younger Qf2b alluvial surfaces lack a well-developed ridge and ravine topographic pattern, are moderately dissected, hummocky, less weathered, and possess granitic boulders that make up to 2% of the alluvial surface (Fig. 23). The mean ^{10}Be model age calculated for a Qf2b surface is 60.9 ± 6.6 ka (Fig. 23).

The areally dominant alluvial fan deposits along the range front are Qf3 deposits (Figs.

22 and 23). Based on the plumose texture caused by the topographic patterns of bars and swales, along with inset geometry, Qf3 surfaces have been subdivided into three units: Qf3a, Qf3b, and Qf3c. The oldest surfaces, Qf3a, are typically planar, densely vegetated, exhibit weakly developed desert varnish, and large boulders are infrequent. Boulder samples collected from a Qf3a alluvial surface yielded a mean ^{10}Be model age of 25.8 ± 7.5 ka (Fig. 23). The next youngest fan surface, Qf3b, extends up to 11 km from the range front, farther than any other alluvial fan surface (Figs. 22 and 23). Qf3b surfaces consist of moderately muted bar and swale morphology and are best distinguished by the incision of dendritic channel networks, which range from 1.0 to 2.5 m deep, and presence of granitic boulders. Qf3b surfaces are typically covered with boulders averaging 1 to 3 m high, comprising $\sim 5\%$ of the surface and locally up to 50% on linear levees. The youngest Qf3 surface, Qf3c, exhibits well preserved bar and swale morphology (Fig. 23). Fan surfaces are undissected, unvarnished, hummocky, and contain many boulder-lined channels. Boulder clasts range in size from ~ 1 m to ~ 9 m high, and comprise up to $\sim 20\%$ of the alluvial surface. Samples collected from a Qf3c fan surface yielded a mean ^{10}Be surface exposure age of 4.4 ± 1.1 ka (Fig. 23).

The youngest surface, Qf4 deposits, cuts all other surfaces, and consists of active channels inset into recently abandoned channels (Figs. 22 and 23). These surfaces contain recent debris-flow deposits, which include tree trunk clasts, unvarnished boulder levee bars, and are densely vegetated. Boulder samples collected from a Qf4 debris flow yielded a mean ^{10}Be model age of 4.1 ± 1.0 ka (Fig. 23).

Exposed along the range front northwest of Independence Creek and north of Onion Valley is a large ~ 1 km² rock slide deposit, Qrs; the ^{10}Be model age for the rockslide is 18.78 ± 3.9 ka. Moraine deposits, Qm, are exposed as narrow elongated lobes on the flanks of Onion Creek.

Fault Geometry, Magnitude of Offset, and Slip Rates

The following summary on fault geometry, magnitude of offset, and slip rates is based on the work of Le et al. (2007). The SNFFZ is composed of multiple fault scarps along the eastern piedmont of the Sierra Nevada, centered on a ~ 35 km long and up to ~ 5 km wide section between Oak and Lubkin creeks (Fig. 22). This part of the SNFFZ is characterized by NNW-striking, dominantly E-dipping with lesser W-dipping normal fault scarps that typically juxtapose Quaternary sediment in the hanging wall upon either Quaternary sediment or granite bedrock in the footwall. The fault scarps cut and offset Qf1, Qf2, and Qf3 surfaces, and the rockslide and glacial moraine deposits, but not Qf4 surfaces. Based on fault zone width, geometry, and strike, this part of the SNFFZ can be subdivided into four distinct, right-stepping segments A-D (Fig. 22). Faults that define each segment have an average strike of $\sim 334^\circ$, whereas faults that define the step-over between segments have an average strike of $\sim 10^\circ$. Debris flow levees offset across the SNFFZ exhibit only dip-slip motion. This observation, combined with no evidence for laterally offset alluvial fan surfaces, indicates that the SNFFZ records only dip-slip.

Topographic profiles measured perpendicular to east-facing fault scarps which cut and offset distinct alluvial fan surfaces define the amount of Quaternary vertical displacement. Measurements across fault scarps yield vertical surface offsets that range from 41.0 ± 2.0 m to 2.0 ± 0.1 m. Older alluvial surfaces record larger vertical offsets and progressively younger surfaces record progressively smaller vertical offsets. Topographic profiles P4, P5, and P6 (Fig. 23) were measured across offset alluvial surfaces for which model ^{10}Be TCN ages were determined.

Combining data from ^{10}Be TCN surface exposure model ages of offset alluvial fan

surfaces with vertical offset measurements across fault scarps yields vertical slip rate estimates of $0.2\text{-}0.3 \pm 0.1$ mm/yr since ~ 124 ka, $0.2\text{-}0.4 \pm 0.1$ mm/yr since ~ 61 ka, $0.3\text{-}0.4 \pm 0.2$ since ~ 26 ka, and 1.6 ± 0.4 since ~ 4 ka. Linear regressions through age vs. vertical offset plots yield average late Pleistocene to Holocene vertical slip rates of $0.2\text{-}0.3$ mm/yr. Assuming a fault dip of 60° yields calculated horizontal extension rates for the late Pleistocene to Holocene that range from $0.1\text{-}0.2 \pm 0.1$ mm/yr to 0.9 ± 0.4 mm/yr. Calculated late Holocene vertical and horizontal slip rates of 1.6 ± 0.4 mm/yr and 0.9 ± 0.4 mm/yr, respectively, are two to 20 times faster than late Pleistocene and calculated average estimates. This indicates either that horizontal extension rates have increased over the last 4,000 years, that these calculated slip rates are maxima because these faults are early in the earthquake cycle, or that the ~ 7 m offset is the result of two or more earthquakes clustering in time.

Tectonic Implications

The following discussion is based on the work of Le et al. (2007). The closely spaced SNFFZ, Lone Pine fault, and Owens Valley fault accommodate both extension and dextral shear along the western boundary of the Basin and Range Province–ECSZ. The mix of normal faulting and strike-slip faulting here has been interpreted as either spatially and/or temporally varying regional stresses (Zoback, 1989; Bellier and Zoback, 1995) or fault slip partitioning within a single regional stress field (Wesnousky and Jones, 1994).

Based on fault slip azimuth data, Zoback (1989) and Bellier and Zoback (1995) postulated that the stress regime along this section of the Sierra Nevada underwent a recent (less than 100,000 years, but greater than 10,000 years) permanent change from normal-slip dominated to strike-slip dominated stress regimes. Although plausible, the pre-1872 rupture along the Owens Valley fault, between 3.3 ± 0.3 and 3.8 ± 0.3 ka (Lee et al., 2001b) or between $10,200 \pm 200$ and 8800 ± 200 cal yr B.P. (Bacon et al., 2007), and the last earthquake along the SNFFZ, $\leq 4.1 \pm 1.1$ ka, occurred $\sim 2000\text{-}6000$ years apart, implying a rapid change in stress regime if this hypothesis is valid.

In the second hypothesis, this region is characterized by a single stress field and motion of the southern Sierra Nevada is partitioned (Wesnousky and Jones, 1994) onto the Owens Valley fault, Lone Pine fault, and SNFFZ. These subparallel faults strike clockwise with respect to the $\sim 313^\circ$ -trending vector that defines motion of the Sierra Nevada microplate relative to stable North America (Dixon et al., 2000). Thus motion of the Sierra Nevada block is partitioned into three different slip vectors—dominant dextral slip along the Owens Valley fault, intermediate oblique slip on the Lone Pine fault, and subordinate normal slip along the SNFFZ (cf Beanland and Clark, 1994; Le et al., 2007; Bacon et al., 2007). The distribution of fault slip along the eastern escarpment of the Sierra Nevada shows that dextral slip dominates, consistent with measured GPS velocities across the western margin of the Basin and Range Province (e.g. Thatcher et al. 1999; Wernicke et al., 2000).

FIELD GUIDE

This guide provides directions to field trip stops relative to nearby towns, landmarks, and major roads. It does not provide distances between individual stops. All field trip stop locations are keyed to the map in Figure 1. In addition, Universal Transverse Mercator (UTM) coordinates of all stops are provided in NAD83 datum, zone 11. It is preferable to have a high-clearance vehicle (and possibly 4WD, depending on road conditions) for many of the stops.

Day 1: Coso Range, Inyo Mountains, and Owens Valley

Stop 1: Northern Coso Range Piedmont

Directions. This stop is located at UTM 413630E, 4019852N. From Olancho, head east on CA-190, ~3.5 miles from the intersection with US-395 (~1 mile west of the well-marked road to Dirty Sock Corporation Yard) and park on the side of the road along the broad shoulder.

Description. This is Stop 7 of Frankel et al. (2008). The thing to look at, stand on, and walk around here is evidence for surface rupture during the 1872 Owens Valley earthquake. With a little searching, you will find a series of right laterally displaced Holocene beach ridges on the north side of the highway that were discovered by Burt Slemmons and his colleagues ~30 years ago and that are on trend with the Owens Valley fault to the north where it heads into the playa from Bartlett Point (Fig. 5). Slemmons et al. (2008) argue that the offset beach ridges indicate that surface rupture during the 1872 earthquake extended all the way to the Coso Range piedmont, rather than dying out at Bartlett Point as suggested by Beanland and Clark (1994). Once you find the offset beach ridges, look to the southeast to view tectonic-geomorphic evidence for dextral shear extending from the southern end of the Owens Valley fault into the northwest Coso Range. There is a large push-up ridge ~3 km south of the road where the fault zone that offsets the beach ridges terminates or makes a left step. About 3–4 km south of the road is a high, N-facing wave-cut scarp at ~1160 m (3800 ft) elevation along the northern Coso Range piedmont. This scarp was last inundated ca. 24 ka during a Tioga-age pluvial highstand of Owens Lake. The wave-cut scarp is visibly warped into a series of low-amplitude folds associated with a fault zone that transfers slip from Owens Valley southward through the Coso Range to the Airport Lake fault zone in Indian Wells Valley. These structures comprise the eastern tectonic margin of the Sierra Nevada microplate at this latitude.

Stop 2: Inyo Mountains Exhumation from Manzanar National Historic Site

Directions: This stop is located at UTM 40653487 E 397580 N. This stop is at the Manzanar National Historic Site on US-395. From Lone Pine, drive north on US-395. After ~11 miles, turn left (west) into the Manzanar National Historic Site.

Description: Across Owens Valley to the east is the western flank of the Inyo Mountains (Fig. 24). Late Cenozoic faults are not exposed along the western flank of the Inyo Mountains except for the oblique slip southern Inyo Mountains fault along the SW Inyo Mountains (Bacon et al., 2005; Casteel, 2005). Nevertheless, a steep, linear gravity gradient along the western front of the Inyo Mountains has been interpreted as a continuous bedrock fault scarp buried beneath thick alluvial fan deposits (Pakiser et al., 1964). (U-Th)/He samples were collected along the Pat Keyes

trail, which extends up the western flank of the Inyo Mountains from ridge north of Reward Mine (Figs. 10 and 24) and down the ridge on the north side of Pat Keyes Canyon on the east side (Fig. 10). Zircon (U-Th)/He samples yield: 1) an elevation invariant (U-Th)/He age of 65.8 ± 7.1 Ma from the west-side of the range and about half-way down the east-side, 2) a decrease in age from ~ 66 Ma to ~ 54 Ma down the middle part of the eastern flank, and 3) an elevation invariant age of 55.0 ± 9.8 Ma at the base of the eastern flank (Fig. 10). Apatite (U-Th)/He samples yield: 1) an elevation invariant age of 53.2 ± 6.6 Ma up the west-side of the range, 2) a decrease in age from ~ 53 Ma to ~ 16 Ma from the top of the range part way down the east flank, 3) an elevation invariant (U-Th)/He age of 15.6 ± 2.4 Ma, that then decrease from ~ 15 Ma to ~ 3 Ma from the middle part of the eastern flank, and 4) an elevation invariant age of 2.8 ± 0.7 Ma at the range front (Fig. 10). The zircon and apatite age patterns are interpreted as indicating: (a) two episodes of moderate to rapid exhumation associated with Laramide deformation during the late Cretaceous/early Tertiary; (b) development of a slowly eroding surface during a prolonged period from early Eocene to middle Miocene (c) rapid cooling, exhumation, and initiation of normal slip along the EIFZ, accommodated by westward tilting of the Inyo Mountains block, at 15.6 Ma; and (d) rapid cooling, exhumation, and renewed normal slip along the EIFZ at 2.8 Ma.

Stop 3: Poverty Hills

Directions: This stop is located at UTM 389062 E 4102142 N. From the intersection of Crocker Road and CA-395 in the town of Big Pine, drive south 4.8 miles on CA-395 and turn right (west) on to Fish Springs Road. After driving 2.1 miles on Fish Springs Road, bear right onto Griffith Road. Go 0.5 miles on Griffith Road and turn right onto Tinemaha Road. Drive 1.3 miles on Tinemaha Road and park in the turnout on the right. Walk northward along Tinemaha Road to view breccia exposures in roadcuts. BE CAREFUL TO WATCH FOR TRAFFIC.

Description: From the parking area along Tinemaha Road, walk north along the road to view excellent exposures of breccia in roadcuts (Fig. 12a). There are several characteristics of importance to note, but first be careful to distinguish between bedrock breccia and similar appearing recent colluvial breccia in the roadcuts. Regarding the bedrock breccia, particularly note the large clast to matrix ratio. In some outcrop areas, there is essentially no matrix material. Also note the preserved source rock stratigraphy within the brecciated masses. Although preserved, stratigraphic layers are strongly deformed by cataclastic flow and zones of concentrated shear. At the far end of the roadcuts a few hundred meters north of the parking area is a zone of breccia consisting of scattered clasts supported within a light-colored, fine grained matrix. This material may be the strongly comminuted basal zone of the rock avalanche, although the underlying substrate is not exposed to confirm this interpretation. None of the breccia is typical of debris flows, which involves turbulent mixing during emplacement. Advocates of the transpressional uplift model for the origin of the hills suggest that the brecciated zone is the result of faulting along a fault buried not far below the road grade, rather than a mass wasting event.

Day 2: Fish Lake Valley and Queen Valley

Stop 4: Fish Lake Valley Fault at Furnace Creek

Directions. This stop is located at UTM 410935E, 4158364N. From Big Pine, take CA-168 east over Westgaard Pass. Continue on CA-168 through Deep Springs Valley to Fish Lake

Valley. At the intersection of CA-168 and CA-266 in Oasis, turn north on CA-266 and go ~7.1 mi to a dirt track leading off to the west (just north of White Wolf Canyon Road to the east). Go ~1.5 mi toward the large shutter-ridge. Continue on the dirt track, bearing to the northwest and paralleling the fault, for another 0.3 mi and park near the incised channel (Fig. 14a). Walk ~0.1 mi west up the westernmost fault scarp to the apex of the fan.

Description. This is, in part, Stop 11 of Frankel et al. (2008). Just south of the canyon mouth at Furnace Creek, the Fish Lake Valley fault is exposed as two parallel NW-striking strands displacing a late Pleistocene alluvial fan complex (Figs. 13 and 25; Frankel et al., 2007b; Reheis et al., 1995; Reheis and Sawyer, 1997). Prominent scarps are exposed in the alluvial fans with the western strand dipping to the NE and the eastern strand dipping to the SW, and with other small normal fault scarps scattered across the fan surfaces (Reheis et al., 1995). The area between the two fault strands is down-dropped in a small pull-apart basin (parking area is at the northern end of this pull-apart structure). Just south of the offset late Pleistocene fan is a large NW-SE-striking shutter-ridge, which is bounded on its northeast and southwest sides by the two fault strands (Reheis et al., 1995).

Although a number of alluvial fan surfaces are mapped in this location (Reheis et al., 1995), the primary surface of interest is the late Pleistocene Q_{fi} deposit (Q_{fi} of Reheis et al., 1995), which is displaced by the fault (Figs. 13 and 14). Cosmogenic nuclide ¹⁰Be dates from the Q_{fi} surface yield an age of 94 ± 11 ka (Frankel et al., 2007b). A recent reexamination of offset channels at this location using lidar data revised the late Pleistocene offset to 290 ± 20 m (Fig. 14; Frankel et al., 2007b). Combining the 290 ± 20 m of displacement determined from lidar topography with the cosmogenic ¹⁰Be age of 94 ± 11 ka for the Q_{fi} surface yields a minimum late Pleistocene, right-lateral slip rate of 3.1 ± 0.4 mm/yr for the Fish Lake Valley fault zone at Furnace Creek (Frankel et al., 2007b). The rate of extension at this site is 0.1 ± 0.1 mm/yr (Fig. 13; Ganey et al., 2010).

Stop 5: Fish Lake Valley Fault at Perry Aiken Creek

Directions: This stop is located at UTM 403197E, 4169042N. From Dyer, NV travel north on NV-264 for ~1.2 m, make a left (west) turn on an unnamed dirt road at approximately UTM 40449E, 4170675N, and continue west for ~1.3 m until you reach the prominent ~74 m high scarp of the Fish Lake Valley fault (Fig. 26). Park at the base of the scarp and climb to the top of it for a good view of the fault (note: this is a steep climb).

Description: The fault zone at Perry Aiken Creek exhibits a complex pattern of sub-parallel, anastomosing fault strands (Fig. 15). This section of the fault includes one of the tallest single fault scarps in Fish Lake Valley, located just north of the mouth of Perry Aiken Creek. The 73.5-m-tall fault scarp provides clear evidence for significant normal displacement. Ganey et al. (2010) measured the total vertical displacement at this site to 85.1 ± 4.3 m from lidar data, which is in agreement with previous estimates by Reheis and Sawyer (1997). The cumulative mean horizontal extensional component of displacement at Perry Aiken Creek is 49.1 ± 2.5 m toward N68°E (assuming a 60° fault dip; Ganey et al. 2010). Cosmogenic nuclide ¹⁰Be ages from boulders on the Q_{fi} surface yield an age of 71 ± 8 ka (Ganey et al., 2010). Combining the cosmogenic nuclide ages with the measured extension yields a late Pleistocene extension rate of $0.7 +0.3/-0.1$ mm/yr toward N68°E (Ganey et al., 2010).

Stop 6: Fish Lake Valley Fault at Indian Creek

Directions. This stop is located at UTM 396137E, 4182771N. From Dyer, Nevada, head ~8.5 mi north on NV-264 (~16.8 mi north of the California-Nevada border). Turn west (left) on Indian Creek Road (well-graded dirt) and continue for ~5 mi until you reach the prominent east-facing scarp near the canyon mouth at UTM 395992E, 4183225N. Park just west of the scarp on the south side of the road (Fig. 27). Walk ~0.3 mi south along the base of the scarp to the third deeply incised channel cutting the footwall. Climb up to the top of the scarp at this location for a good view of the fault zone.

Description: This is, in part, Stop 12 of Frankel et al. (2008). The fault scarps at Indian Creek are located at the northern end of the Fish Lake Valley fault system. The fault zone splays into numerous normal faults in this location (Reheis et al., 1993), but a significant strike-slip component is still present (Figs. 16 and 17; Frankel et al., 2007; Reheis et al., 1993; Reheis and Sawyer, 1997). Most of the faulting at this site displaces the late Pleistocene Qf₁ surface. The dextral component of slip at this location is restricted to a single strand cutting the late Pleistocene Qf₁ and Holocene Qf₁ surfaces near the eastern White Mountains range-front (Figs. 17 and 18; Frankel et al., 2007b; Reheis et al. 1993; Reheis and Sawyer, 1997). Frankel et al. (2007) used lidar data to revise the late Pleistocene dextral displacement history to 178 ± 20 m on the basis of six offset channels; the Holocene Qf₁ surface is displaced right-laterally by 15 ± 2 m (Frankel et al., 2008, in review).

The normal component of slip is restricted to a set of normal fault scarps east of the main dextral fault strand, two scarps west of dextral strand, and some vertical displacement on the main dextral fault strand (Fig. 16). The cumulative vertical displacement across all fault strands from the recent lidar survey at this site adds up to 75.4 ± 3.8 m, which yields a cumulative mean horizontal extensional displacement at Indian Creek of 43.7 ± 2.1 m toward S88°E when assuming a 60° fault dip (Ganev et al., 2010).

Eight tightly clustered cosmogenic nuclide ¹⁰Be surface exposure dates from boulders on the Qf₁ fan surface have a mean age and standard deviation of 71 ± 8 ka (Frankel et al., 2007b). Combining the cosmogenic surface exposure ages with measured offset yields a late Pleistocene strike-slip rate of 2.5 ± 0.4 mm/yr, a Holocene strike-slip rate of $2.1 +0.7/-0.6$ mm/yr, and an extensional rate of $0.6 +0.2/-0.1$ mm/yr toward N68°E (Frankel et al., 2007b, 2008a; Ganev et al., 2010).

Stop 7: Queen Valley Normal Fault

Directions: This stop is located at UTM 379376 E 4197445 N. This stop is at the mouth of Queen Canyon, about 12 miles northeast of Benton. From the intersection of US-6 and CA-120 in Benton, drive north on US-6. After ~9.5 miles, turn left (southeast) onto the dirt road. Drive southeast ~2 miles and park along the side of the road inside a small graben. Walk north onto the footwall of the southeast dipping fault scarp.

Description: At the mouth of Queen Canyon, six alluvial fan surfaces and several west- and east-facing normal fault scarps are exposed (Figs. 19, 20, and 29). The oldest surface, an erosional remnant Qcf₁, is preserved along a ridge extending along the south side of Queen Canyon. The extensive surface at the mouth of the canyon is a Qcf₂ surface. Inset into this surface is Qcf_{3a}, which in turn is inset by Qcf_{3b}, c, and d. Cosmogenic radionuclide dating of

quartz collected from surface boulders on Qcf2 yielded ^{10}Be TCN model ages of 52.2 ± 1.6 ka and ~ 70 ka for an interpreted remnant older debris flow. The alluvial fan surfaces are cut by a zone of NE-striking, west- and east-dipping normal fault scarps and small grabens, with no evidence for a lateral component of slip (Figs. 19, 20, and 29). Topographic profiling across fault scarps cutting Qcf2 surfaces at the mouth of Queen Canyon yields a minimum 9.4 ± 4.4 m of horizontal extension (assuming a fault dip of $60 \pm 10^\circ$) towards 282° . Combining this calculated horizontal extension measurement with the ^{10}Be model Qcf2 surface age of 53.6 ± 10.7 ka yields a minimum horizontal extension rate of 0.2 ± 0.1 mm/yr.

Stop 8: Queen Valley Thrust Fault

Directions: This stop is located at UTM 4192349 E 370028 N. This stop is along US-6 about 4 miles north of Benton. From the intersection of US-6 and CA-120, drive north on Highway 6. After ~ 3.3 miles, turn left (northwest) onto the dirt road. Drive northwest ~ 0.4 miles and park at the base of the hill on the east side of the road. Walk to the northeast to the top of the hill.

Description: At the southwestern end of Queen Valley, three faults, with different orientations and sense of offset, are exposed (Figs. 19, 20, and 29). To the northwest, is the well-exposed, NW-striking, linear Coyote Springs fault. This is a dextral fault based on the relatively topographically high exposure of a probable Qf2 surface, which is interpreted as a pressure ridge at a left step along the trace of the fault. To the northeast, at the base of the northern end of the White Mountains, is the NE-striking Queen Valley normal fault. And here at this stop are a set of small, east-west to northwest-southeast-trending hills underlain by Pliocene(?) basalt lavas, and Qf1 and Qf2 alluvial fan surfaces. In general, these hills are characterized by long, steep southern flanks and shorter, shallower northern flanks. These hills are interpreted as anticlines in the hanging wall of a flower structure defined by south-vergent and north-vergent thrust faults. In support of this interpretation are playa deposits exposed to the northeast, implying ponding up fan from these hills. On the basis of the style and geometry of faults, we suggest that dextral slip along the WMFZ is partitioned here into two components—normal slip along the NE-striking Queen Valley fault and thrust slip along these WNW-striking thrust faults. The latter transfers slip to the dextral slip NW-striking Coyote Springs fault.

Day 3: Volcanic Tableland, Round Valley, and Sierra Nevada Frontal Fault

Stop 9: Volcanic Tableland Relay Ramp

Directions: This stop is located at UTM 374296E 4143620 N. The Volcanic Tableland is a prominent broad plateau located north of the town of Bishop, California (Fig. 21). It is readily accessible via highways US-395 and US-6. From the intersection of US-395 and US-6 at the north end of Bishop, follow US-6 north. After ~ 1.4 miles, US-6 begins to curve east; exit left here onto Five Bridges Road and follow this north. Stay on this road as it turns west, becoming Jean Blanc Road and passing a gravel quarry. After 1.8 miles (measured from the US-6 turn-off) this road intersects with Fish Slough Road, Chalk Bluff Road and Casa Diablo Road. Follow Casa Diablo Road for ~ 1.2 miles towards the northwest up onto the Tableland. The road parallels a prominent north striking, east facing scarp on your left; go past the tip of this fault, then pull over and park along the westward curve in the road.

Description: Northeast of the road is a relatively small fault comprised of two simple en echelon segments forming a relay ramp; a much smaller segment and relay near the northern tip (Fig. 30). Maximum throw is about 9 m and forms the west boundary of a horst. Walk up the relay ramp to the footwall for a view of the Fish Slough fault; this is a useful place to discuss the sizes of faults, from the small displacement example here to the >120 m maximum displacement on the Fish Slough fault. Dawers et al. (1993) used displacement and length data from the horst bounding faults at this site, as well as the Fish Slough and a number of other faults on the Tableland to address displacement-length (D-L) scaling here. Data here are consistent with a linear D-L scaling relationship, with the along-strike average throw equaling roughly 0.01L. Some points for discussion include the notion that en echelon segments interact mechanically prior to linking, as evidenced displacement gradient anomalies along relays, i.e. steep gradients that imply deformation has to be distributed through a relay. Compare the simplicity of the relay on this fault with the breached relays at the southern end of the Fish Slough fault (these are discussed in detail in Ferrill et al. (1999)). Walk back to the vehicles via the relay ramp towards the north end of this fault.

Stop 10: Volcanic Tableland Segmented Normal Fault

Directions: This stop is located at UTM 367653 E 4148830 N. From Stop 9, Continue up Casa Diablo Road ~5.1 mi; four fumarolic mounds (in the form of small oval hills aligned SE8 NW) will be on your left; pull over and park. Beyond the fumaroles, a large array of en echelon, east-dipping fault scarps is visible (Fig. 31). A large relay ramp is visible sloping towards the northeast, between the two center-most fault segments. Walk about 3/4 mile to the relay ramp..

Description: This fault is a classic example of a segmented normal fault. Dawers and Anders (1995) measured along strike throw profiles that show that most of the displacement occurs on 4 large en echelon fault segments. Breached relays separate the segments, suggesting that the main segments formed as small faults, which grew into an interacting array that later became well linked. It is noteworthy that, taken as a whole, this fault has a D/L scaling ratio similar to much simpler and smaller faults on the Tableland (see details in Dawers and Anders, 1995). Of particular interest here is the large relay ramp with an incised paleo-channel (Fig. 31a and b). As one walks up the channel note changing patterns of incision, knickpoints upstream from faults, variation in across-channel profile, and wind gaps with paleo-waterfalls at the faults. Gilpin (2002) conducted a detailed field study here that concluded that the growth of overlapping fault segment tips determined the path the channel took, and that later breaching of the relay via a prominent linking fault led to incision that is evident in the footwall of the linking fault (Fig 31c)

Stop 11: Margin of Volcanic Tableland across Owens River Terraces

Directions: This stop is located at UTM 373846 E 4142152 N. From the intersection of US-395 and US-6 at the north end of Bishop, follow US-6 north. After ~1.4 miles, US-6 begins to curve east; exit left here onto Five Bridges Road and follow this north. Stay on this road as it turns west, becoming Jean Blanc Road and passing a gravel quarry. After 1.8 miles (measured from the US-6 turn-off) this road intersects with Fish Slough Road, Chalk Bluff Road and Casa Diablo Road. Turn left onto Chalk Bluff Road and follow this westward for about a mile along the southern margin of the Volcanic Tableland.

Description: From this vicinity one can view terraces along the Owens River to the south (Fig. 32). These have been mapped by Bateman (1965) and Pinter et al. (1994). The extent of the terrace deposits is illustrated on the generalized map shown in Figure 21. Sheehan (2007) evaluated the role of distributed E-W extensional strain across this region of northern Owens Valley by comparing summed displacements measured across the Tableland with fault strain measured on the terraces. This encompasses therefore several geomorphic units ranging in age from ~760 ka to ~20 ka. Sheehan found a two to three-fold increase in extension rates during late Pleistocene time. Though the spatial extent of the terrace data is limited, and thus this may only be a locally significant result, it is noteworthy that an increase in E-W extension rate from mid-Pleistocene to Holocene time is also reported for Fish Lake Valley (Reheis and Sawyer, 1997). In addition, dextral slip on the nearby White Mountain fault has slowed during this time frame (Kirby et al., 2006). This suggests a change in the orientation of regional shear from NNW to NW during the late Pleistocene. If one continues by vehicle further westward along Chalk Bluff Road, within the next mile or so, several normal faults are exposed in cross-section, suggesting a relatively steep dip ($>60^\circ$) for the Tableland faults, at least in the near surface.

Stop 12: Sierra Nevada Frontal Fault

Directions: This stop is located at UTM 386698 E 4064619 N. This stop is along the Sierran range front southeast of Independence. From the center of Independence, drive west on Onion Valley Road. After ~4.5 miles, turn left (south) onto Foothill Road. At ~3.0 miles, cross Symmes Creek at the Shepherd Pass (stock) trailhead sign. Continue ~0.5 miles further to a fork; bear right. At the next fork, ~0.5 miles further, bear left at the sign to the Shepherd Pass trailhead (do NOT drive to the trailhead) and continue for ~0.6 miles southwest to a small parking area on a terrace on the north side of Shepherd Creek.

Description: This is Stop 5 of Glazner et al. (2005). Between Symmes Creek to the north and Shepherd Creek to the south (Fig. 22), seven alluvial fan surfaces and several east-facing normal fault scarps are exposed. These are part of the Sierra Nevada frontal fault zone (Figs. 22, 23, and 33). Distinct alluvial fan surfaces have been identified based on fan surface height, slope, inset geometry, and surface morphologic features such as the degree of channel incision, fan dissection, desert pavement development, presence or absence of bar and swale morphology, relative weathering of surface boulders, and cross-cutting relationships. The oldest surface, an erosional remnant Qf1, is preserved as a small mound to the north of Symmes Creek. These surfaces are typically located at the apexes of drainage basins, are strongly dissected and contain scarce, highly weathered boulder clasts. Younger Qf2a surfaces are exposed at the range front between Symmes and Shepherd creeks and are defined by their ridge and ravine morphology, smooth surfaces located a few meters to tens of meters above the modern channel, and absence of large granitic boulders. Qf2b surfaces, exposed on either side of Symmes Creek, are inset into Qf2a surfaces and characterized by relatively smooth surfaces that contain large, moderately weathered granitic boulders. Based on the degree of bar and swale morphology development, along with inset geometry, Qf3 surfaces have been divided into three subunits, Qf3a, b, and c. These surfaces form the extensive alluvial aprons between Symmes and Shepherd creeks. The youngest surfaces, Qf4, cut across all other surfaces and are defined by active channels and channels that have been abandoned for a short period of time. These surfaces are typically densely vegetated, contain unvarnished granitic clasts, and recent debris flow deposits which include tree trunks and fresh boulder levee bars.

TCN dating of quartz collected from surface boulders yielded ^{10}Be TCN model ages of 60.9 ± 6.6 ka, 25.8 ± 7.5 ka, 4.4 ± 1.1 ka, and 4.1 ± 1.0 ka for surfaces Qf2b, Qf3a, Qf3c, and Qf4 surfaces, respectively, in the Symmes-Shepherd creek area. The alluvial fan surfaces are cut by a zone of parallel NNW-striking, east-dipping normal fault scarps with no evidence for a lateral component of slip. Topographic profiling across fault scarps yield vertical surface offsets of 41.0 ± 8.2 m of Qf2a, 11.9 ± 2.3 m of Qf2b, and 10.2 ± 2.0 m of Qf3a; Qf4 surfaces have not been offset. Combining data from ^{10}Be TCN ages with vertical offsets yield vertical slip rate estimates of $0.2\text{--}0.4 \pm 0.1$ mm/yr since ~ 61 ka, $0.3\text{--}0.4 \pm 0.2$ since ~ 26 ka, and 1.6 ± 0.4 since ~ 4 ka. Combining measured offsets with TCN ages, and assuming a fault dip of 60° , late Pleistocene to Holocene horizontal extension rates range from $0.1\text{--}0.2 \pm 0.1$ mm/yr to 0.9 ± 0.4 mm/yr. Vehicles are parked on a Qf3a surface, which is in the footwall of an east-facing fault scarp that exhibits 10.2 m of vertical offset.

ACKNOWLEDGMENTS

Research presented in this guidebook was supported by the National Science Foundation, the Geothermal Program Office of the China Lake Naval Air Warfare Center, the National Aeronautics and Space Administration, Lawrence Livermore National Laboratory, The Geological Society of America, the University of California White Mountain Research Station, Louisiana Board of Regents' Support Fund, Central Washington University, University of Southern California, and Georgia Institute of Technology. Lidar data were collected by the National Center for Airborne Laser Mapping (NCALM). Ideas and interpretations expressed herein benefited greatly from discussions with J. Bartley, J. Dewey, T. Dixon, J. Dolan, R. Finkel, J. Gosse, E. Hauksson, J. Helms, C. Henry, K. Le, F. Monastero, G. Roquemore, D. Slemmons, D. Stockli, and J. D. Walker. Aerial reconnaissance courtesy of A. Glazner.

REFERENCES

- Argus, D.F., and Gordon, R.G., 1991, Current Sierra Nevada-North America motion from very long baseline interferometry: implications for the kinematics of the western United States: *Geology*, v. 19, p. 1085-1088.
- Argus, D.F., and Gordon, R.G., 2001, Present tectonic motion across the Coast Ranges and San Andreas fault system in central California: *Geological Society of America Bulletin*, v. 113, p. 1580-1592.
- Bacon, S.N. and Pezzopane, S.K., 2007, A 25,000-year old record of earthquakes on the Owens Valley fault near Lone Pine, California: Implications for recurrence intervals, slip rates, and segmentation models: *Geological Society of America*, v. 95, p. 2472-2485 doi:10.1785/0120040228.
- Bacon, S.N., Jayko, A.S., and McGeehin, J.P., 2005, Holocene and latest Pleistocene oblique dextral faulting on the southern Inyo Mountains fault, Owens Lake Basin, California, *Bulletin of the Seismological Society of America*, v. 95, p. 2472-2485, doi:10.1785/0120040228.
- Bacon, S.N., Burke, R.M., Pezzopane, S.K., and Jayko, A.S., 2006, Last glacial maximum and Holocene lake levels of Owens Lake, eastern California, USA: *Quaternary Science Reviews*, v. 25, p. 1264-1282.
- Bartley, J.M., Glazner, A.F., Coleman, D.S., Kylander-Clark, A., Mapes, R., and Friedrich, A.M., 2007, Large Laramide dextral offset across Owens Valley, California, and its possible relation to tectonic unroofing of the southern Sierra Nevada, *in* Till, A.B. et al., eds., *Exhumation associated with continental strike-slip fault systems*: Geological Society of America Special Paper 434, p. 129-148.
- Bateman, P.C., 1965, Geology and tungsten mineralization of the Bishop district, California: U.S. Geological Survey Professional Paper 470, 208 p.
- Bateman, P.C., and Wahrhaftig, C., 1966, Geology of the Sierra Nevada, in Bailey, E.H., ed., *Geology of Northern California*: California Division of Mines and Geology Bulletin 190, p. 107-172.
- Beanland, S., and Clark, M.M., 1994, The Owens Valley fault zone, eastern California, and surface faulting associated with the 1872 earthquake: *U.S. Geological Survey Bulletin* 1982, 29 p.
- Bellier, O., and Zoback, M.L., 1995, Recent state of stress change in the Walker Lane zone, western Basin and Range Province, United States: *Tectonics*, v. 14, p. 564-593, doi:10.1029/94TC00596.

- Bennett, R.A., Davis, J.L., and Wernicke, B.P., 1999, Present-day pattern of Cordilleran deformation in the Western United States: *Geology*, v. 27, p. 371–374.
- Bennett, R.A., Wernicke, B.P., Niemi, N.A., Friedrich, A.M., and Davis, J.L., 2003, Contemporary strain rates in the northern Basin and Range Province from GPS data: *Tectonics*, v. 22, doi:10.1029/2001TC001355.
- Berry, M.E., 1997, Geomorphic analysis of late Quaternary faulting on Hilton Creek, Round Valley and Coyote Warp faults, east-central Sierra Nevada, California, USA: *Geomorphology*, v. 20, p. 177–195, doi: 10.1016/S0169-555X(97)00033-0.
- Bishop, K.M. and Clements, S., 2006, The Poverty Hills, Owens Valley, California: transpressional uplift or ancient landslide deposit?: *Environmental and Engineering Geoscience*, v. 12, p. 301-314.
- Blakely, R.J., and Ponce, D.A. 2001, Map showing depth to pre-Cenozoic basement in the Death Valley groundwater model area, Nevada and California: U.S. Geological Survey Miscellaneous Field Studies Map MF-2361-3, 1:250,000.
- Bradley, D., 2005, The kinematic history of the Coaldale Fault, Walker Lane Belt, Nevada [M.S. thesis]: Lawrence, University of Kansas, 96 p.
- Brogan, G.E., Kellog, K.S., Slemmons, D.B., and Terhune, C.L., 1991, Late Quaternary faulting along the Death Valley–Furnace Creek Fault System, California and Nevada: U.S. Geological Survey Bulletin 1991, 23 p.
- Buck, W.R., 1988, Flexural rotation of normal faults: *Tectonics*, v.7, p. 959-973.
- Burchfiel, B.C., Hodges, K.V., and Royden, L.H., 1987, Geology of Panamint Valley-Saline Valley pull-apart system, California: Palinspastic evidence for low angle geometry of a Neogene range-bounding fault: *Journal of Geophysical Research*, v. 92, p. 10,422-10,426.
- Carter, B.A., 1980, Quaternary displacement on the Garlock fault, California, *in* Fife, D.L., and Brown, A.R., eds., *Geology and mineral wealth of the California desert*: Santa Ana, South Coast Geological Society Guidebook [Dibblee Volume], p. 457–466.
- Casteel, J.C., 2005, Late Miocene to Holocene faulting along the southwestern Inyo Mountains fault zone, eastern California [M.S. thesis]: Ellensburg, Central Washington University, 72 p.
- Clark, M.K., Maheo, G., Saleeby, J., and Farley, K.A., 2005, The non-equilibrium landscape of the southern Sierra Nevada, California: *GSA Today*, v. 15, p. 4-10, doi:10.1130/1052- 5173(2005)015[4:TNLOTS]2.0.CO;2.
- Conrad, J.E., 1993, Late Cenozoic tectonics of the southern Inyo Mountains, eastern California [M.S. thesis]: San Jose, San Jose State University, 84 p.
- Davis, G.A., and Burchfiel, B.C., 1973, Garlock fault: An intracontinental transform structure, southern California: *Geological Society of America Bulletin*, v. 84, p. 1407–1422, doi: 10.1130/0016-7606(1973)84<1407:GFAITS>2.0.CO;2.
- Dawers, N. H., and Anders, M. H., 1995, Displacement-length scaling and fault linkage: *Journal of Structural Geology*, v. 17, p. 607-614.
- Dawers, N. H., Anders, M. H., and Scholz, C. H., 1993, Growth of normal faults: displacement length scaling: *Geology*, v. 21, p. 1107-1110.
- Dawson, T.E., McGill, S.F., and Rockwell, T.K., 2003, Irregular recurrence of paleoearthquakes along the central Garlock fault near El Paso Peaks, California: *Journal of Geophysical Research*, v. 108, doi: 10.1029/2001JB001744.
- Dilles, J.H., and Gans, P.B., 1995, The chronology of Cenozoic volcanism and deformation in the Yerington Area, western Basin and Range and Walker-Lane: *Geological Society of America Bulletin*, v. 107, p. 474-486
- Dixon, T.H., Robaudo, J.L., and Reheis, M.C., 1995, Constraints on present-day Basin and Range deformation from space geodesy: *Tectonics*, v. 14, p. 755-772.
- Dixon, T.H., Miller, M., Farina, F., Wang, H., and Johnson, D., 2000, Present-day motion of the Sierra Nevada block, and some tectonic implications for the Basin and Range Province: *North American Cordillera: Tectonics*, v. 19, p. 1–24, doi: 10.1029/1998TC001088.
- Dixon, T.H., Norabuena, E., and Hotaling, L., 2003, Paleoseismology and global positioning system: earthquake-cycle effects and geodetic versus geologic fault slip rates in the eastern California shear zone: *Geology*, v. 31, p. 55–58, doi: 10.1130/0091 7613(2003)031<0055: PAGPSE>2.0.CO;2.
- Dokka, R.K., and Travis, C.J., 1990, Late-Cenozoic strike-slip faulting in the Mojave Desert, California: *Tectonics*, v. 9, p. 311–340.
- Dooley, T., Monastero, F.C., Hall, B., McClay, K., and Whitehouse, P., 2004, Scaled sandbox modeling of transtensional pull-apart basins – Applications to the Coso geothermal system; *Geothermal Resources Council Transactions*, v. 28, p.637-641.
- Duffield, W.A., and Bacon, C.R., 1981, Geologic map of the Coso Volcanic field and adjacent areas, Inyo County, California: U.S. Geological Survey Miscellaneous Investigations Series Map I-1200, 1:50,000.

- Faulds, J.E., Henry, C.D., and Heinz, N.H., 2005, Kinematics of the northern Walker Lane: An incipient transform fault along the Pacific–North America plate boundary: *Geology*, v. 33, p. 505–508, doi: 10.1130/G21274.1.
- Ferrill, D. A., and Morris, A. P., 2001, Displacement gradient and deformation in normal fault systems: *Journal of Structural Geology*, v. 32, p. 619–638.
- Ferrill, D. A., Stamatakos, J. R., and Sims, D., 1999, Normal fault corrugation: implications for growth and seismicity of active normal faults: *Journal of Structural Geology*, v. 21, p. 1027–1038.
- Fillmore, R.P. and Walker, J.D., 1996, Evolution of a supradetachment extensional basin: the lower Miocene Pickhandle Basin, central Mojave Desert, California, in, Beratan, K.K., ed., *Reconstructing the history of Basin and Range extension using sedimentology and stratigraphy: Geological Society of America Special Paper 303*, p.107–126.
- Fillmore, R.P., Walker, J.D., Bartley, J.M., and Glazner, A.F., 1994, Development of three genetically related basins associated with detachment-style faulting: predicted characteristics and an example from the central Mojave Desert, California: *Geology*, v. 22, p. 1087–1090.
- Flesch, L.M., Holt, W.E., Haines, A.J., and Shen-Tu, B., 2000, Dynamics of the Pacific–North American plate boundary zone in the western United States: *Science*, v. 287, p. 834–836, doi:10.1126/science.287.5454.834.
- Frankel, K.L., Brantley, K.S., Dolan, J.F., Finkel, R.C., Klinger, R.E., Knott, J.R., Machette, M.N., Owen, L.A., Phillips, F.M., Slate, J.L., and Wernicke, B.P., 2007a, Cosmogenic ¹⁰Be and ³⁶Cl geochronology of offset alluvial fans along the northern Death Valley fault zone: Implications for transient strain in the eastern California shear zone: *Journal of Geophysical Research-Solid Earth*, v. 112, doi:10.1029/2006JB004350.
- Frankel, K. L., Dolan, J. F., Finkel, R. C., Owen, L. A., and Hoeft, J. S., 2007b, Spatial variations in slip rate along the Death Valley-Fish Lake Valley fault system determined from LiDAR topographic data and cosmogenic ¹⁰Be geochronology: *Geophysical Research Letters*, v. 34, doi:10.1029/2007GL030549.
- Frankel, K.L., Glazner, A.F., Kirby, E., Monastero, F.C., Strane, M.D., Oskin, M.E., Unruh, J.R., Walker, J.D., Anandakrishnan, S., Bartley, J.M., Coleman, D.S., Dolan, J.F., Finkel, R.C., Greene, D., Kylander-Clark, A., Morrero, S., Owen, L.A., and Phillips, F., 2008, Active tectonics of the eastern California shear zone, in Duebendorfer, E.M., and Smith, E.I., eds., *Field guide to plutons, volcanoes, faults, reefs, dinosaurs, and possible glaciation in selected areas of Arizona, California, and Nevada: Geological Society of America Field Guide 11*, p. 43–81, doi: 10.1130/2008.fld011(03).
- Frankel, K.L., Dolan, J.F., Owen, L.A., Ganev, P., and Finkel, R.C., in review, Spatial and temporal constancy of seismic strain release along an evolving segment of the Pacific–North America plate boundary: *Earth and Planetary Science Letters*.
- Gan, W., Svarc, J.L., Savage, J.C., and Prescott, W.H., 2000, Strain accumulation across the eastern California shear zone at latitude 36°30'N: *Journal of Geophysical Research*, v. 105, p. 16,229–16,236, doi: 10.1029/2000JB900105.
- Ganev, P.N., Dolan, J.F., Frankel, K.L., and Finkel, R.C., 2010, Rates of extension along the Fish Lake Valley fault and transensional deformation in the eastern California shear zone-Walker Lane: *Lithosphere* v. 2, p. 33–49, doi:10.1130/L51.
- Gans, P.B., Miller, E.L., McCarthy, J., and Ouldcutt, M.L., 1985, Tertiary extensional faulting and evolving brittle-ductile transition zones in the northern Snake Range and vicinity: New insights from seismic data: *Geology*, v.13, p. 189–193.
- Gilpin, R. E., 2002, Interaction between stream development and propagating extensional faults [PhD thesis]: Edinburgh, University of Edinburgh, 415 p.
- Glazner, A.F., Lee, J., Bartley, J.M., Coleman, D.S., Kylander-Clark, A., Greene, D.C., and Le, K., 2005, Large dextral offset across Owens Valley, California from 148 Ma to 1872 A.D., in Stevens, C., and Cooper, J., eds., *Western great basin geology: Fieldtrip guidebook and volume for the joint meeting of the Cordilleran section–GSA and Pacific Section–AAPG, April 29–May 1, 2005, San José, California: Fullerton, Pacific Section SEPM (Society for Sedimentary Geology) Book 99*, p. 1–35.
- Goethals, M. M., Niedermann, S., Hetzel, R., and Fenton, C. R., 2009, Determining the impact of faulting on the rate of erosion in a low-relief landscape: a case study using in situ produced Ne-21 on active normal faults in the Bishop Tuff, California: *Geomorphology*, v. 103, p. 401–413.
- Guest, B., Niemi, N.A., and Wernicke, B.P., 2007, Stateline fault system: a new component of the Miocene–Quaternary eastern California shear zone: *Geological Society of America Bulletin*, v. 119, p. 1337–1346.
- Hammond, W.C., and Thatcher, W., 2004, Contemporary tectonic deformation of the Basin and Range province, western United States: 10 years of observation with the global positioning system: *Journal of Geophysical Research*, v. 109, B08403, doi:10.1029/2003JB002746.

- Hauksson, E., and Unruh, J., 2007, Regional tectonics of the Coso geothermal area along the intra-continental plate boundary in central-eastern California: three-dimensional VP and VP/VS models, spatial-temporal seismicity patterns, and seismogenic strain deformation: *Journal of Geophysical Research*, v. 112, doi:10.1029/2006JB0044721.
- Hearn, E.H., and Humphreys, E.D., 1998, Kinematics of the southern Walker Lane belt and motion of the Sierra Nevada block, California: *Journal of Geophysical Research*, v. 103, p. 27,033–27,049, doi:10.1029/98JB01390.
- Henry, C.D., and Perkins, M.E., 2001, Sierra Nevada–Basin and Range transition near Reno, Nevada: two-stage development at 12 and 3 Ma: *Geology*, v. 29, p. 719–722.
- Hill, E.M., and Blewitt, G., 2006, Testing for fault activity at Yucca Mountain, Nevada, using independent GPS results from the BARGEN network: *Geophysical Research Letters*, v. 33, doi:10.1029/2006GL026140.
- Hoefl, J.S., and Frankel, K.L., in review, Temporal variations in extension rate along the Lone Mountain fault and strain partitioning in the eastern California shear zone-Walker Lane belt: *Geosphere*.
- Hoefl, J.S., and Frankel, K.L., 2010, Late Pleistocene rates of extension on the Lone Mountain fault and strain distribution in the eastern California shear zone-Walker Lane: *Geological Society of America Abstracts with Programs*, v. 42, p. 55.
- Hough, S.E., and Hutton, K., 2008, Revisiting the 1872 Owens Valley, California, Earthquake: *Bulletin of the Seismological Society of America*, v. 98, p. 931–949.
- Humphreys, E.D., and Weldon, R.J., 1994, Deformation across the western United States: a local estimate of Pacific–North America transform deformation: *Journal of Geophysical Research*, v. 99, p. 19,975–20,010, doi:10.1029/94JB00899.
- Ingersoll, R.V., Devaney, K.A., Geslin, J.K., Cavazza, W., Diamond, D.S., Heins, W.A., Jagiello, K.J., Marsaglia, K.M., Paylor, E.D., II, and Short P.F., 1996, The Mud Hills, Mojave Desert, California: structure, stratigraphy, and sedimentology of a rapid extended terrane *in*, Beratan, K.K., *ed.*, *Reconstructing the history of Basin and Range extension using sedimentology and stratigraphy*: *Geological Society of America Special Paper 303*, p. 61–84.
- Jones, C.H., Farmer, G.L., and Unruh, J., 2004, Tectonics of Pliocene removal of lithosphere of the Sierra Nevada, California: *Geological Society of America Bulletin*, v. 116, p. 1408–1422.
- Kirby, E., Burbank, D. W., Reheis, M., and Phillips, F., 2006, Temporal variations in slip rate of the White Mountain fault zone, eastern California: *Earth and Planetary Science Letters*, v. 248, p. 168–185.
- Le, K., Lee, J., Owen, L., and Finkel, R.C., 2007, Late Quaternary slip rates along the Sierra Nevada frontal fault zone, California: evidence for slip partitioning across the western margin of the eastern California shear zone-Basin and Range Province: *Geological Society of America Bulletin*, v. 119, p. 240–256; doi: 10.1130/B25960.1.
- Lee, J., Rubin, C.M., and Calvert, A., 2001a, Quaternary faulting history along the Deep Springs fault, California: *Geological Society of America Bulletin*, v. 113, p. 855–869, doi:10.1130/00167606(2001)113<0855:QFHATD>2.0.CO;2.
- Lee, J., Spencer, J., and Owen, L., 2001b, Holocene slip rates along the Owens Valley fault, California: Implications for the recent evolution of the eastern California shear zone: *Geology*, v. 29, p. 819–822, doi: 10.1130/00917613(2001)029<0819:HSRATO>2.0.CO;2.
- Lee, J., Stockli, D. F., Owen, L. A., Finkel, R. C., and Kislitsyn, R., 2009a, Exhumation of the Inyo Mountains, California: implications for the timing of extension along the western boundary of the Basin and Range Province and distribution of dextral fault slip rates across the eastern California shear zone: *Tectonics*, v. 28, TC1001, doi:10.1029/2008TC002295.
- Lee, J., Garwood, J., Stockli, D., and Gosse, J., 2009b, Quaternary faulting in Queen Valley, California-Nevada: implications for kinematics of fault slip transfer in the eastern California shear zone-Walker Lane belt: *Geological Society of America Bulletin*, v. 121, p. 599–614, doi:10.1130/B26352.1.
- Martel, S.J., 1984, Structure of the Owens Valley fault zone near Poverty Hills, Owens Valley, California: *Geological Society of America Abstracts with Programs*, v. 16, no. 6, p. 585.
- Martel, S.J., 1989, Structure and late Quaternary activity of the northern Owens Valley fault zone, Owens Valley, California: *Engineering Geology*, v. 27, p. 489–507.
- McClusky, S.C., Bjornstad, S.C., Hager, B.H., King, R.W., Meade, B.J., Miller, M.M., Monastero, F.C., and Souter, B.J., 2001, Present day kinematics of the eastern California shear zone from a geodetically constrained block model: *Geophysical Research Letters*, v. 28, p. 3369–3372, doi:10.1029/2001GL013091.
- McGill, S.F., and Sieh, K., 1991, Surficial offsets on the central and eastern Garlock fault associated with prehistoric earthquakes: *Journal of Geophysical Research*, v. 96, p. 21,597–21,621.

- McKenzie, D., and Jackson, J., 1983, The relationship between strain rates, crustal thickening, paleomagnetism, finite strain and fault movements within a deforming zone: *Earth and Planetary Science Letters*, v. 65, p. 182–202.
- McKenzie, D., and Jackson, J., 1986, A block model of distributed deformation by faulting: *Journal of the Geological Society, London*, v. 143, p. 349–353.
- Miller, M.M., Johnson, D.J., Dixon, T.H., and Dokka, R.K., 2001, Refined kinematics of the eastern California shear zone from GPS observations, 1993–1994: *Journal of Geophysical Research*, v. 106, p. 2245–2263, doi:10.1029/2000JB900328.
- Monastero, F.C., and Unruh, J.R., 2002, Definition of the brittle-plastic transition in the Coso geothermal field, east-central California, USA: EAGE 64th Conference and Exhibition, Florence, Italy, May 27-30.
- Monastero, F.C., Katzenstein, A.M., Miller, J.S., Unruh, J.R., Adams, M.C., and Richards-Dinger, K., 2005, The Coso geothermal field: a nascent metamorphic core complex: *Geological Society of America Bulletin*, v. 117, p. 1534-1553.
- Neponset Geophysical Corporation and Aquila Geosciences, 1997, Phase 3 and Phase 4 Seismic Program, Owens Lake, Inyo County, California: Final Report prepared for Great Basin Unified Air Pollution Control District, Bishop, California, 146 p.
- Oldow, J.S., Kohler, G., and Donelick, R.A., 1994, Late Cenozoic extensional transfer in the Walker Lane strike-slip belt, Nevada: *Geology*, v. 22, p. 637–640.
- Oskin, M., and Iriondo, A., 2004, Large-magnitude transient strain accumulation on the Blackwater fault, eastern California shear zone: *Geology*, v. 32, p. 313–316, doi: 10.1130/G20223.1.
- Oskin, M., Perg, L., Blumentritt, D., Mukhopadhyay, S., and Iriondo, A., 2007, Slip rate of the Calico fault: implications for geologic versus geodetic rate discrepancy in the eastern California shear zone: *Journal of Geophysical Research*, v. 112, B03402, doi: 10.1029/2006JB004451.
- Oskin, M., Perg, L., Shelef, E., Strane, M., Gurney, M., Singer, B., and Zhang, X., 2008, Elevated shear zone loading rate during and earthquake cluster in eastern California: *Geology*, v. 36, p. 507-510, doi:10.1130/G24814A.1.
- Oswald, J.A., and Wesnousky, S.G., 2002, Neotectonics and Quaternary geology of the Hunter Mountain fault zone and Saline Valley region, southeastern California: *Geomorphology*, v. 42, p. 255-278.
- Pakiser, L.C., Kane, M. F., and Jackson, W. H., 1964, Structural geology and volcanism of Owens Valley region, California: a geophysical study: U.S. Geological Survey Professional Paper 438, 65 p.
- Peltzer, G., Crampe, F., Hensley, S., and Rosen, P., 2001, Transient strain accumulation and fault interaction in the eastern California shear zone: *Geology*, v. 29, p. 975–978, doi:10.1130/0091-7613(2001)029<0975:TSAAFI>2.0.CO;2.
- Petronis, M.S., 2005, Cenozoic evolution of the central Walker Lane belt, west-central Nevada Ph.D. thesis]: Albuquerque, University of New Mexico, 286 p.
- Petronis, M.S., Geissman, J.W., Oldow, J.S., and McIntosh, W.C., 2002, Paleomagnetic and $^{40}\text{Ar}/^{39}\text{Ar}$ geochronologic data bearing on the structural evolution of the Silver Peak extensional complex, west-central Nevada: *Geological Society of America Bulletin*, v. 114, p. 1108–1130, doi: 10.1130/00167606(2002)114<1108:PAAAGD>2.0.CO;2.
- Petronis, M.S., Geissman, J.W., Oldow, J.S., and McIntosh, W.C., 2009, Late Miocene to Pliocene vertical axis rotation attending development of the Silver Peak–Lone Mountain displacement transfer zone, west-central Nevada, *in* Oldow, J.S., and Cashman, P.H., eds., Late Cenozoic structure and evolution of the Great Basin–Sierra Nevada transition: *Geological Society of America Special Paper 447*, p. 215–253, doi:10.1130/2009.2447(12).
- Pinter, N., 1995, Faulting on the Volcanic Tableland, Owens Valley, California: *Journal of Geology*, v. 103, p. 73-83.
- Pinter, N., Keller, E. A., and West, R. B., 1994, Relative dating of terraces of the Owens River, northern Owens valley, California, and correlation with moraines of the Sierra Nevada: *Quaternary Research*, v. 42, p. 266-276.
- Reasenber, P., Ellsworth, W., and Walter, A., 1980, Teleseismic evidence for a low-velocity body under the Coso geothermal resource area: *Research*, v. 85, p. 2471-2,483.
- Reheis, M.C., 1992, Geologic Map of late Cenozoic deposits and faults in parts of the Soldier Pass and Magruder Mountain 15' Quadrangles, Inyo and Mono Counties, California and Esmeralda County, Nevada: U.S. Geological Survey Map I-2268, 1:24,000.
- Reheis, M.C., and Dixon, T.H., 1996, Kinematics of the eastern California shear zone: evidence for slip transfer from Owens and Saline Valley fault zones to Fish Lake Valley fault zone: *Geology*, v. 24, p. 339–342, doi:10.1130/0091-7613(1996)024<0339:KOTECES>2.3.CO;2.

- Reheis, M.C., and Sawyer, T.L., 1997, Late Cenozoic history and slip rates of the Fish Lake Valley, Emigrant Peak, and Deep Springs fault zones, Nevada and California: *Geological Society of America Bulletin*, v. 109, p. 280–299, doi: 10.1130/0016 7606(1997)109<0280:LCHASR>2.3.CO;2.
- Reheis, M.C., Sawyer, T.L., Slate, J.L., and Gillispie, A.R., 1993, Geologic map of late Cenozoic deposits and faults in the southern part of the Davis Mountain 15' Quadrangle, Esmeralda County, Nevada: U.S. Geological Survey Map I-2342, 1:24,000.
- Reheis, M.C., Slate, J.L., and Sawyer, T.L., 1995, Geologic map of late Cenozoic deposits and faults in parts of the Mt. Barcroft, Piper Peak, and Soldier Pass 15' Quadrangles, Esmeralda County, Nevada, and Mono County, California: U.S. Geological Survey Map I-2464, 1:24,000.
- Rockwell, T.K., Lindvall, S., Herzberg, M., Murbach, D., Dawson, T., and Berger, G., 2000, Paleoseismology of the Johnson Valley, Kickapoo, and Homestead Valley faults: Clustering of earthquakes in the eastern California shear zone: *Bulletin of the Seismological Society of America*, v. 90, p. 1200–1236, doi:10.1785/0119990023.
- Ross, D.C., 1965, Geology of the Independence Quadrangle, Inyo County, California: U.S. Geological Survey Bulletin 1181-O, p. O1-O64.
- Ross, D. C., 1967, Generalized geologic map of the Inyo Mountains region, California, U.S. Geological Survey Miscellaneous Geologic Investigations Map, I-0506, 1:125,000.
- Ross, D.C., 1969, Descriptive petrography of three large granitic bodies in the Inyo Mountains, California: U.S. Geological Survey Professional Paper 601, 47p.
- Sarna-Wojcicki, A. M., Pringle, M. S., and Wijbrans, J., 2000, New Ar-40/Ar-39 age of the Bishop Tuff from multiple sites and sediment rate calibration for the Matuyama-Brunhes boundary: *Journal of Geophysical Research-Solid Earth*, v. 105, p. 21,431-21,443.
- Savage, J.C., Lisowski, M., and Prescott, W.H., 1990, An apparent shear zone trending north35 northwest across the Mojave Desert into Owens Valley, California: *Geophysical Research Letters*, v. 17, p. 2113–2116.
- Sawyer, T.L., 1990, Quaternary Geology and Neotectonic activity along the Fish Lake Valley fault zone, Nevada and California [M.S. thesis]: Reno, University of Nevada, 379p.
- Serpa, L. and Pavlis, T.L., 1996, Three-dimensional model of the late Cenozoic history of the Death Valley region, southeastern California: *Tectonics*, v. 15, p. 1113-1128.
- Sheehan, T. P., 2007, Evolution of Neogene fault populations in northern Owens Valley, California and implications for the eastern California shear zone [Ph.D. thesis]: New Orleans, Tulane University, 203 p.
- Slemmons, D.B, Vittori, E., Jayko, A.S., Carver, G.A., and Bacon, S.N., 2008, Quaternary fault and lineament map of Owens Valley, Inyo County, eastern California: *Geological Society of America Map and Chart 96*, 1:100,000, 2 sheets, doi: 10.1130/2008.MCH096.
- Spencer, J.E., 1984, The role of tectonic denudation in the warping and uplift of low-angle normal faults: *Geology*, v.12, p. 95-98.
- Sternlof, K.R., 1988, Structural style and kinematic history of the active Panamint-Saline extensional system, Inyo County, California [M.S. thesis]: Cambridge, Massachusetts Institute of Technology, 40 p.
- Stockli, D.F., Farley, K.A., and Dumitru, T.A., 2000, Calibration of the apatite (U-Th)/He thermochronometer on an exhumed fault block, White Mountains, California: *Geology*, v. 28, p. 983-986.
- Stockli, D.F., Surpless, B.E., Dumitru, T.A., and Farley, K.A., 2002, Thermochronological constraints on the timing and magnitude of Miocene and Pliocene extension in the central Wassuk Range, western Nevada: *Tectonics*, v. 21, doi:10.1029/2001TC001295.
- Stockli, D.F., Dumitru, T.A., McWilliams, M.O., and Farley, K.A., 2003, Cenozoic tectonic evolution of the White Mountains, California and Nevada: *Geological Society of America Bulletin*, v. 115, p. 788-816.
- Surpless, B.E., Stockli, D.F., Dumitru, T.A., and Miller, E.L., 2002, Two-phase westward encroachment of Basin and Range extension into the northern Sierra Nevada: *Tectonics*, v. 21, doi:10.1029/2000TC001257.
- Taylor, T.R., 2002, Origin and structure of the Poverty Hills, Owens Valley fault zone, Owens Valley, California [M.S. Thesis]: Oxford, Miami University, 93p.
- Taylor, T.R. and Dilek, Y., 2001, Origin of the Poverty Hills, Owens Valley, California and implications for the tectonic evolution of the Owens Valley Basin: *Geological Society of America Abstracts with Programs*, v. 33, no. 6, p. A-395.
- Thatcher, W., Foulger, B.P., Julian, B.R., Svarc, J., Quilty, E., and Bawden, G.W., 1999, Present-day deformation across the Basin and Range Province, western United States: *Science*, v. 282, p. 1,714-1,718.
- Tincher, C.R., and Stockli, D.F., 2009, Kinematics of multistage Tertiary faulting in the Queen Valley area, central Walker Lane belt, Nevada, *in* Oldow, J.S. and Cashman, P.H., eds., *Late Cenozoic structure and evolution of the Great Basin-Sierra Nevada transition*: *Geological Society of America Special Paper 447*, p. 255-274.

- Unruh, J.R., Hauksson, E., Monastero F.C., Twiss, R.J., and Lewis, J.C., 2002, Seismotectonics of the Coso Range-Indian Wells Valley region, California: transtensional deformation along the southeastern margin of the Sierran microplate, *in* Glazner, A.F., Walker J.D., and Bartley, J.M., eds., *Geologic evolution of the Mojave Desert and southwestern Basin and Range: Geological Society of America Memoir 195*, p. 277-294.
- Unruh, J.R., Humphrey, J., and Barron, A., 2003, Transtensional model for the Sierra Nevada frontal fault system, eastern California: *Geology*, v. 31, p. 327-330.
- Unruh, J.R., Monastero, F.C., and Pullammanappallil, S., 2008, The nascent Coso metamorphic core complex, east-central California: brittle upper plate structure revealed by seismic reflection data: *International Geology Review*, v. 50, p. 245-269.
- Walker, J.D., and Whitmarsh, R.W., 1998, A tectonic model for the Coso geothermal area: U.S. Department of Energy Proceedings Geothermal Program Review XVI, April 1-2, Berkeley, California, p. 2-17 to 2-24.
- Wernicke, B., Friedrich, A.M., Niemi, N.A., Bennett, R.A., and Davis, J.L., 2000, Dynamics of plate boundary fault systems from Basin and Range Geodetic Network (BARGEN) and geologic data: *GSA Today*, v. 10, p. 1-7.
- Wernicke, B.P., Davis, J.L., Bennett, R.A., Normandeau, J.E., Friedrich, A.M., and Niemi, N.A., 2004, Tectonic implications of a dense continuous GPS velocity field at Yucca Mountain, Nevada: *Journal of Geophysical Research*, v. 109, doi:10.1029/2003JB002832.
- Wesnousky, S.G., 2005, The San Andreas and Walker Lane fault systems, western North America: transpression, transtension, cumulative slip and the structural evolution of a major transform plate boundary: *Journal of Structural Geology*, v. 27, p. 1505-1512, doi: 10.1016/j.jsg.2005.01.015.
- Wesnousky, S.G., and Jones, C.H., 1994, Oblique slip, slip partitioning, spatial and temporal changes in the regional stress field, and the relative strength of active faults in the Basin and Range, western United States: *Geology*, v. 22, p. 1031-1034, doi: 10.1130/0091-7613(1994)022<1031:OSSPSA>2.3.CO;2.
- Whitmarsh, R.S., 1998, Geologic map of the Coso Range: Geological Society of America Map and Chart Series, Online Map, DOI: 10.1130/1998-whitmarsh-coso.
- Wilcox, R.E., Harding, T.P., and Seely, D.R., 1973, Basic wrench tectonics: *American Association of Petroleum Geologists Bulletin*, v. 57, p. 74-96.
- Willemsse, E. J. M., Pollard, D. D., and Aydin, A., 1996, 3D analyses of slip distributions on normal fault arrays with consequences for fault scaling: *Journal of Structural Geology*, v. 18, p. 295-309.
- Wilson, C. K., Jones, C. H. , and Gilbert, H. J., 2003, Single-chamber silicic magma system inferred from shear wave discontinuities of the crust and uppermost mantle, Coso geothermal area, California: *Journal of Geophysical Research*, v. 108, doi:10.1029/2002JB001798.
- Wood, J., and Saleeby, J., 1997, Late Cretaceous-Paleocene extensional collapse and disaggregation of the southernmost Sierra Nevada batholith: *International Geology Review*, v. 39, p. 973-1009.
- Yarnold, J.C. and Lombard, J.P., 1989, A facies model for large rock avalanche deposits formed in dry climates, *in* Colburn, I. P., Abbott, P. I., and Minch, J., eds., *Conglomerates in basin analysis: a symposium dedicated to A. O. Woodford: Pacific Section, Society of Economic Paleontologists and Mineralogists*, p. 9-31.
- Zoback, M.L., 1989, State of stress and modern deformation

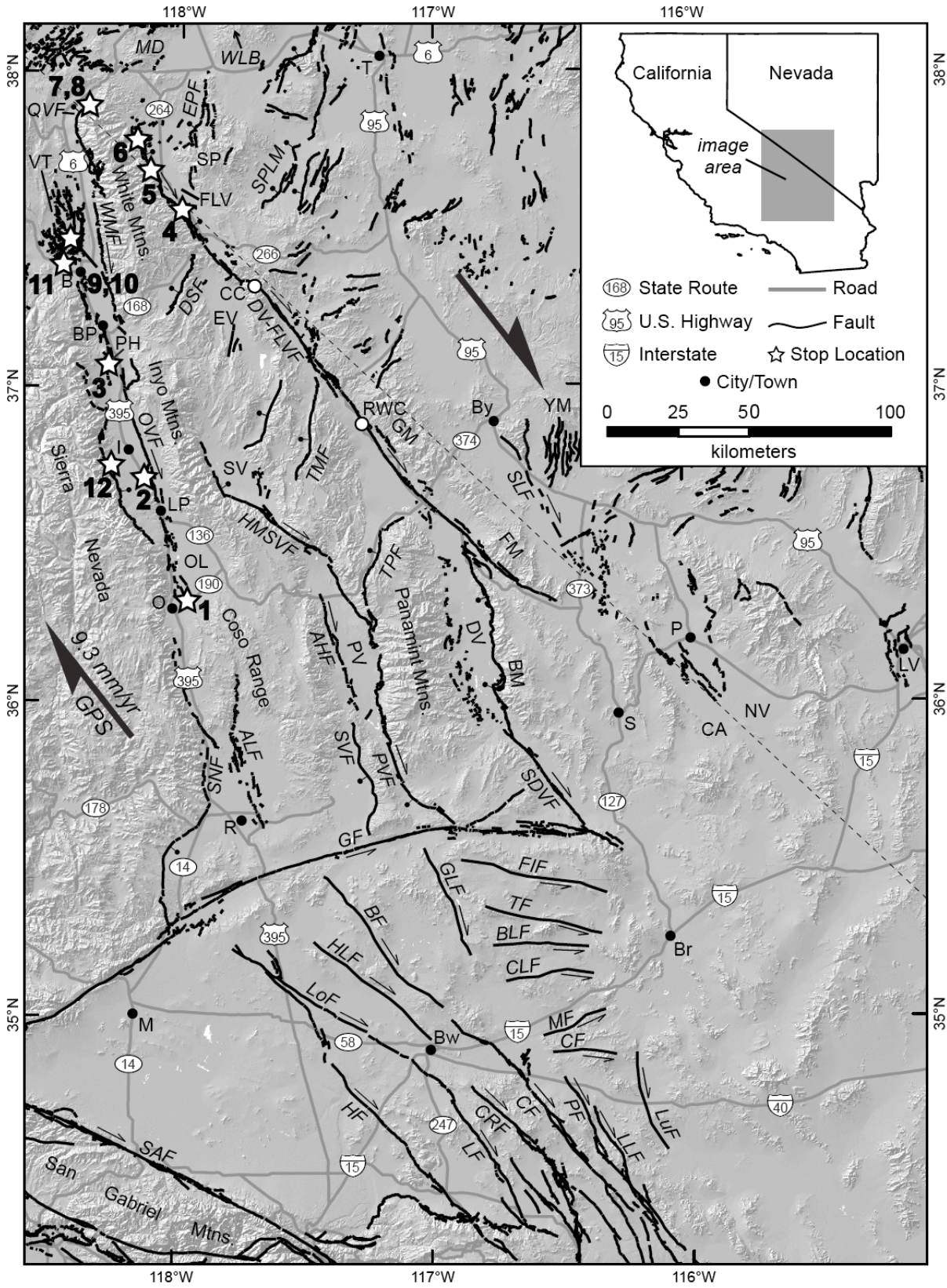


Figure 1. Shaded relief index map of the eastern California shear zone showing Quaternary faults, roads, towns, and field trip stops. Full caption on next page.

Figure 1. Shaded relief index map of the eastern California shear zone showing Quaternary faults, roads, towns, and field trip stops. Most faults are from the U.S. Geological Survey Quaternary fault and fold database (<http://earthquake.usgs.gov/regional/qfaults>). Arrows indicate relative fault motion for strike slip faults. Bar and circle indicates the hanging wall of normal faults. Field trip stop location numbers are tied to site descriptions in the field guide section. AHF—Ash Hill fault; ALF—Airport Lake fault; B—Bishop; BF—Blackwater fault; BLF—Bicycle Lake fault; BM—Black Mountains; BP—Big Pine; Br—Baker; Bw—Barstow; By—Beatty; CA—California; CC - Cucumongo Canyon; CF—Cady fault; CLF—Coyote Lake fault; CoF—Calico fault; CRF—Camp Rock fault; DSF—Deep Springs fault; DV-FLVF—Death Valley–Fish Lake Valley fault; EPF—Emigrant Peak fault; EV—Eureka Valley; FIF—Fort Irwin fault; FM—Funeral Mountains; GF—Garlock fault; GFL—Goldstone Lake fault; GM—Grapevine Mountains; HF—Helendale fault; HLF—Harper Lake fault; HMSVF—Hunter Mountain–Saline Valley fault; I—Independence; LF—Lenwood fault; LLF—Lavic Lake fault; LoF—Lockhart fault; LP—Lone Pine; LuF—Ludlow fault; LV—Las Vegas; M—Mojave; MF—Manix fault; MD—Mina deflection; NV—Nevada; O—Olancho; OL—Owens Lake; OVF—Owens Valley fault; P—Pahrump; PF—Pisgah fault; PH—Poverty Hills; PV—Panamint Valley; PVF—Panamint Valley fault; RWC—Red Wall Canyon; R—Ridgecrest; S—Shoshone; SAF—San Andreas fault; SDVF—southern Death Valley fault; SLF—Stateline fault; SPLM—Silver Peak–Lone Mountain extensional complex; SNF—Sierra Nevada frontal fault; SP—Silver Peak Range; SVF—Saline Valley fault; T—Tonopah; TF—Tiefort Mountain fault; TMF—Tin Mountain fault; TPF—Towne Pass fault; VT—Volcanic Tableland; WLB—Walker Lane belt; WMF—White Mountains fault; YM—Yucca Mountain.

Figure 2. Northward branching of the Holocene-active Airport Lake fault zone (ALFZ) in northern Indian Wells Valley, Rose Valley, the Coso Range and Wild Horse Mesa. WB=Western branch; CB=Central branch; EB=Eastern branch; WHM = Wild Horse Mesa; WHMFZ = Wild Horse Mesa fault zone; CWF = Coso Wash fault; WHA = White Hills anticline; AL = Airport Lake playa; HS = Haiwee Spring; GF = geothermal field; BR = basement ridge; UCF = Upper Centennial Flat; LCF = Lower Cactus Flat; MF = McCloud Flat. Faults with especially prominent scarps in Wild Horse Mesa are highlighted in bold. Late Quaternary faults modified from Duffield and Bacon (1981) and Whitmarsh (1998), with additional original mapping.

Figure 3. Hillshade map showing extent of a Quaternary pediment surface that fringes the northern and northwestern Coso Range. The pediment is crossed by two zones of faulting that can be traced northward from Lower Cactus flat (i.e., faults A and B). The easternmost of the fault zones (A) strikes north to north-northeast and joins the Red Ridge fault zone in the northern Coso Range piedmont, which in turn may merge with the “Central Valley fault zone” in southern Owens Lake basin (faults in Owens Lake basin from Neponset and Aquila, 1997). Fault B to the west is part of a discontinuous northwest-striking zone that can be traced to the southern end of the Owens Valley fault, and which experienced surface rupture during the 1872 Owens Valley earthquake (Slemmons et al., in press). The pediment surface folded into a series of anticlines about west-northwest trending axes west of the Red Ridge fault zone

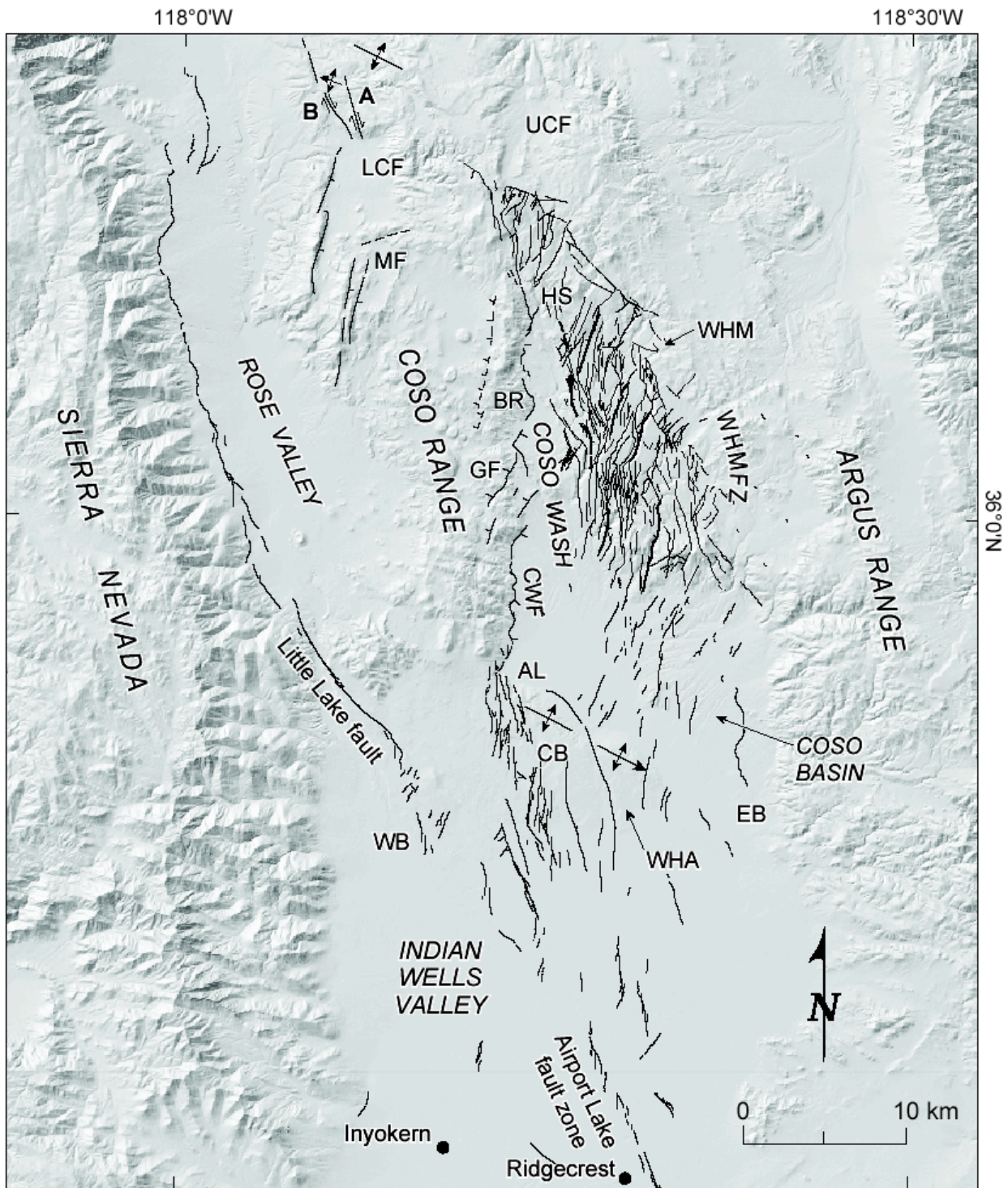


Figure 2. Northward branching of the Holocene-active Airport Lake fault zone (ALFZ) in northern Indian Wells Valley, Rose Valley, the Coso Range and Wild Horse Mesa. WB=Western branch; CB=Central branch; EB=Eastern branch; WHM = Wild Horse Mesa; WHMFZ = Wild Horse Mesa fault zone; CWF = Coso Wash fault; WHA = White Hills anticline; AL = Airport Lake playa; HS = Haiwee Spring; GF = geothermal field; BR = basement ridge; UCF = Upper Centennial Flat; LCF = Lower Cactus Flat; MF = McCloud Flat. Faults with especially prominent scarps in Wild Horse Mesa are highlighted in bold. Late Quaternary faults modified from Duffield and Bacon (1981) and Whitmarsh (1998), with additional original mapping.

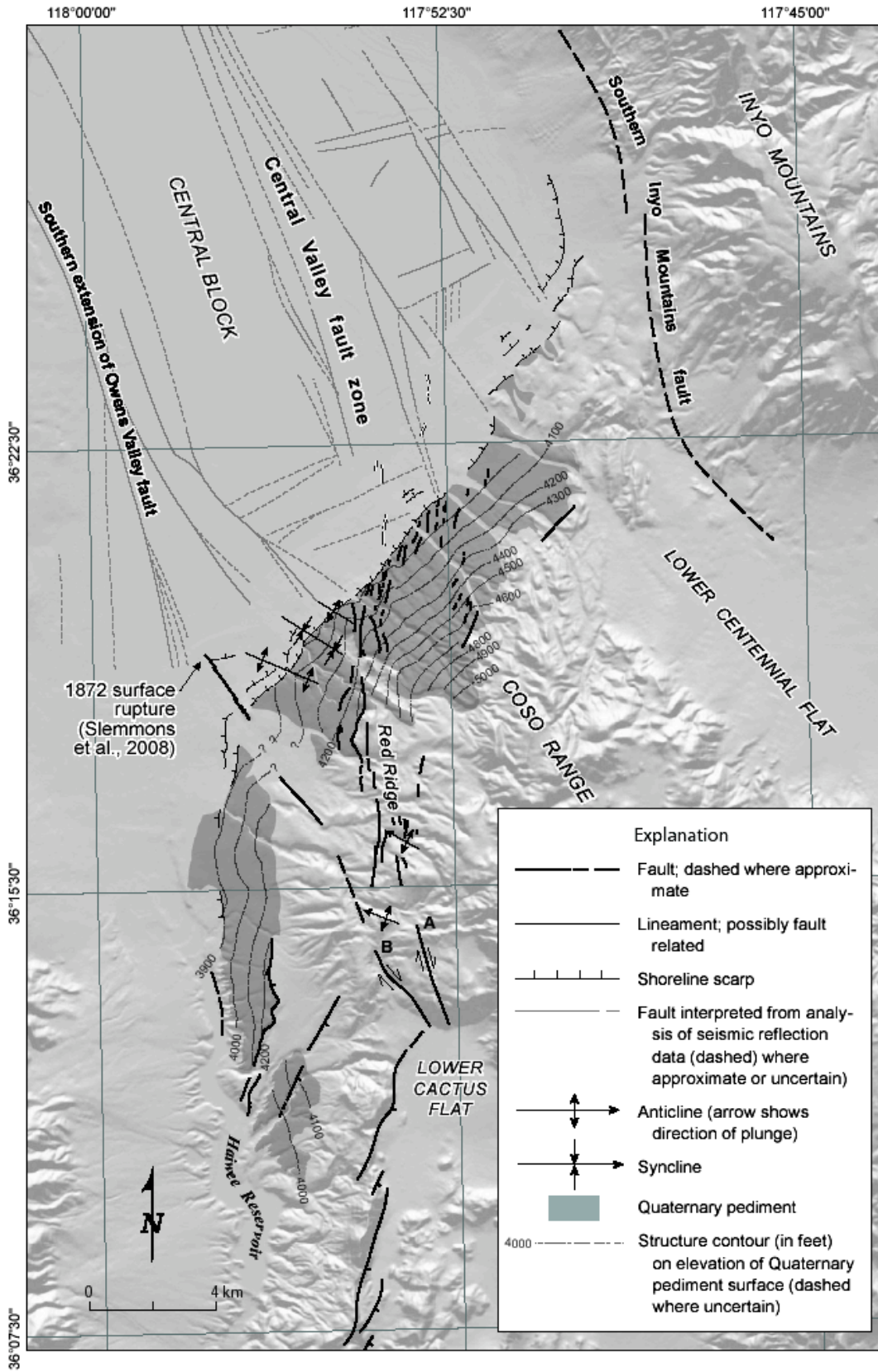


Figure 3. Hillshade map showing extent of a Quaternary pediment surface that fringes the northern and northwestern Coso Range. Full caption on page .

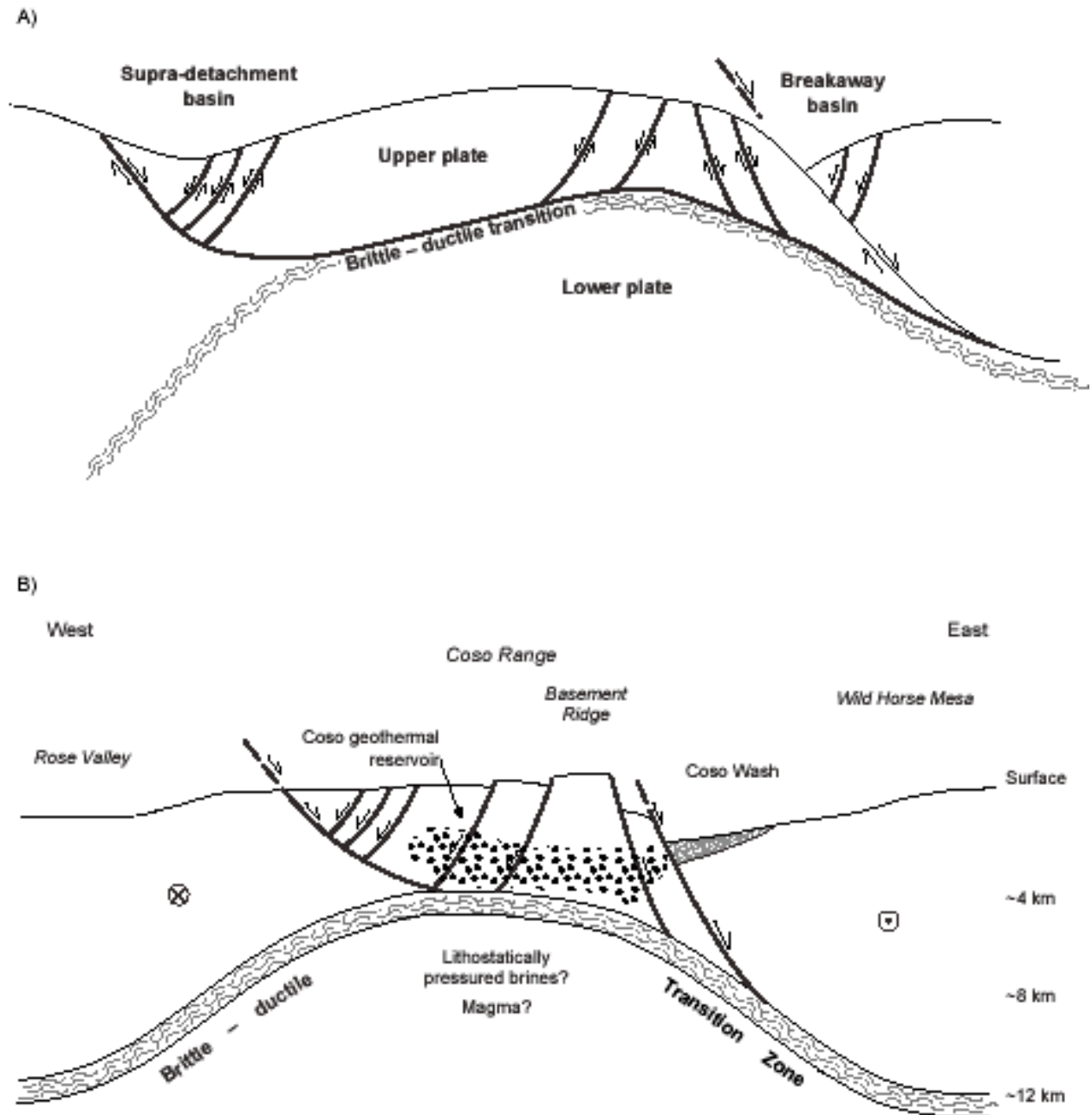


Figure 4. Model for the central Coso Range as a nascent metamorphic core complex. 4A. Generalized model for a metamorphic core complex (after Gans et al., 1985). 4B. Structural cartoon of the central Coso Range at the latitude of the geothermal field, modified from Unruh et al., 2008. Stippled pattern shows the depth and general geometry of the geothermal reservoir. Oblique horizontal extension within the plane of the cross section is driven by a right-releasing transfer of NW-dextral shear across the central Coso Range.



Figure 5. Slightly oblique aerial view to the southeast of lineaments (arrows) associated with the southern Owens Valley fault zone (see Figure 3 for location). The field trip stop is along state highway 190 at the curve in the road. Beach ridges on the north side of the highway associated with an older Holocene shoreline of Owens Lake are offset in a right-lateral sense by the Owens Valley fault (the displacement is not visible at this scale). Slemmons et al. (2008) interpret that the displacement occurred during the 1872 Owens Valley earthquake, indicating that coseismic rupture on the Owens Valley fault extended at least as far south as the Coso Range piedmont.



Figure 6. Oblique aerial view to the east of a hill located about 3 km southeast of the field trip stop on highway 190. The west flank of the hill is cut by a series of left-stepping splays of the fault shown in Figure 4 (dark lineaments aligned with arrows). The fault splays are expressed as west-facing scarps (shadowed).

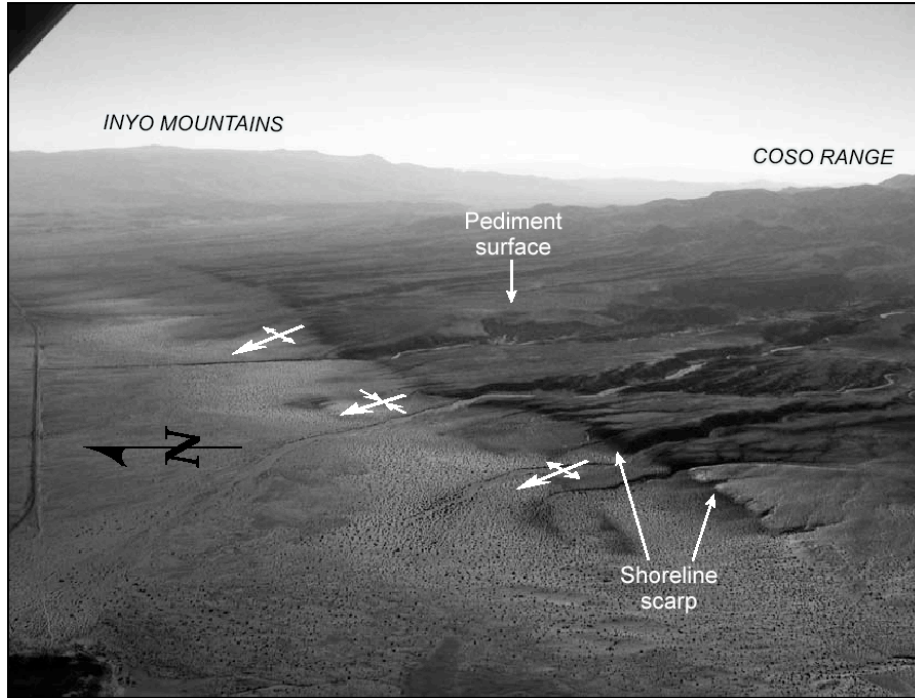


Figure 7. Oblique aerial view to the east of the northern Coso Range piedmont and southern Owens Valley. The darker, more eroded surface to the south (right) is a pediment surface cut across tilted strata of the Pliocene Coso Formation. The pediment terminates to the north against a wave-cut escarpment associated with one or more Pleistocene high stands of pluvial Owens Lake. The pediment and wave-cut scarp are noticeably folded about west-northwest-trending axes into a series of broad, low amplitude anticlines. As demonstrated by the varying width of the shadowed escarpment, the scarp is higher across the axes of the anticlines and lower through the syncline. See Figure 3 for location of folds relative to faults cutting the pediment surface



Figure 8. Oblique aerial view to the southeast of the northern Coso Range pediment surface broken up in a series of horst and graben by the Red Ridge fault zone (see Figure 3 for location).

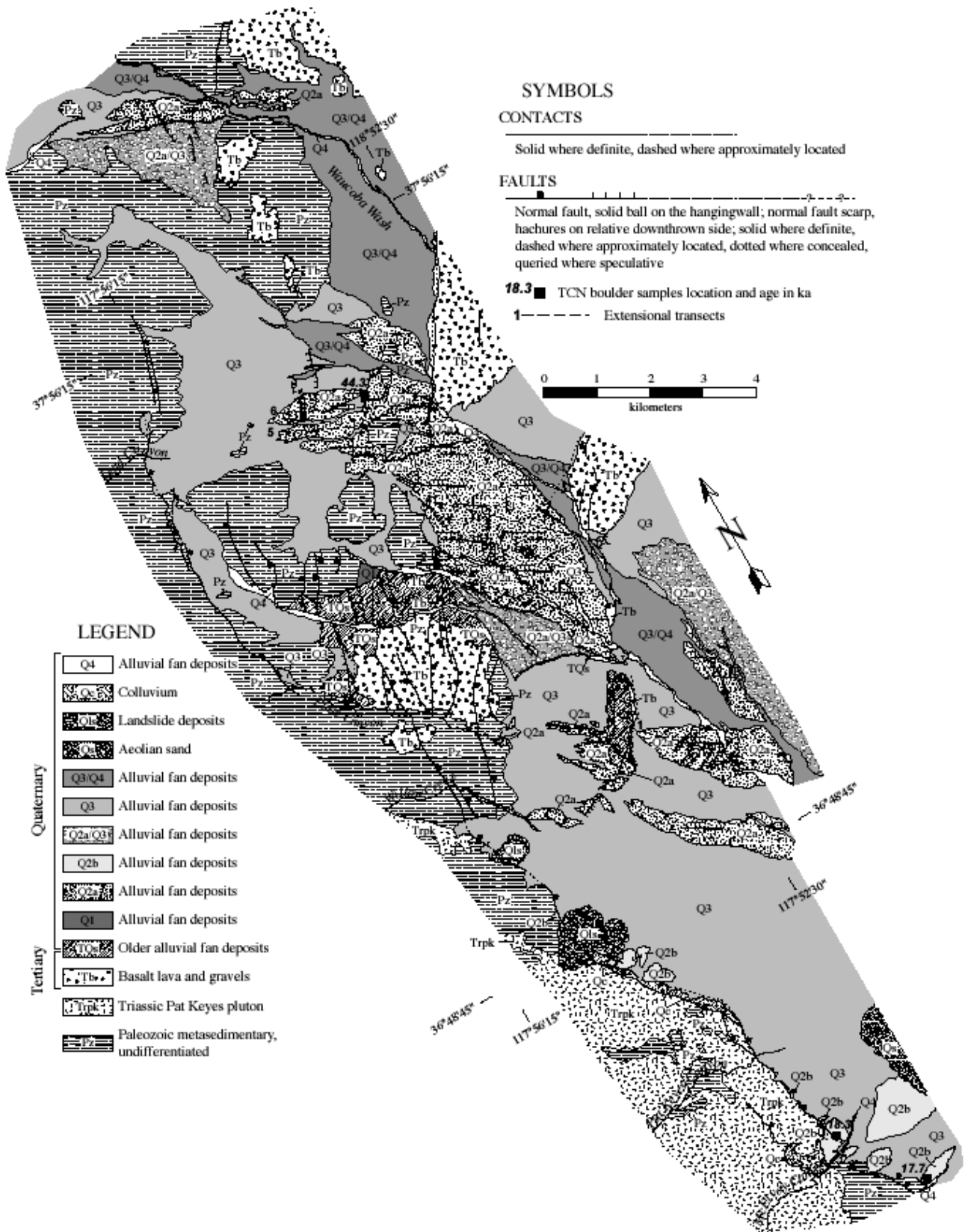


Figure 9. Geologic map along the eastern Inyo fault zone (east of stop 2 in Fig. 1) showing pre-Tertiary rocks, Tertiary volcanic rocks, Quaternary sedimentary deposits and alluvial fan surfaces, and Quaternary faults. See Figure 1 for location of the Inyo Moutnain. Bedrock geology from Ross (1967). Modified from Lee et al. (2009a).

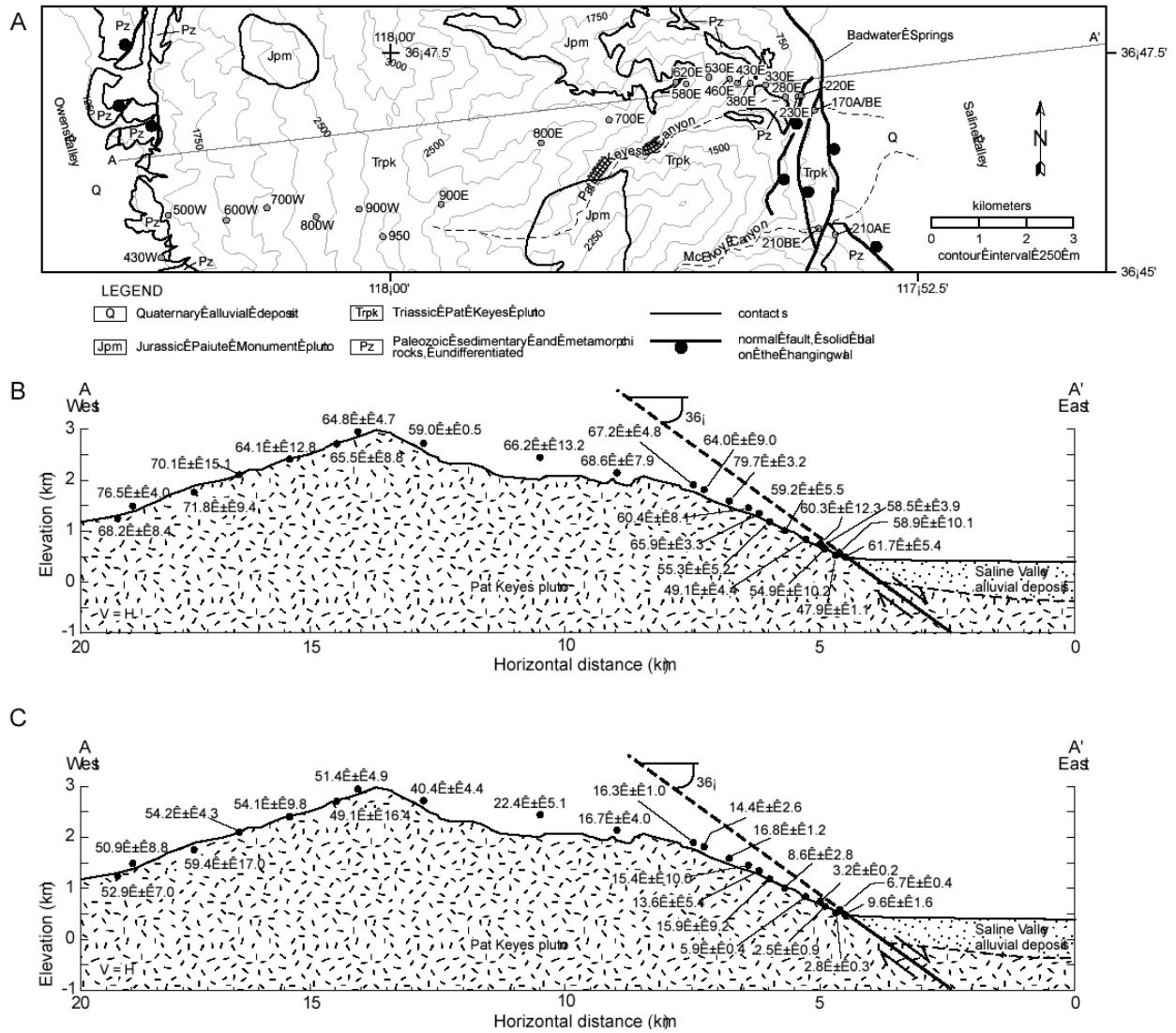


Figure 10. (a) Simplified geologic map across the central Inyo Mountains showing location of (U-Th)/He thermochronometric samples. Geology from Ross (1967). (b) Zircon and (c) apatite (U-Th)/He ages projected onto cross-section across the Inyo Mountains. Location of cross section shown in (a). Modified from Lee et al. (2009a).

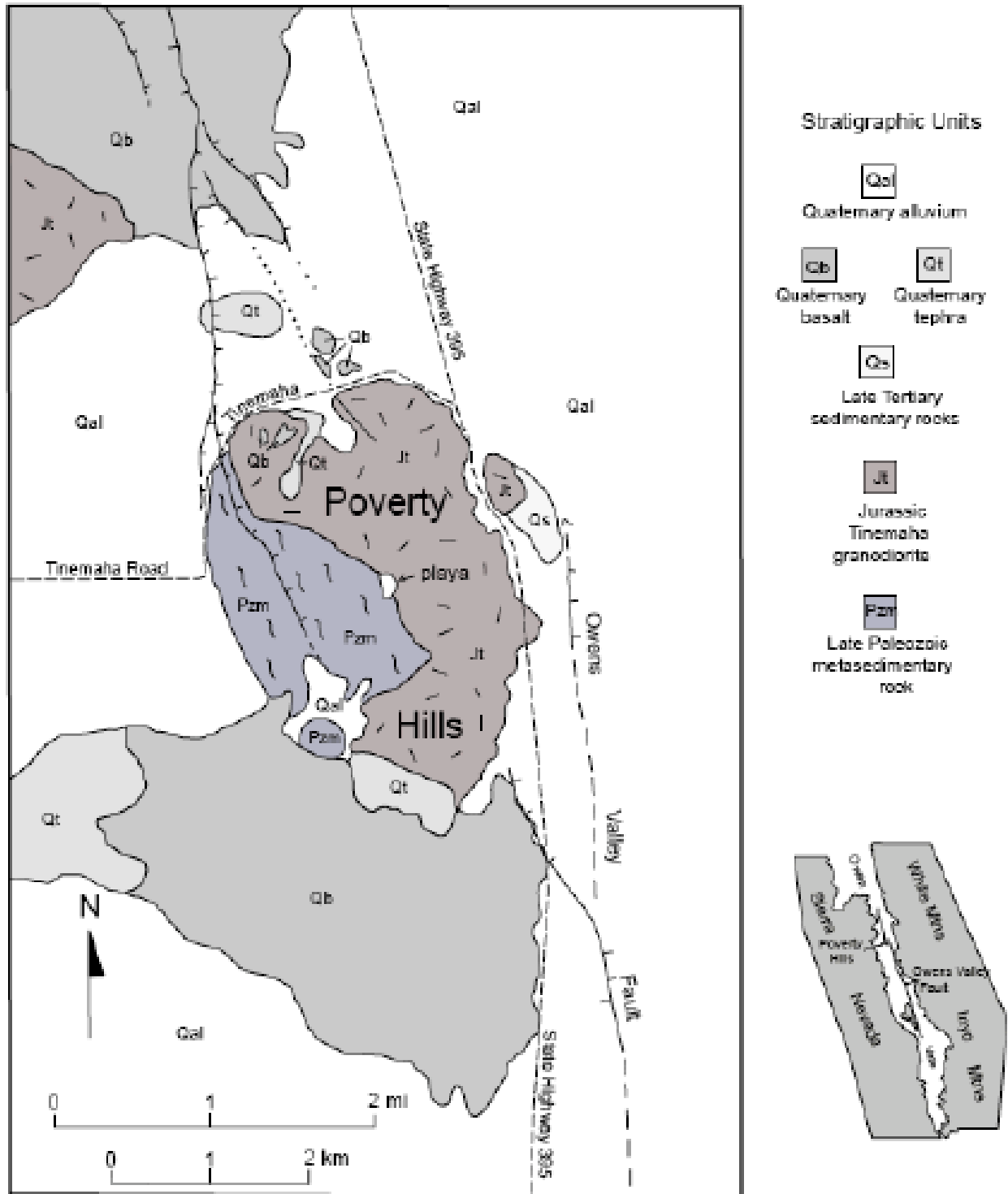


Figure 11. Geologic map of the Poverty Hills and adjacent Owens Valley fault.



Figure 12. Photographs for comparison of breccia in the Poverty Hills and Blackhawk landslides. (a) View toward the northeast of breccia in a roadcut along Tinemaha Road at the northwest side of the Poverty Hills. Note the light colored bed that has been contorted by cataclastic flow interpreted to have occurred during emplacement of the Poverty Hills mass as a rock avalanche. (b) For comparison, a similarly distorted bed (outlined) in the Pleistocene Blackhawk landslide, a well-documented rock avalanche deposit in the southern Mojave Desert.

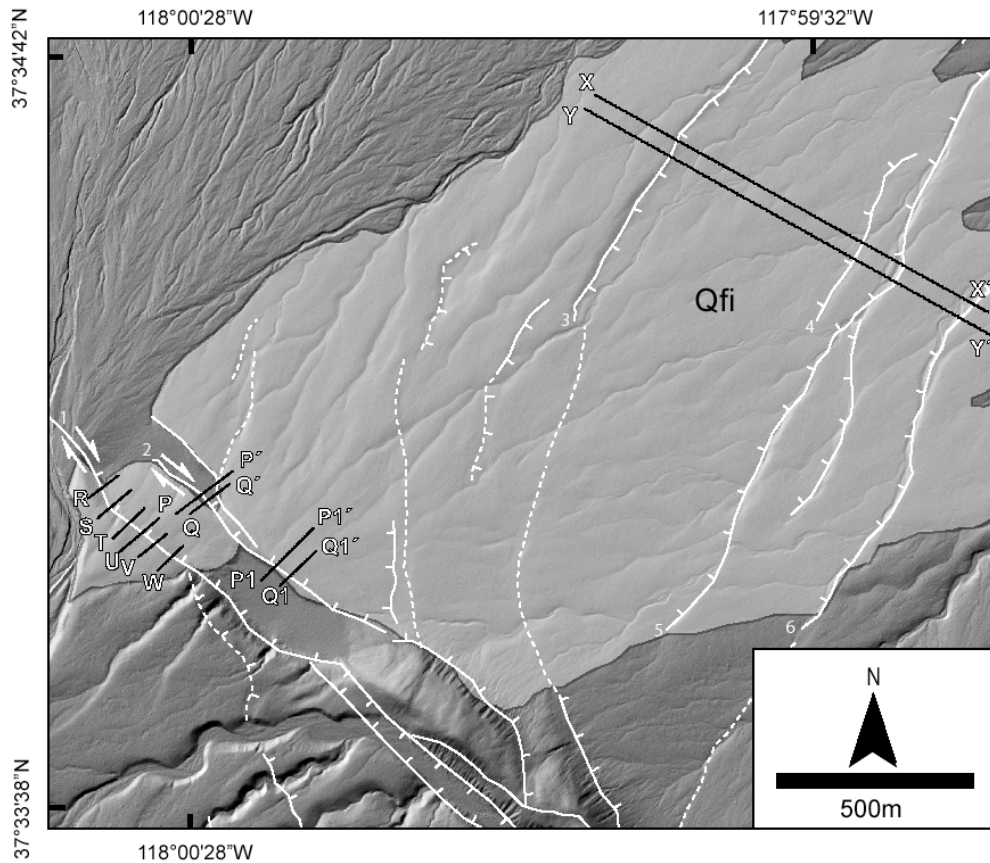


Figure 13. Hillshaded lidar-derived DEM of the Furnace Creek alluvial fan showing the topographic profiles analyzed for extension rates. The number by each fault scarp represents the scarps that were included in the analysis. The mapped Quaternary deposits are modified from Reheis et al. (1995). See Ganev et al. (2010) for the detailed measurements of scarp heights. Solid lines are fault scarps (used in analysis), dashed lines are fault scarps visible on shaded relief maps but not detectible on topographic profiles (not used in analysis), arrows show sense of motion on strike slip faults, tick marks are on the hanging wall of normal faults, lines with question marks denote inferred fault scarps and sense of motion. Modified from Ganev et al. (2010)

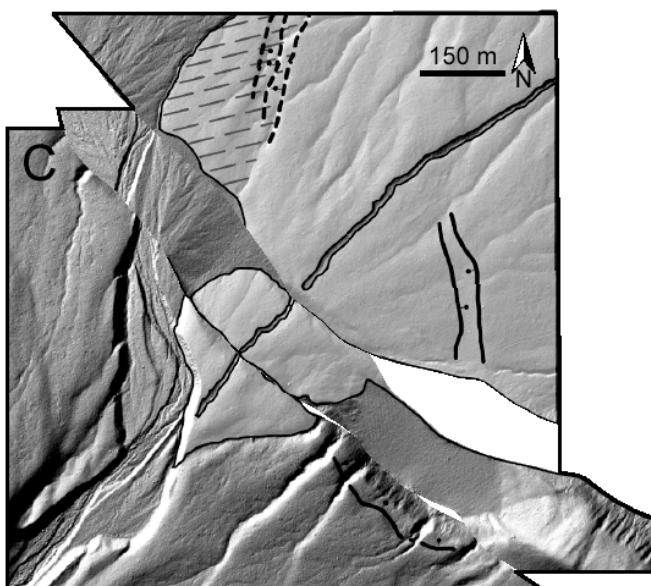
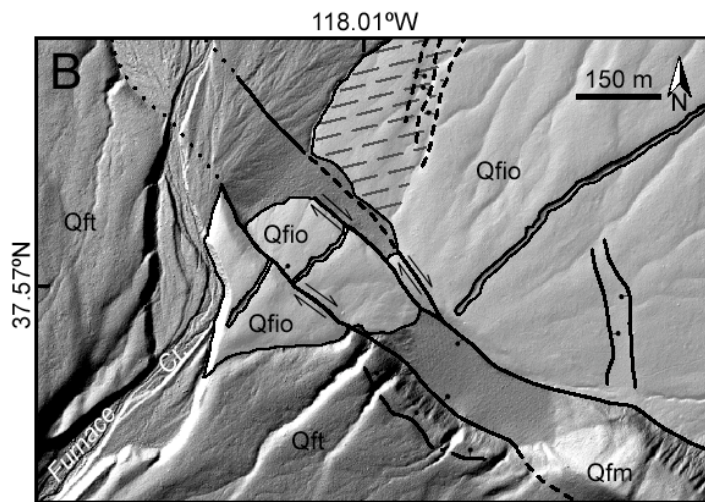
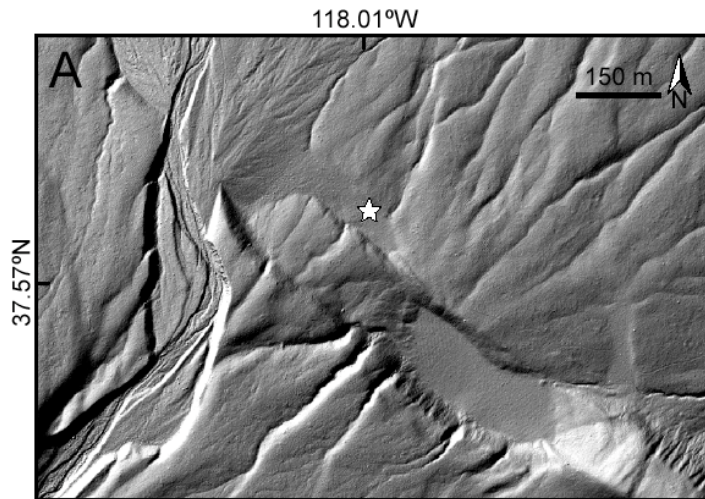


Figure 14. Maps of Furnace Creek alluvial fan in Fish Lake Valley (after Frankel et al., 2007b). (a) Hillshaded 1-m-resolution lidar digital elevation model of the Furnace Creek alluvial fan. Star indicates parking area for field trip. (b) Geologic map (modified from Reheis et al., 1995) of the Furnace Creek alluvial fan draped over the hillshaded image from A. Qfio—Older alluvium of Indian Creek (late Pleistocene); Qft—Alluvium of Trail Canyon (middle Pleistocene); Qfm—Alluvium of McAfee Creek (middle Pleistocene). (c) Furnace Creek alluvial fan retro-deformed 290 ± 20 m to its pre-faulting position based on the high-resolution lidar digital elevation data. Hatched pattern on northwest section of the offset fan indicates a surface of similar age, but set into the Qfio unit. Combining the late Pleistocene displacement history with the 94 ± 11 ka cosmogenic ^{10}Be model age from the offset Qfio surface yields a slip rate of 3.1 ± 0.4 mm/yr (Frankel et al., 2007b).

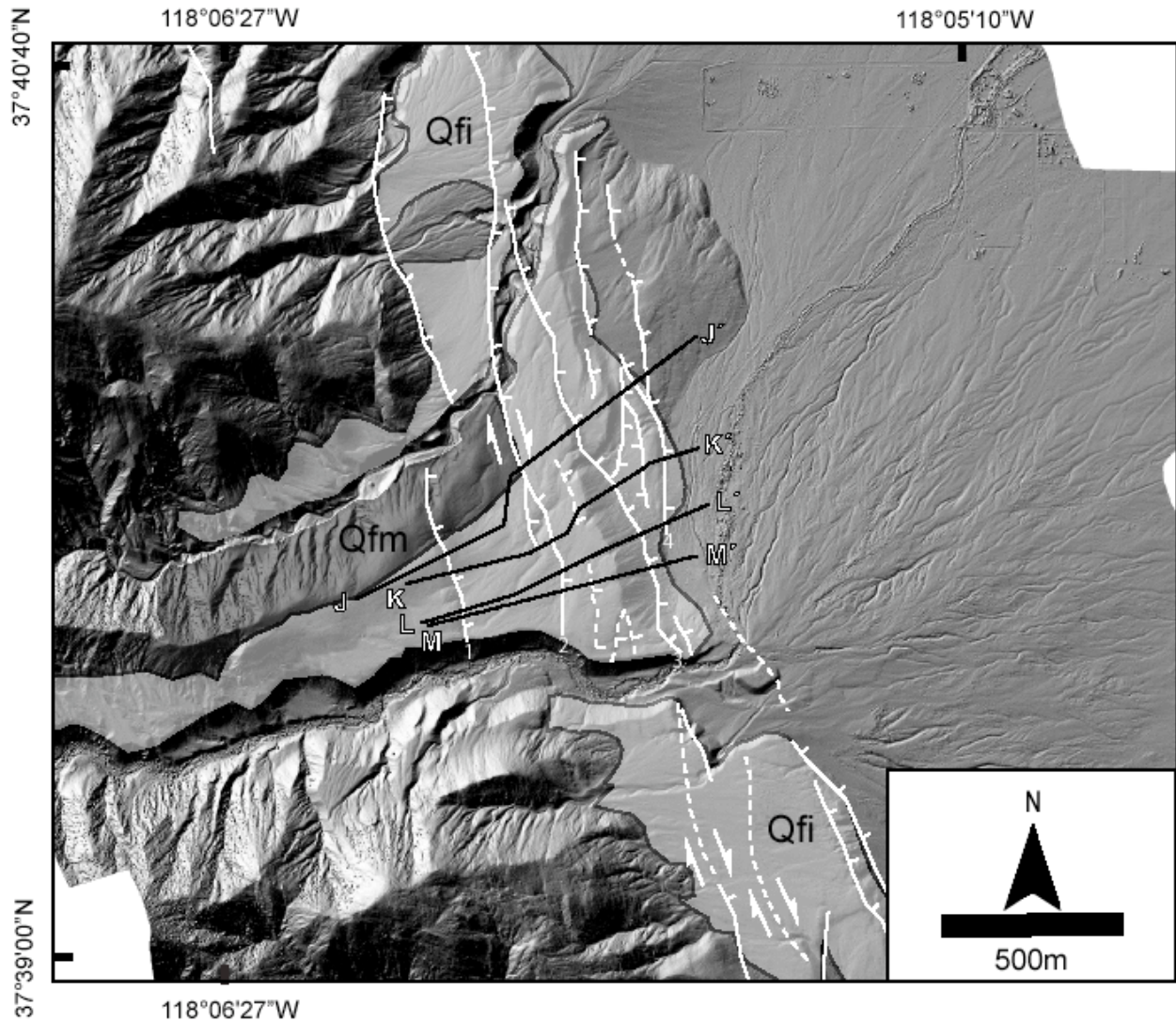


Figure 15. Hillshaded lidar-derived DEM of the Perry Aiken Creek site showing the topographic profiles analyzed. The number by each fault scarp represents the scarps that were included in the analysis. The mapped Quaternary deposits are modified from Reheis et al. (1993). See Ganev et al. (2010) for the detailed measurements of scarp heights. Solid lines are fault scarps (used in analysis), dashed lines are fault scarps visible on shaded relief maps but not detectible on topographic profiles (not used in analysis), arrows show sense of motion on strike slip faults, tick marks are on the hanging wall of normal faults, lines with question marks denote inferred fault scarps and sense of motion. Modified from Ganev et al. (2010).

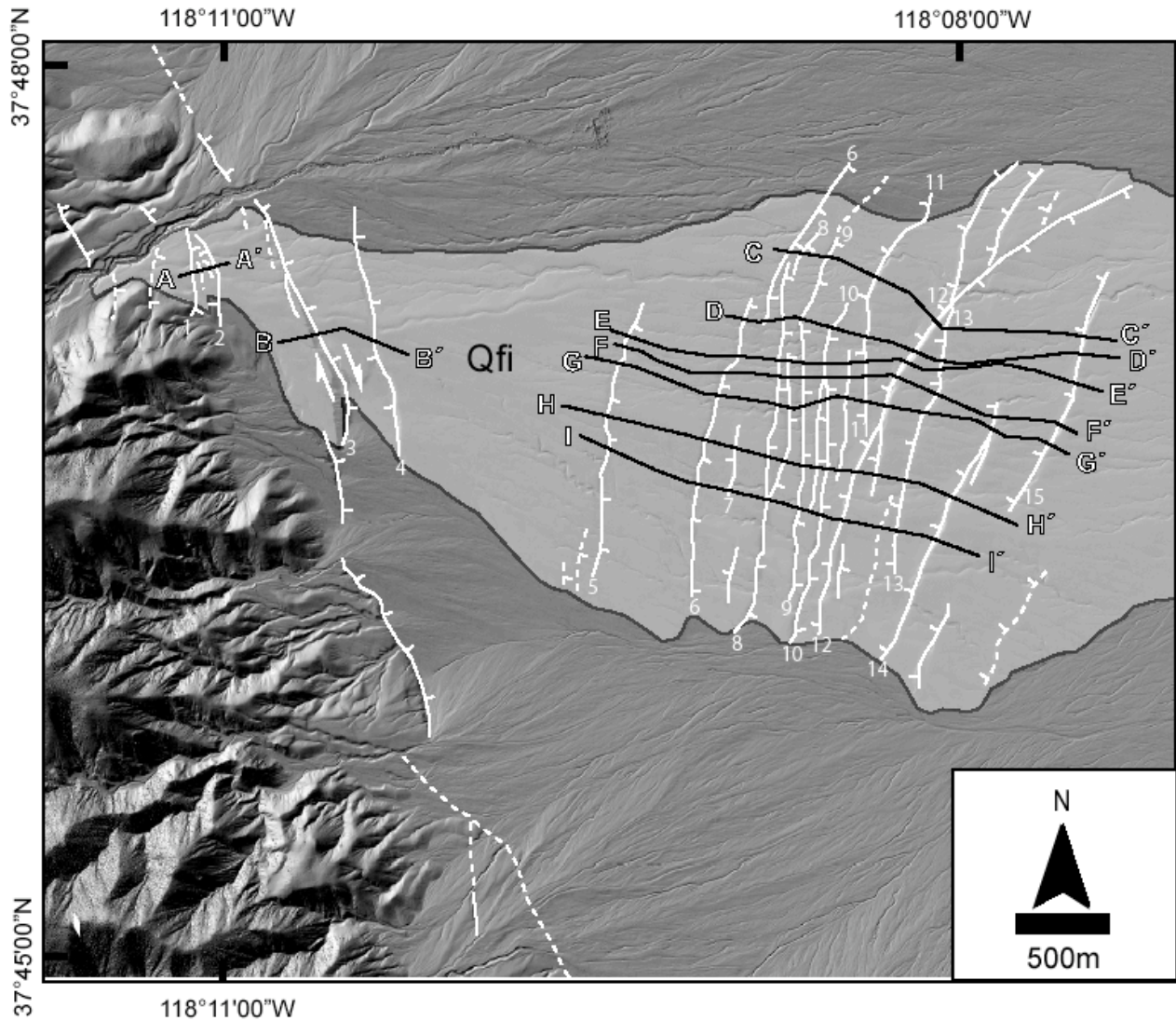


Figure 16. Hillshaded lidar-derived DEM of the Indian Creek site showing the topographic profiles analyzed. The number by each fault scarp represents the scarps that were included in the analysis. The mapped Quaternary deposits are modified from Reheis et al. (1995). See Ganev et al. (2010) for the detailed measurements of scarp heights. Solid lines are fault scarps (used in analysis), dashed lines are fault scarps visible on shaded relief maps but not detectable on topographic profiles (not used in analysis), arrows show sense of motion on strike slip faults, tick marks are on the hanging wall of normal faults, lines with question marks denote inferred fault scarps and sense of motion. Modified from Ganev et al. (2010).

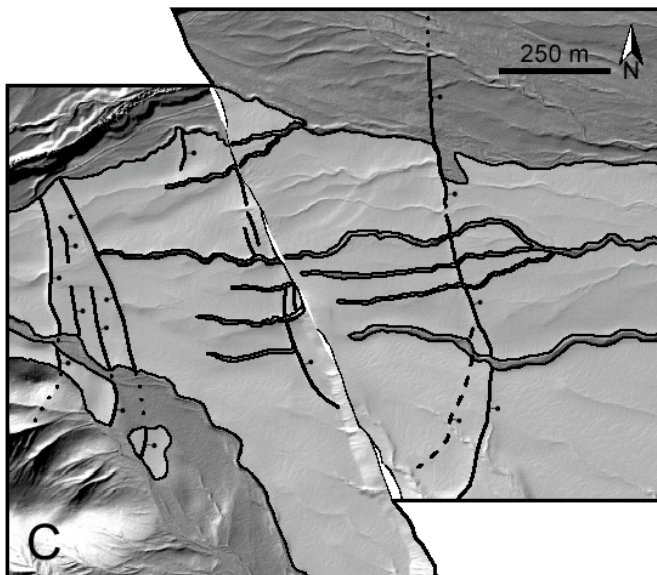
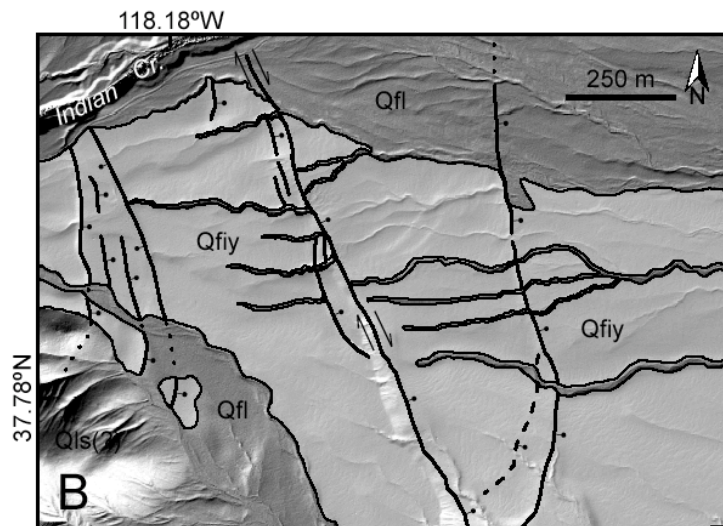
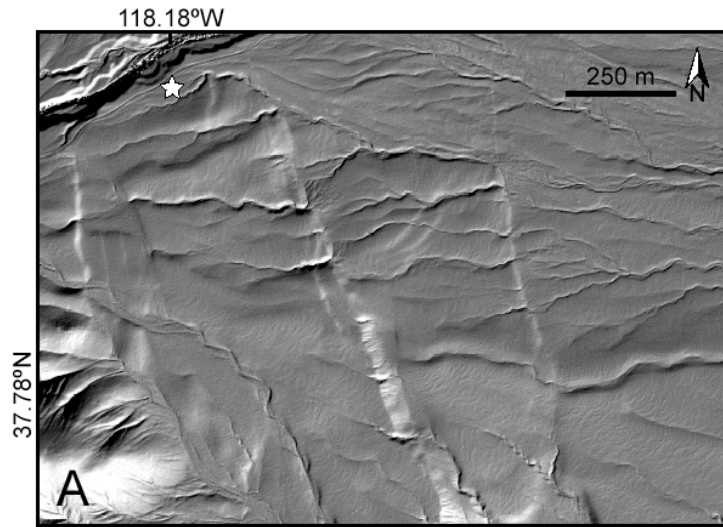


Figure 17. Maps of the Indian Creek alluvial fan in Fish Lake Valley (after Frankel et al., 2007b). (a) Hillshaded 1 m resolution lidar digital elevation model of the Indian Creek alluvial fan. Star indicates parking area for field trip. (b) Geologic map (modified from Reheis et al., 1993) of the Indian Creek alluvial fan and surrounding areas draped over the hillshaded image in A. Qfi y—Younger alluvium of Indian Creek (late Pleistocene); Qfl —Alluvium of Leidy Creek (early Holocene and late Pleistocene); Qls—Holocene to late Pleistocene landslide deposits. (c) Indian Creek alluvial fan retrodeformed 178 ± 20 m to its pre-faulting position based on lidar data. A cosmogenic ^{10}Be model age for the Qfi y surface of 71 ± 8 ka yields a slip rate of 2.5 ± 0.4 mm/yr when combined with the late Pleistocene offset measurement (Frankel et al., 2007b).

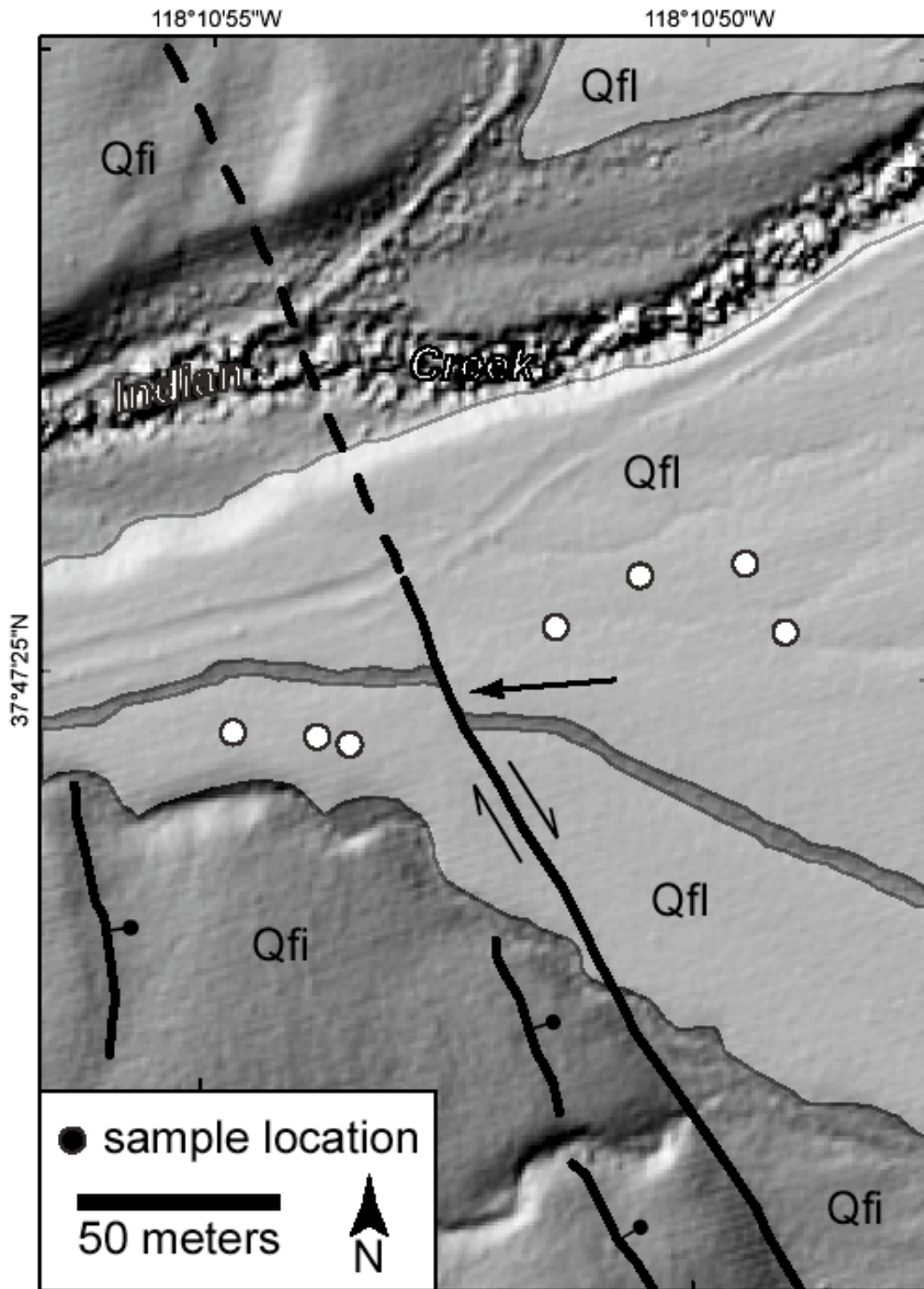


Figure 18. Simplified Quaternary geologic map of the northern Indian Creek alluvial fan in Fish Lake Valley modified from Reheis et al. (1993). Map highlights the right-laterally offset channel in Holocene alluvium. Displacement of this channel based on measurements from lidar data is 15 ± 2 m. When combined with the cosmogenic ^{10}Be surface exposure age of 7 ± 1.8 ka for the Qfl fan unit, this yields a slip rate of $2.1 +0.7/-0.6$ mm/yr, which is indistinguishable from the late Pleistocene rate determined to the south on the same fan complex (Fig. 17).

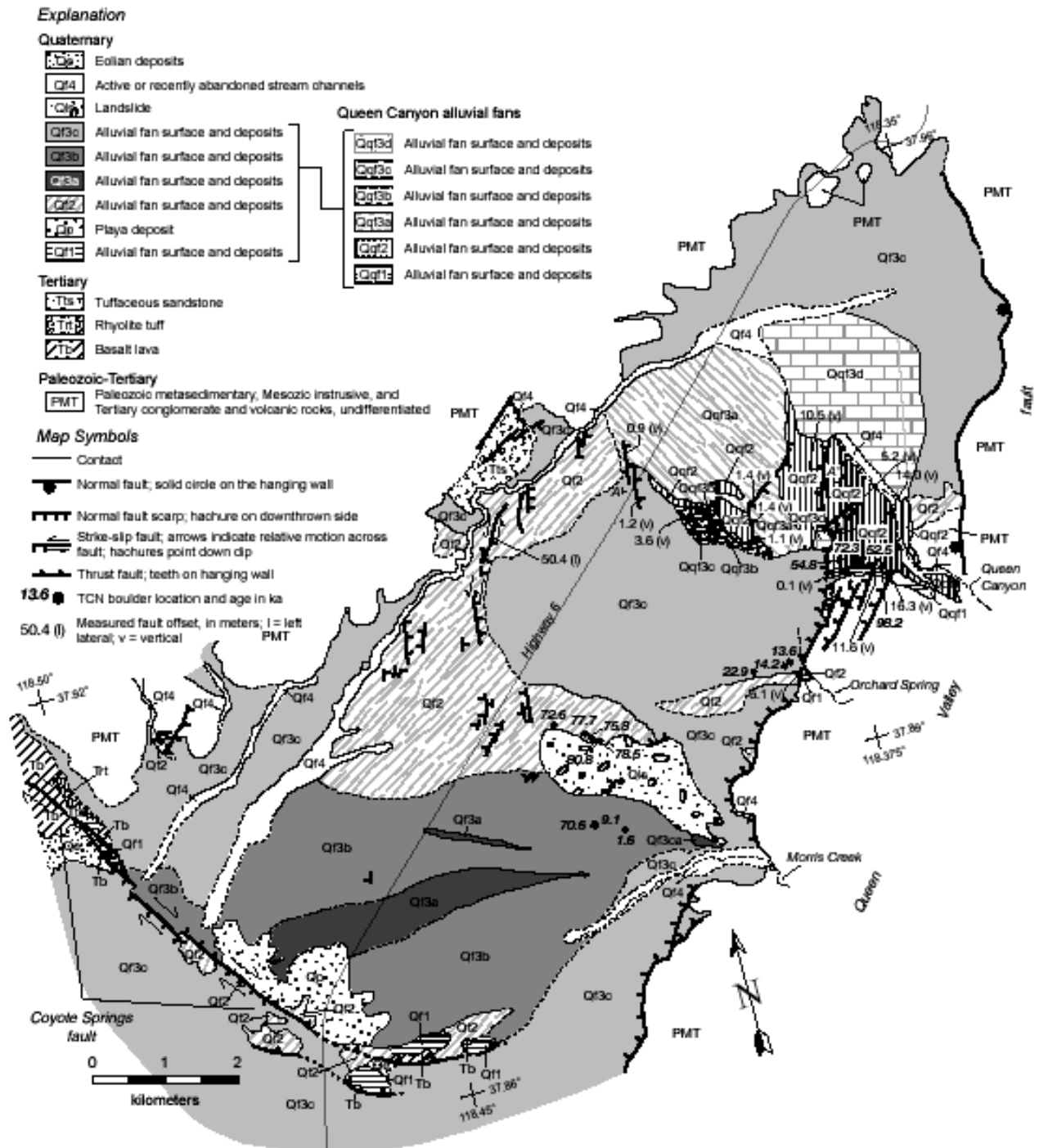


Figure 19. Simplified geologic map of the Queen Valley area (stops 7 and 8, Fig. 1) showing Tertiary volcanic rocks, Quaternary sedimentary deposits and alluvial fan surface, and Quaternary faults. Modified from Lee et al. (2009b).

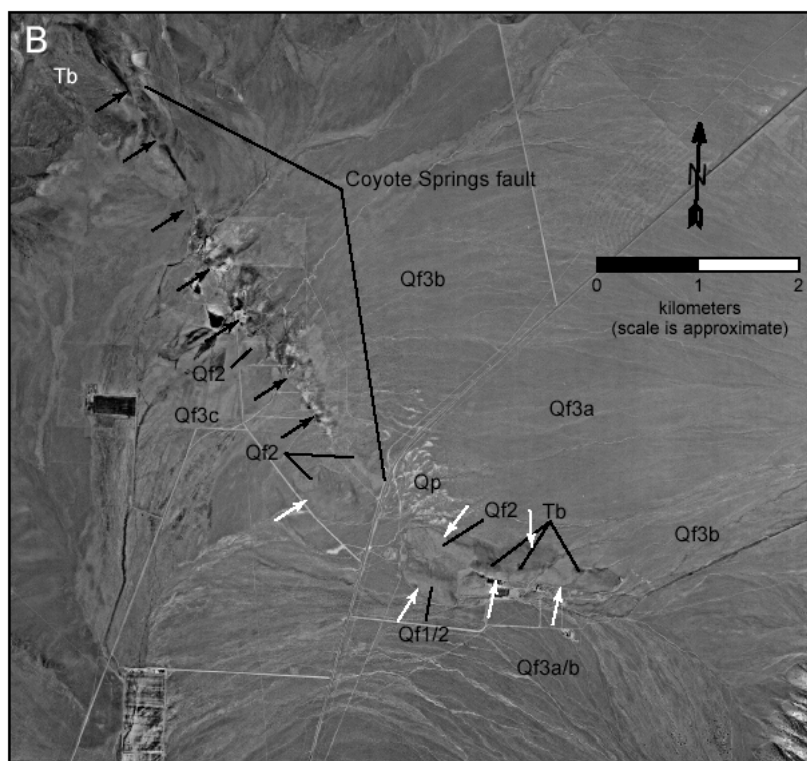
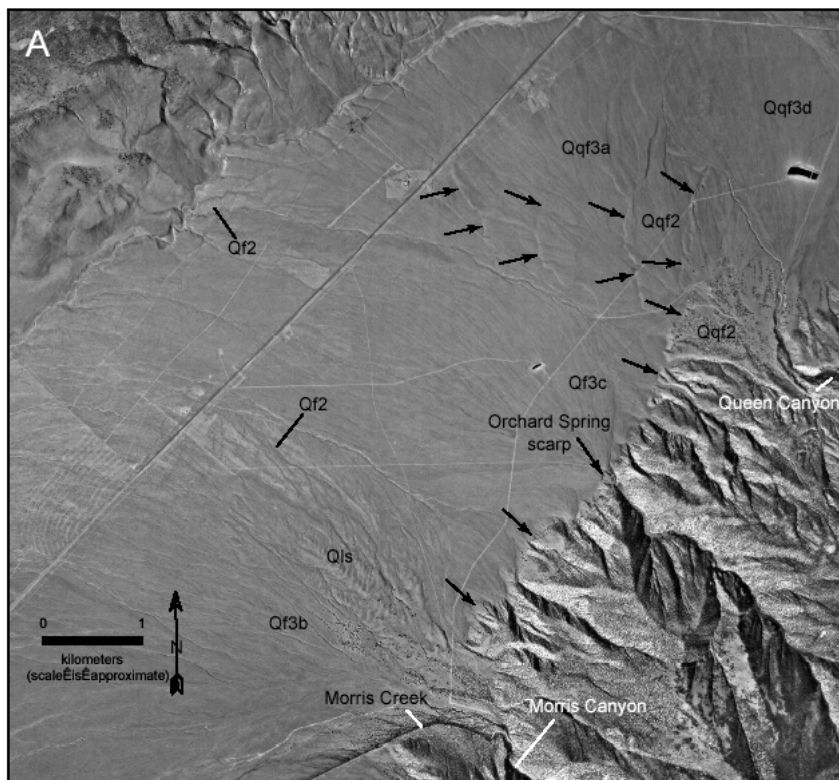


Figure 20. (a) Aerial photograph of the central part of Queen Valley highlighting different alluvial fan surfaces and prominent fault scarps (arrows). (b) Aerial photograph of the southern part of Queen Valley highlighting different alluvial fan surfaces and the dextral Coyote Springs fault (black arrows) and thrust faults (white arrows). See Figure 19 for unit abbreviations. Modified from Lee et al. (2009b).

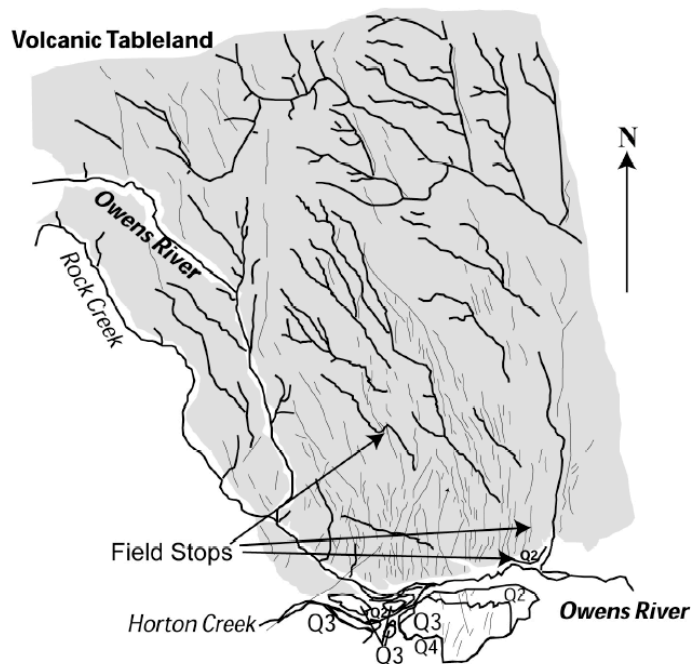
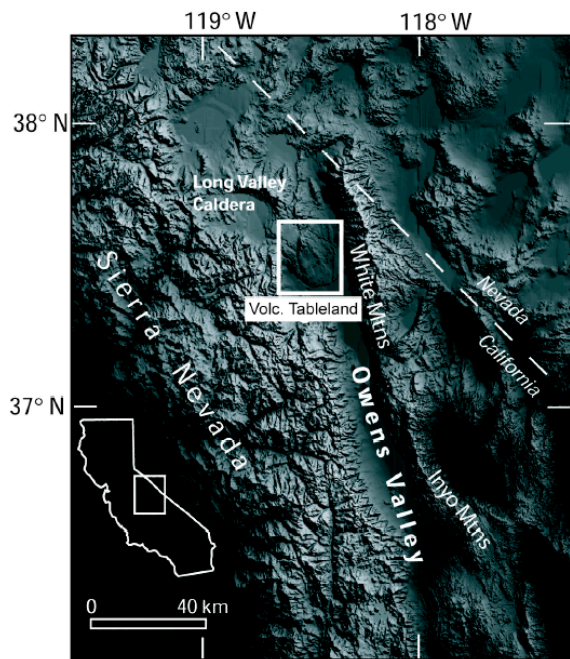


Figure 21. Location of the Volcanic Tableland with field stops noted. Faults and drainage pattern at right are after Pinter (1995).

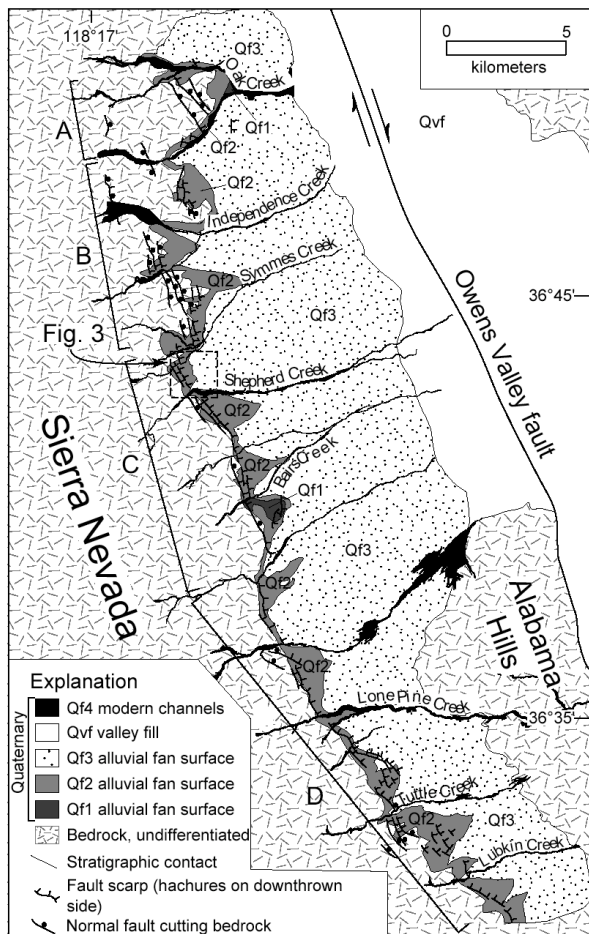


Figure 22. Simplified geologic map along the southern Sierra Nevada frontal fault zone (stop 12, Fig. 1) showing major normal fault scarps cutting Quaternary alluvial fan surfaces and fault zone segments. Modified from Le et al. (2007).

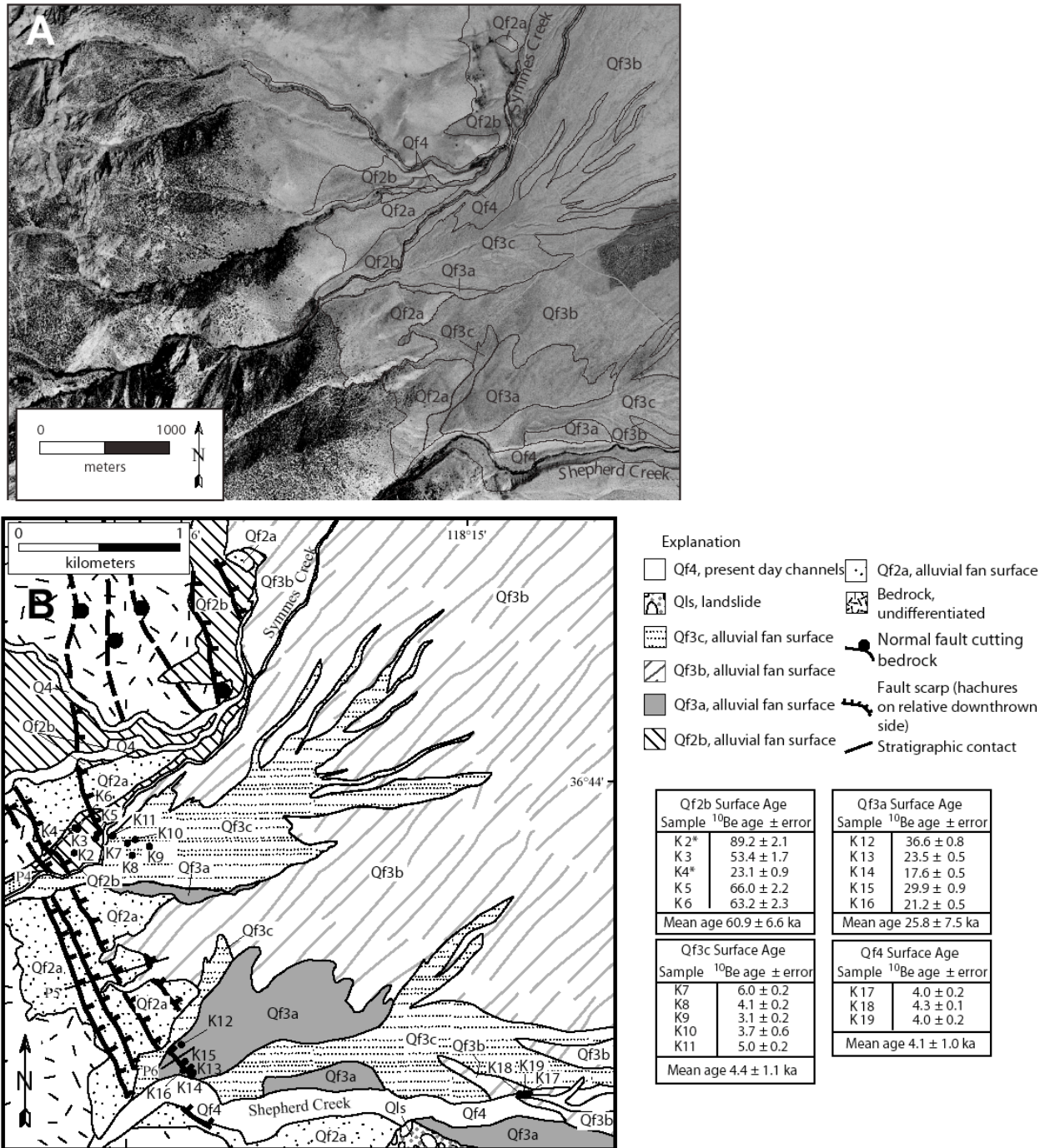


Figure 23. (a) Aerial photograph of the area of Symmes and Shepherd creeks, highlighting different alluvial fan surfaces. (b) Detailed geologic map of area shown in (a) and showing normal fault scarps cutting Quaternary alluvial fan surfaces, cosmogenic nuclide (TCN) sample locations (black circles), and topographic profile locations. Boxes show calculated ¹⁰Be boulder age for each sample and age of abandonment for each surface; asterisk (*) indicates boulder sample not calculated in the mean. TCN model ages incorporate an erosion rate of 0.3 cm/k.y. Location shown in Figure 22. Modified from Le et al. (2007).

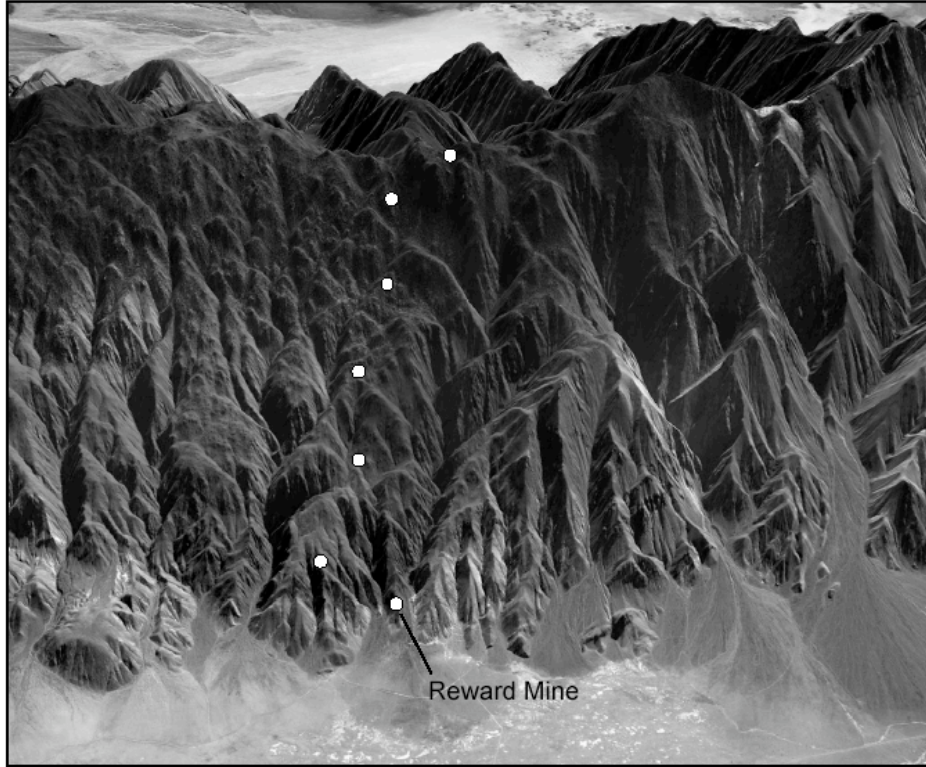


Figure 24. Vertically exaggerated (2.5x) oblique eastward view of the central part of the western flank of the Inyo Mountains showing locations of (U-Th)/He sample locations. Image from Google Earth.



Figure 25. View to the northwest along the Death Valley–Fish Lake Valley fault zone at Furnace Creek in central Fish Lake Valley. Note the two prominent fault scarps cutting the Furnace Creek alluvial fan. White Mountain Peak is the prominent summit along the skyline ridge.



Figure 26. View looking to the southwest at the west-facing normal fault scarp at Perry Aiken Creek. This scarp is the largest late Pleistocene vertical offset along the entire Death Valley–Fish Lake Valley fault system.



Figure 27. Photograph looking southwest along the right-lateral oblique fault scarp at Indian Creek in Fish Lake Valley at the northern end of the Death Valley–Fish Lake Valley fault zone. The eastern White Mountains range front is visible beyond the scarp. Numerous normal faults displace the distal portion of the Indian Creek; all dextral deformation at this location is accommodated on the pictured fault.



Figure 28. Vertically exaggerated (2.5x) oblique northeastward view of an anticlinal hill at the southwestern end of Queen Valley. Break in slope near the base of the hill is interpreted as a north- to northeast-dipping thrust fault. Playa deposits, which ponded up-fan of this set of hills, are poorly exposed in the upper right corner of the image. Image from Google Earth.

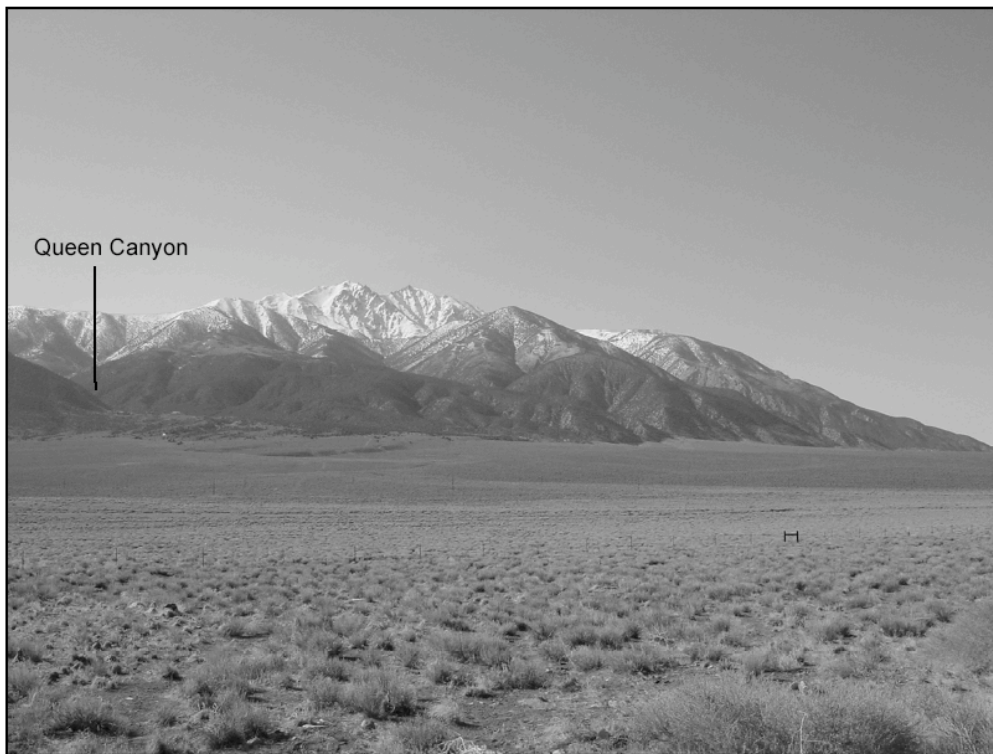


Figure 29. View looking south at the Queen Valley fault exposed at the base of the northern end of the White Mountains. Well-developed triangular facets are exposed along the southwestern part of the fault and fault scarps are well-developed in alluvial fans at the mouth of Queen Canyon.



Figure 30. View looking to the northeast at a relay ramp developed in a normal fault cutting the Volcanic Tableland. The highest summit on the skyline ridge in background is White Mountain Peak.

Figure 31, On following page

Figure 31. (a) Aerial photograph an extensional fault array on the Volcanic Tableland (see Dawers and Anders, 1995, for along strike displacement data and discussion of growth by fault linkage). Dark shadows are normal fault scarps, dipping east. Paleo-channels incise into the Bishop tuff surface both perpendicular and parallel to the array. The box highlights the warped overlap, or relay ramp, between the tips of the larger displacement fault segments; this is an excellent fieldtrip stop for observing channel incision in footwalls of normal faults, knick-zones upstream from faults, wind gaps and paleo-waterfalls at displaced channels. (b) Annotated sketch highlighting the ‘linking fault’ and nearby channel patterns. (c) Gilpin (2002) interpreted this pattern of fault array evolution, based on field observations of channel incision here; a=earliest stream initiation stage through f=current fault and pale-channel geometry.

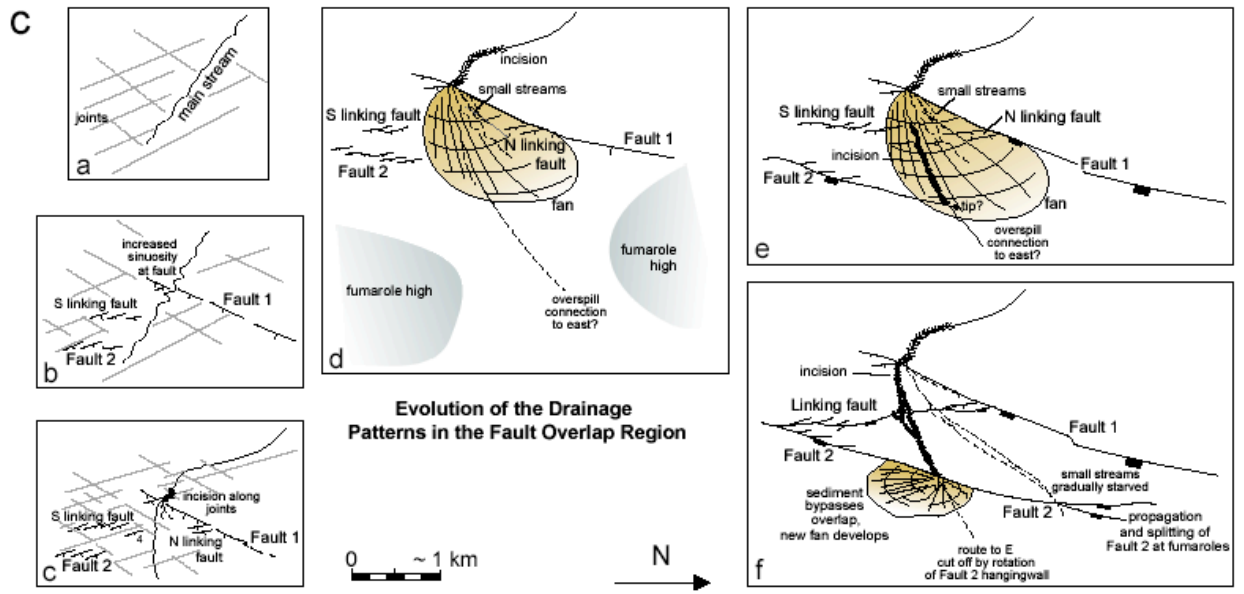
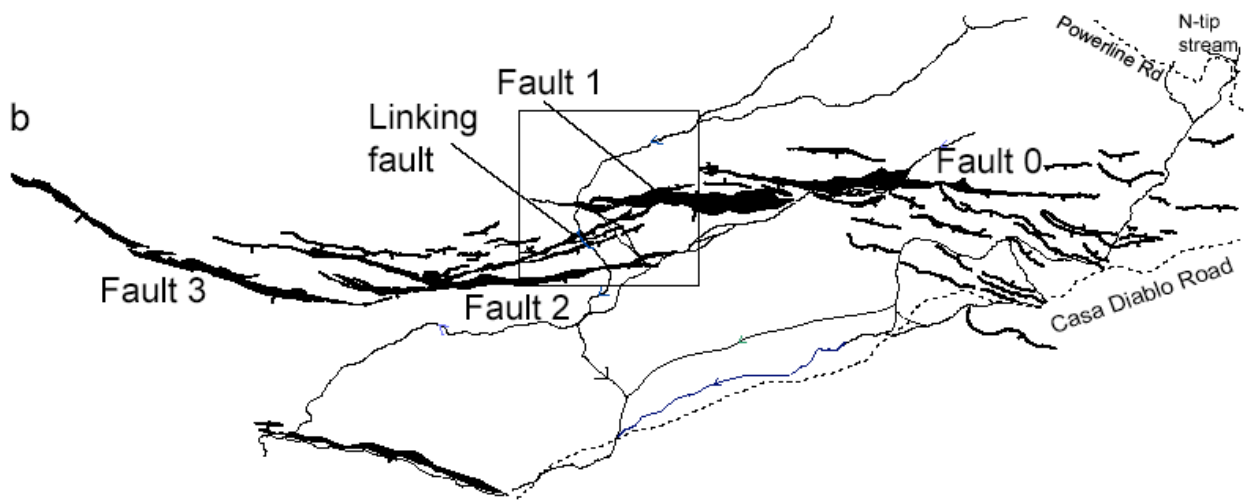
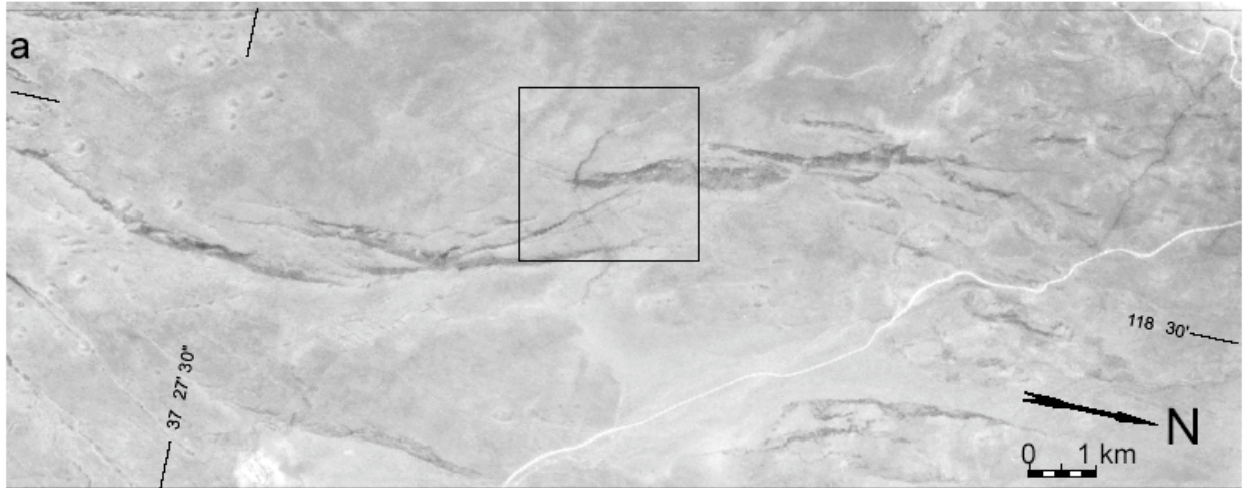


Fig.31. For full caption, see preceding page.



Figure 32. Photograph taken looking the southwest across the Owens River and Owens River terraces.



Figure 33. Field photo of an east-facing fault scarp north of Symmes Creek along the Sierra Nevada frontal fault zone. Fault scarp vertically offsets aQf2b alluvial fan surface. View to the southwest.

